Geological History, Chronology and Magmatic Evolution of Merapi

6

Ralf Gertisser, Mary-Ann del Marmol, Christopher Newhall, Katie Preece, Sylvain Charbonnier, Supriyati Andreastuti, Heather Handley, and Jörg Keller

Abstract

This chapter provides a synthesis of the geological history, chronology and magmatic evolution of Merapi. Stratigraphic field and geochronological data are used to divide Merapi into three main evolutionary stages and associated volcanic edifices (Proto-, Old and New Merapi) and eight broad volcano-stratigraphic units to characterise the eruptive activity and structural evolution of the volcano through time. Complementary petrological, geochemical and isotopic data are used to characterise the eruptive products of Merapi and shed light on the geochemical evolution and petrogenetic processes. The data indicate that the eruptive products of Merapi are mainly basaltic andesite of both medium-K and high-K type and support a two-stage petrogenetic model, where primary magmas are derived from a heterogenous, Indian Ocean MORB-like mantle source metasomatised by slab-derived components. Subsequently, these magmas are modified during transfer through the crust by complex magmatic differentiation processes, including contamination by carbonate rocks of the local upper crust. The available data indicate that, since ~ 1900 ^{14}C y BP, the lavas and pyroclastic rocks of Merapi are essentially of the high-K type and that regular geochemical variations with systematic shifts in whole rock SiO_2 content occurred since at least the Late Holocene, although erupted magma

R. Gertisser (✉)
School of Geography, Geology and the Environment, Keele University, Keele ST5 5BG, UK
e-mail: r.gertisser@keele.ac.uk

M.-A. del Marmol
Department of Geology, Ghent University, 9000 Gent, Belgium

C. Newhall
Mirisbiris Garden and Nature Center, Sitio Mirisbiris, 4508 Barangay Salvacion, Santo Domingo, Albay, Philippines

K. Preece
Department of Geography, Swansea University, Swansea SA2 8PP, UK

S. Charbonnier
School of Geosciences, University of South Florida, Tampa, FL 33620-5201, USA

S. Andreastuti
Center for Volcanology and Geological Hazard Mitigation, Geological Agency, Bandung 40122, Indonesia

H. Handley
Department of Applied Earth Sciences, University of Twente, 7514 AE Enschede, The Netherlands

School of Earth, Atmosphere and Environment, Monash University, Clayton, VIC 3800, Australia

J. Keller
Institut für Geo- und Umweltnaturwissenschaften, Mineralogie-Petrologie, Albert-Ludwigs-Universität Freiburg, 79104 Freiburg, Germany

R. Gertisser et al. (eds.), *Merapi Volcano*, Active Volcanoes of the World,
https://doi.org/10.1007/978-3-031-15040-1_6

compositions have remained broadly uniform since the mid-twentieth century.

Keywords

Merapi · Stratigraphy · Chronology · Petrology · Geochemistry · Isotope geochemistry · Petrogenesis · Magmatic evolution · Merapi-type volcanism

6.1 Introduction

Merapi, located 25–30 km north of the city of Yogyakarta in Central Java (Fig. 6.1), is one of Indonesia's most active and hazardous volcanoes. Eruptions during the twentieth and early twenty-first century have mostly consisted of lava dome growth, typically lasting for weeks or months each time, and subsequent gravitational dome collapse to generate small volume pyroclastic density currents (PDCs) or block-and-ash flows, in the classic volcanological literature termed Merapi-type nuées ardentes. The well-recorded historical activity of Merapi (Voight et al. 2000 and references therein; Global Volcanism Program 2013), particularly since the late eighteenth century, indicates that eruptions have occurred every few years and have been dominated by effusive, lava dome-formation and intermittent short-lived explosive outbursts,

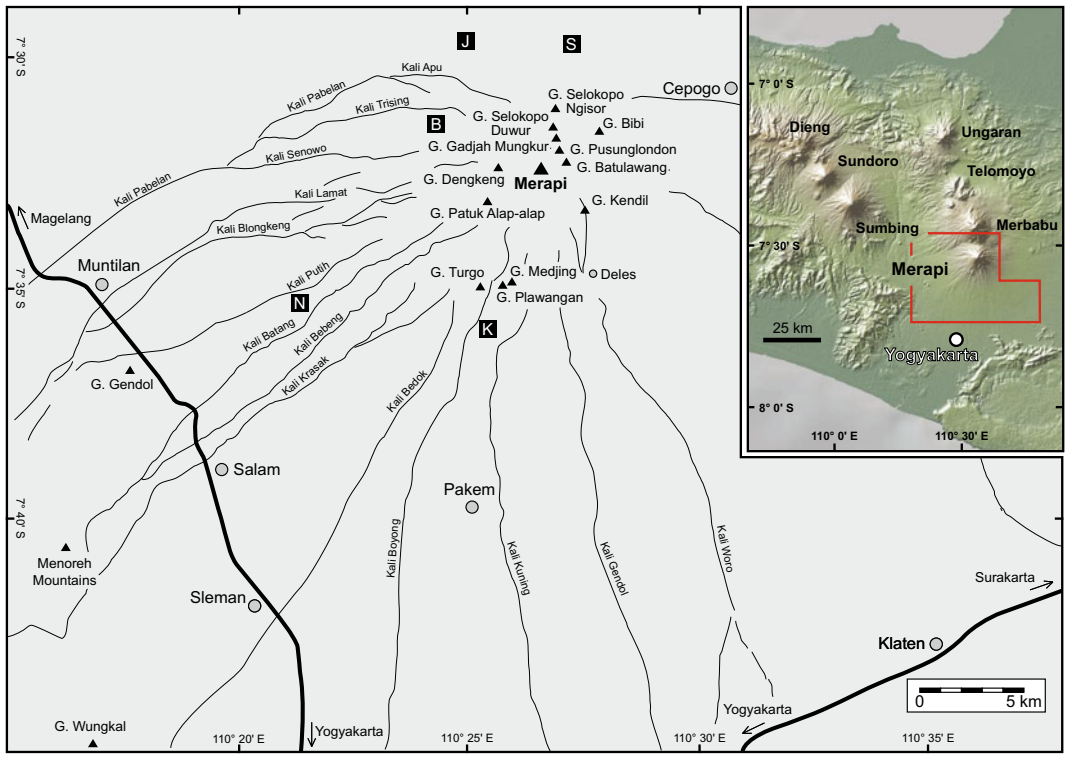

Fig. 6.1 Map of Merapi, showing locations referred to in the text. Major towns and villages are shown by filled circles, while volcano observation posts (K = Kaliurang; N = Ngepos; B = Babadan; J = Jrakah; S = Selo) are marked by black squares. The grey lines indicate main river valleys and the thick black lines show major roads. The summit of Merapi and a series of hills (Indon. = Gunung (G.)) that rise from the volcanic complex or from the surrounding plain are indicated by black triangles. The three-dimensional inset map shows the location of Merapi north of the city of Yogyakarta and nearby Quaternary volcanoes in Central Java

producing PDCs. Stratigraphic and geochronological studies published since the 1980s have provided a detailed picture of Merapi's prehistoric activity, which was often explosive, as well as the overall structural and geological evolution of the volcanic complex. The results of these investigations, which built on earlier work of, for example, Kemmerling (1921), Hartmann (1935) and van Bemmelen (1949, 1956), are included in reports (e.g. Wirakusumah et al. 1980) and Ph.D. theses (Bahar 1984; del Marmol 1989; Berthommier 1990; Andreastuti 1999; Gertisser 2001), a collection of landmark papers published in a special issue 'Merapi volcano' of the Journal of Volcanology and Geothermal Research (Andreastuti et al. 2000; Camus et al. 2000; Newhall et al. 2000) and subsequent studies (e.g. Gertisser and Keller 2003a; Gertisser et al. 2012a; Bronto et al. 2014; Selles et al. 2015). A 1:50,000 geological map of Merapi was published by Wirakusumah et al. (1989). Complementary petrological, geochemical and isotopic studies of the eruptive products of Merapi have shed light on magma generation in the mantle wedge above the subducting Indo-Australian plate, magma storage and magmatic differentiation processes in the arc crust, and the magmatic evolution of Merapi in space and time. Such studies either focused on Merapi itself (e.g. Kerinec 1982; Bahar 1984; Luais 1986; del Marmol 1989; Berthommier 1990; Andreastuti 1999; Andreastuti et al. 2000; Camus et al. 2000; Newhall et al. 2000; Gertisser 2001; Gertisser and Keller 2003a, b; Gertisser et al. 2012a; Chadwick et al. 2013; Costa et al. 2013; Troll et al. 2013a; Deegan et al. 2016; Handley et al. 2018), or used rock samples from Merapi and other Indonesian volcanoes to discuss magma genesis on an arc-wide scale or in the global context of subduction zone magmatism (e.g. Whitford 1975a, b; Whitford and Nicholls 1976; Whitford et al. 1979, 1981; White and Patchett 1984; McDermott and Hawkesworth 1991; Turner and Foden 2001; Woodhead et al. 2001; Debaille et al. 2006; Handley et al. 2011, 2014; Deegan et al. 2021).

This chapter provides a synthesis of the geological history, chronology and magmatic evolution of Merapi, and discusses the underlying petrogenetic processes. Following a description of the geological evolution of Merapi, the compositional variations of the eruptive products are presented, including petrographical and mineral chemical information, major and trace element geochemistry as well radiogenic (Sr, Nd, Pb, Hf), stable (O) and uranium-series isotopic compositions of samples that span the entire geological history of the volcanic complex. The available petrological, geochemical and isotopic data are then placed into a stratigraphic framework, linked to the major evolutionary stages and associated edifices of the volcanic complex, to discuss the processes of magma genesis and magmatic differentiation at Merapi, and the geochemical variations through time.

6.2 Geological Evolution of Merapi

6.2.1 Previous Research and the Development of Ideas

6.2.1.1 Early Work

Merapi is a volcanic complex consisting of an active stratocone which has grown on top of the remains of an older volcanic edifice, a structure mentioned by Kemmerling (1921) and Hartmann (1935), and elaborated upon by van Bemmelen (1949, 1956) (Fig. 6.2). Based on an idea first articulated by Ijzerman (1891) and Scheltema (1912), van Hinloopen Labberton (1921) advocated that a devastating eruption of Merapi in AD 1006 turned the surrounding area into a wasteland, buried the great temples of Borobudur, Mendut and Prambanan, and destabilised the Mataram Kingdom, a prosperous Hindu State in Central Java, forcing its migration to East Java. Both Hartmann (1935) and van Bemmelen (1949, 1956) expanded upon the idea of a major eruption of Merapi in AD 1006 and its effects on

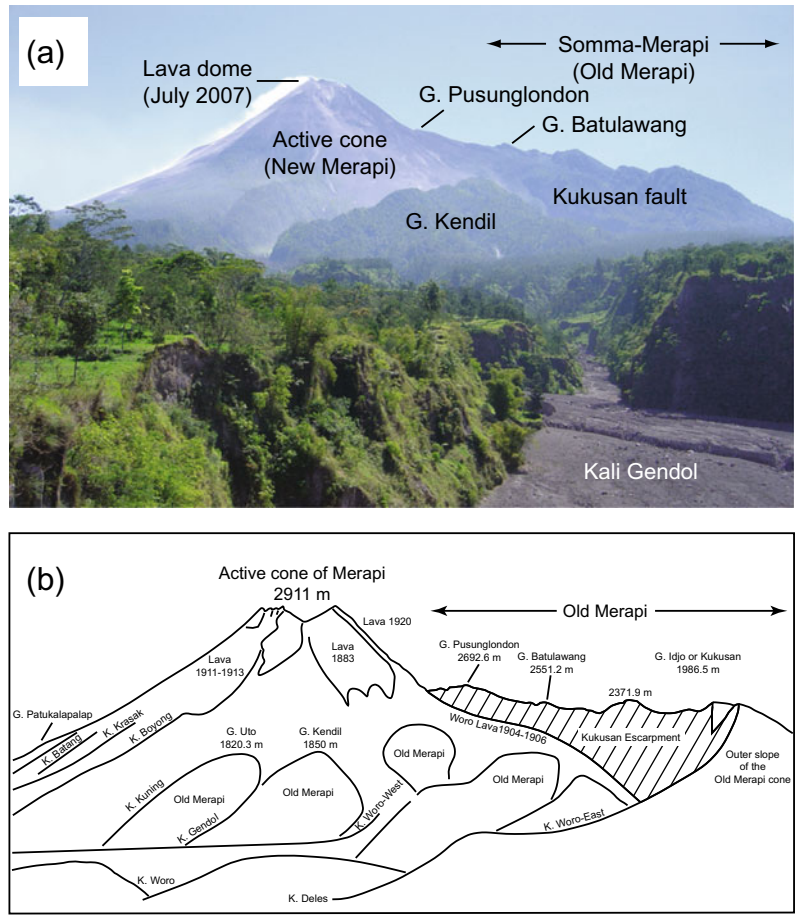

Fig. 6.2 **a** View of the Merapi volcanic complex from the south, with the active cone of Merapi (New Merapi) on the left in the picture and Somma-Merapi, the remnants of Old Merapi, on the right (eastern) side. The Gendol river valley (Kali Gendol), filled with block-and-ash flow deposits from the 2006 eruption, is in the foreground. **b** Redrawing of the original sketch of van Bemmelen made at Deles, illustrating the morphology and structure of Merapi (after van Bemmelen 1956)

the structure of the volcano. Hartmann (1935) speculated that that the oldest known crater (depression) of Merapi with a diameter of 3.5 km was a result of this eruption, while van Bemmelen (1949, 1956) suggested that the "cataclysmic outburst" led to the collapse of the western side of the old Merapi edifice along a major fault zone, known as the Kukusan fault, leaving a horseshoe-shaped crater or Somma rim on the northern and eastern flanks. In this context, Gunung (Indon. = hill or mountain) Gendol and nearby Gunung Sari, Gunung Ukir and several other hills located ~ 20 km west-southwest of Merapi, known collectively as the Gendol Hills, were interpreted as folded units of the older edifice, formed during the gravitational collapse of Merapi's western flank and the buttressing effect of the Menoreh Mountains further west (Fig. 6.3). The active Merapi cone started to grow soon after the assumed paroxysmal eruption in AD 1006 (Hartmann 1935; van Bemmelen 1949, 1956).

6.2.1.2 Research from 1980 to 2000

Since the early work of Kemmerling, Hartmann and van Bemmelen, more recent studies have built upon the idea of an Old and New Merapi, although the views are somewhat conflicting (Fig. 6.4). Hartmann's and van Bemmelen's catastrophic eruption in AD 1006 has been disputed by subsequent authors who have not found evidence for a catastrophic eruption of Merapi in AD 1006, even though this date has become deeply engraved in the literature. Consequently, the exact timing and process of what, in modern volcanology, is called a sector collapse or debris

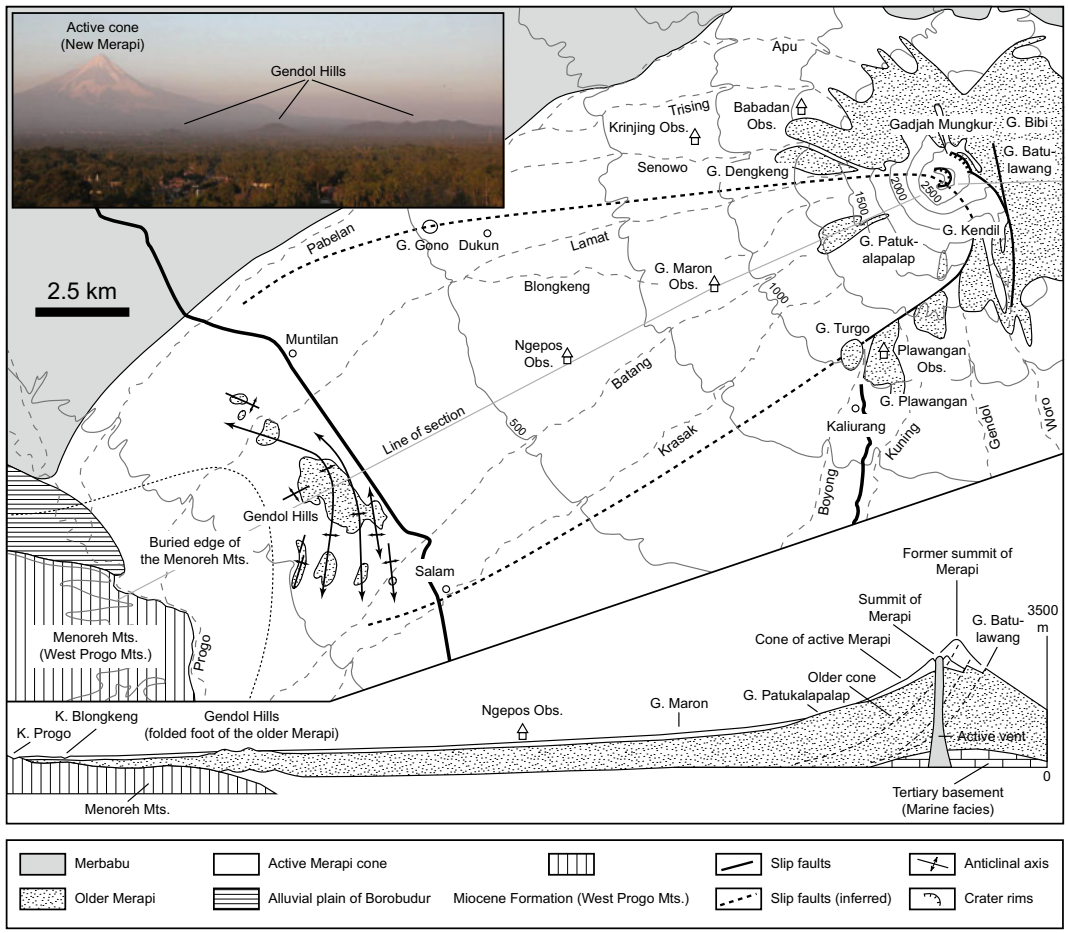

Fig. 6.3 Volcano-tectonic sketch map of Merapi and cross section through the western sector and foot of the volcanic edifice (after van Bemmelen 1949, 1956). The inset shows a field photograph of the Gendol Hills ~ 20 km west-southwest of Merapi, as seen from Candi (Indon. = temple) Borobudur. The active cone of Merapi can be seen in the background

avalanche failure of Old Merapi has remained controversial; an important new contribution by Bronto and co-workers is included in this volume (Bronto et al. 2023, Chap. 7). Additional details of the overall geological evolution of Merapi and its eruptive history, particularly over the past few millennia, have emerged from detailed field investigations. Considerable advances were made in the 1990s, when the volcano was designated a 'Decade Volcano' by the International Association of Volcanology and Chemistry of the Earth's Interior (IAVCEI) as part of the United Nations' International Decade for Natural Disaster Reduction.

The Ph.D. thesis of Bahar (1984) presented the geochemical compositions and stratigraphic relationships of the lava sequences of Merapi, distinguishing, based on the broad stratigraphic framework established by van Bemmelen (1949) and Wirakusumah et al. (1980), the ancient lavas of Gunung Plawangan that were followed by the units of Gunung Turgo and the parasitic cones of Gunung Bibi and Gunung Patuk Alap-alap, the younger lavas of the Batulawang Series, the recent and modern lavas of the Kali (Indon. = river) Kuning and Kali Selokopo Series (AD 1006–AD 1888), and those of the summit area (AD 1888–Present).

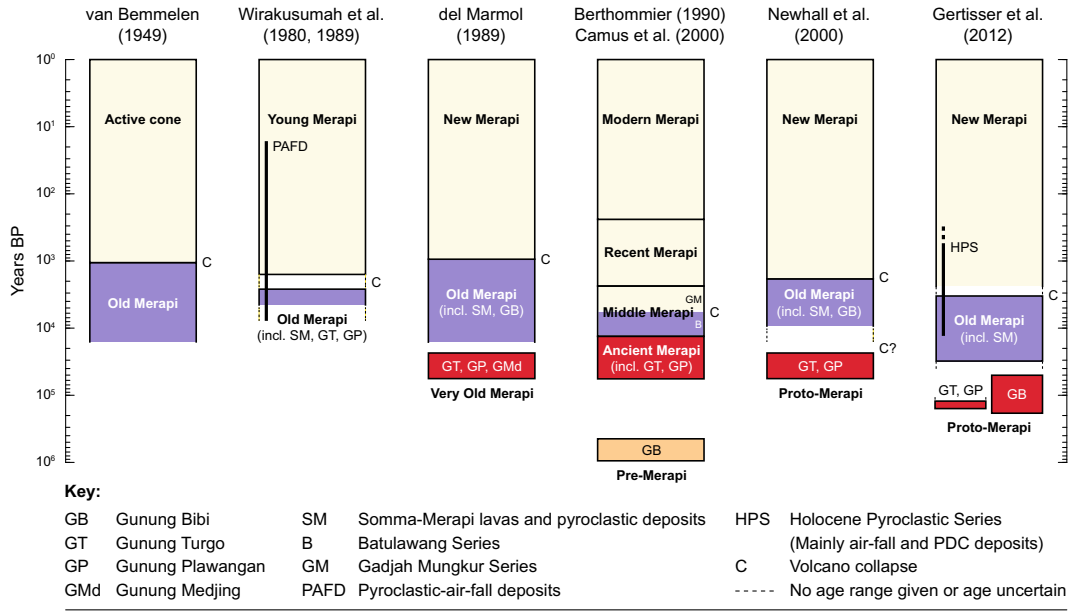

Fig. 6.4 Different interpretations of the stratigraphy and chronology of Merapi. Where available, the analytical uncertainty of the published dates was considered when compiling the figure. A logarithmic time scale was chosen for clarity of presentation

Djumarma et al. (1986) quoted newly available archaeological evidence suggesting that the Mataram Kingdom left Central Java several decades earlier (i.e. in AD 928 or 929) than proposed by van Bemmelen (1949, 1956) and earlier studies. However, the authors did not find archaeological indications for a catastrophic, Somma rim-forming eruption of Merapi in either AD 928-929 or AD 1006, and argued that "the eruption of 1006 A.D. is a classic example of a reasonable speculation that has been transformed into a fact by uncritical repetition". Instead, the authors suggested that the climactic eruption of the pre-Somma or Old Merapi according to van Bemmelen (1949, 1956) might have occurred up to three centuries before AD 1006, although no direct evidence was found for a westward directed landslide from Merapi and for a link between this eruption and the depopulation of the Mataram Kingdom of Central Java.

A key development in the history of geological research on Merapi was the publication of a 1:50,000 geological map of the volcano and preliminary radiocarbon dates by Wirakusumah et al. (1989). Based on the earlier work of Wirakusumah et al. (1980), the geological map—a simplified version of which is shown in Fig. 6.5—identifies an Old Merapi and a Young Merapi edifice, as recognised by Kemmerling (1921), Hartmann (1935) and van Bemmelen (1949, 1956). Within Old Merapi, the authors distinguish the older lavas of Gunung Turgo, Gunung Plawangan and Gunung Bibi (their Ml 1 lavas) from those that constitute the Somma-Merapi in the northern and eastern parts of the volcanic complex (their Ml 2 lavas). Prehistoric lavas and those that erupted since AD 1888 (their Ml 3 and Ml 4 lavas, respectively) comprise Young Merapi. Based on the few available radiocarbon dates at the time, pyroclastic and lahar deposits on the slopes of Merapi dated back to ~ 4350 ^{14}C y BP. These deposits were produced by eruptions from both Old Merapi and Young Merapi, the transition of which was inferred to have occurred between ~ 2870 and 1700 ^{14}C y BP. The pronounced NE-SW curved escarpment at Merapi, shown as a tectonic (normal) fault on the geological map of Yogyakarta (Rahardjo et al.

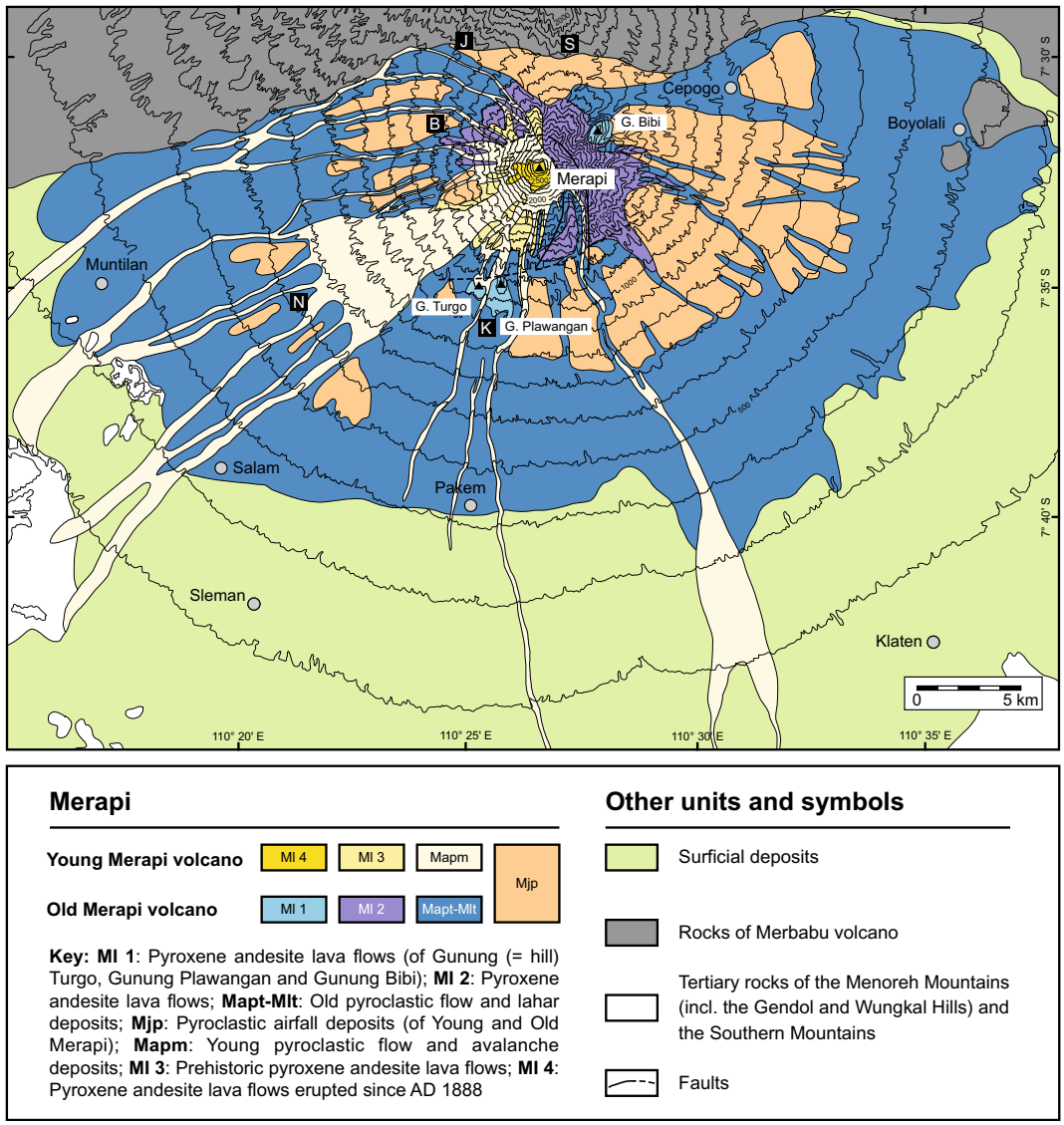

Fig. 6.5 Simplified version of the 1:50,000 geological map of Merapi published in 1989 (Wirakusumah et al. 1989), using the original terminology for the two major volcanic edifices distinguished and for the volcanic products of the different geological units. Some of the original subdivisions were combined for clarity of presentation. Contours are shown in 100 m intervals. Other map symbols as in Fig. 6.1 (after Gertisser et al. 2012a)

1977), is marked as the Kukusan fault on the map of Wirakusumah et al. (1989).

Also in 1989, the Ph.D. thesis of del Marmol provided further detailed insights into the geology and petrology of Merapi, in particular its lavas. Like previous authors, del Marmol (1989) used the terms Old Merapi and New Merapi to refer to the Somma-Merapi edifice and the active or young Merapi cone, respectively (Fig. 6.4). The author considered the rocks that were deposited before the inferred catastrophic sector collapse of the Somma-Merapi edifice, assumed to have occurred in AD 928, as part of Old Merapi with an ancestral part, referred to as Very

Old Merapi, and those that erupted afterwards as part of New Merapi. Very Old Merapi, according to del Marmol (1989), consists of Gunung Turgo and Gunung Plawangan, two steep-sided hills on Merapi's southern flank rising above the villages of Turgo and Kaliurang, as well as the lower part of Gunung Medjing (Figs. 6.1 and 6.4). Composite stratigraphic sections of the Somma-Merapi edifice, constructed by C. Newhall and co-authors and included in del Marmol (1989), were the first detailed descriptions of the explosive eruptive activity of Old Merapi, with representative sections in the Candi (Indon. = temple) Duwur and Candi Lumbung area as well as at Gunung Turgo-Kali Tritis. The lavas and pyroclastic deposits of the Batulawang Formation, as described by Bahar (1984), make up the main part of Old Merapi (del Marmol 1989). These were followed, in different sectors of the volcano, by the Selokopo, Gunung Gadjah Munkur, Gunung Pusonglondon and Djengger Series, which were also thought to be from Old Merapi. According to del Marmol (1989), Gunung Bibi, a distinct hill situated on the northeast flank of Merapi, belongs to the Old Merapi stage or Somma-Merapi edifice, although an older age was not ruled out. Following the catastrophic eruption, New Merapi developed, consisting of the Kali Kuning Formation, the most recent eruptive products in the southwestern sector, and the lava dome complex (<AD 1883) of the summit area.

The Ph.D. thesis of Berthommier (1990), much of which formed the basis for a paper by Camus et al. (2000), presented a geological history of Merapi, supported by a few radiocarbon and U-Th disequilibrium ages, as well as a single $^{40}K/^{40}Ar$ age, and complemented by whole-rock and mineral chemical data. The thesis, as well as Camus et al. (2000), divided Merapi into four evolutionary stages (Ancient, Middle, Recent and Modern Merapi) and an older (pre-Merapi) volcanic structure (Fig. 6.4). Based on a $^{40}K/^{40}Ar$ date of 670 ± 250 ka, Gunung Bibi was attributed to remnants of a pre-Merapi structure. Ancient Merapi (40–14 ka) comprises Gunung Turgo and Gunung Plawangan, interpreted as parasitic structures, as well as the oldest deposits of the Merapi cone sensu stricto (Fig. 6.6). Thus, Ancient Merapi corresponds to the Very Old Merapi or Proto-Merapi as well as part of the Old Merapi cone in the sense of van Bemmelen (1949, 1956) and del Marmol (1989). Middle Merapi (14.0–2.2 ka) consists of two thick andesitic lava sequences, namely the Batulawang Series, dated at ~ 6.7 ka using U-Th disequilibria, and the Gadjah Mungkur Series, which comprises the lava sequences of Gunung Pusunglondon, Gunung Gadjah Mungkur and Gunung Selokopo near the present-day summit of Merapi. Berthommier (1990) and Camus et al. (2000) postulated that during the time of Middle Merapi, a Mount St. Helens-type edifice collapse occurred between ~ 6.7 ka and 2200 ± 160 ^{14}C y BP, the oldest age obtained for pyroclastic deposits attributed to Recent Merapi (Fig. 6.6). They outlined an avalanche caldera open to the west and slightly wider than proposed by van Bemmelen (1949, 1956), with a northern limit that follows roughly the Senowo river valley and the Kukusan fault as the southern extension (cf. Figs. 6.1 and 6.3). Moreover, they interpreted the Gendol Hills as hummocks of a debris-avalanche deposit resulting from the inferred sector collapse, protruding from younger volcaniclastic deposits. A conspicuous, widespread and topography-controlled pyroclastic unit, consisting of a basal layer with moulds of bamboo, a middle layer with normal grading and tractional features and an upper layer of coarse grained, partly cross-bedded ash, was interpreted as a violent PDC or blast deposit emplaced at low temperature. Recent Merapi (2220 ± 160 ^{14}C years BP to AD 1786) and Modern Merapi (since AD 1786) overlie the lava sequences of Middle Merapi and are the main units that constitute the active Merapi cone or New Merapi (Fig. 6.6). Recent Merapi consists of lava flows and PDC deposits often produced by explosive eruptions and fountain collapse. Twice in the evolution of Recent Merapi, extended episodes of violent magmatic to phreatomagmatic eruptions occurred. These produced the widespread sub-Plinian and phreatoplinian deposits of the Gumuk ashes (2220 ± 160 to 1470 ± 140 ^{14}C y BP) that cover the entire edifice, as well as the overlying

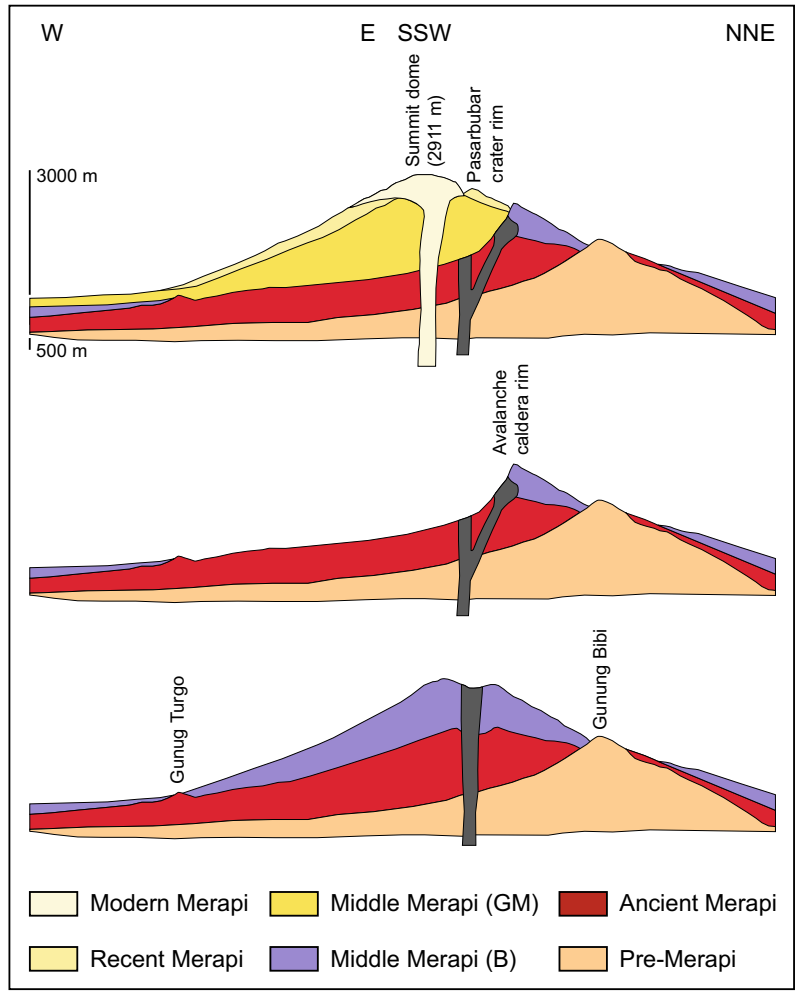

Fig. 6.6 The geological evolution of Merapi after Camus et al. (2000). GM = Gadjah Mungkur Series; B = Batulawang Series

Sambisari ashes on Merapi's southern slope that were emplaced by dilute PDCs and covered Candi Sambisari at the beginning of the fifteenth century (Berthommier 1990; Camus et al. 2000). Modern Merapi has been characterised by lava dome growth within the Pasarbubar crater since AD 1786 and mostly gravitational dome failures that produced small-volume PDCs.

Newhall et al. (2000) provided a comprehensive stratigraphy and many radiocarbon dates of pyroclastic deposits extending the explosive activity of Merapi back to ~ 10,000 years ago. The paper questioned conclusions of Berthommier (1990) and Camus et al. (2000) regarding the edifice failure of Old Merapi and the stratigraphic position of Gunung Bibi. Due to its weathered nature, Gunung Bibi was interpreted by the authors as a vent which built up on the flank of Old Merapi. For the latter, a date of 9630 ± 60 ^{14}C y BP, obtained for a PDC deposit on Merapi's east-northeast flank, marked the oldest age for an explosive eruption of Old Merapi (Fig. 6.4). Old Merapi was inferred to have collapsed one or more times, with hints for an early collapse event from impoundment of Kali Progo to form an early Lake Borobudur at 3430 ± 50 ^{14}C y BP. The latest sector collapse of Old Merapi was postulated to have occurred at ~ 1900 ^{14}C y BP based on their youngest PDC deposit found on the eastern side of the

volcano, if the Somma rim stopped all later PDCs from travelling in an easterly direction. In contrast to Berthommier (1990) and Camus et al. (2000), Newhall et al. (2000) argued that the Gendol Hills are Upper Pliocene in age and hence significantly older than Merapi. Furthermore, the authors found no other evidence of a large-scale debris avalanche deposit and suggested that it has probably been buried by younger deposits. New Merapi began to grow soon after ~ 1900 ^{14}C y BP (Fig. 6.4). Relatively large eruptions from New Merapi were significant enough to affect, destroy or bury many of the larger and smaller temples in the surrounding area, possibly contributing to the eastward migration of the Mataram Kingdom in AD 928 or 929. A smaller partial edifice collapse of New Merapi may have occurred after 1130 ± 50 ^{14}C y BP. Newhall et al. (2000) also coined the term Proto-Merapi (Fig. 6.4), which corresponds to the Very Old Merapi stage of del Marmol (1989) but without Gunung Medjing. The authors concluded that Gunung Plawangan and Gunung Turgo are erosional remnants of the earliest Proto-Merapi cone that precedes van Bemmelen's Old Merapi.

Largely based on the Ph.D. thesis of Andreastuti (1999), Andreastuti et al. (2000) established a detailed tephrostratigraphic framework at Merapi from 3000 to 250 years ago. Recognising important stratigraphic marker horizons around the volcano, some of which were dated by the radiocarbon method, Andreastuti (1999) and Andreastuti et al. (2000) identified a number of tephra units associated with moderate to large eruptions, which include, from old to young, the Sumber, Kadisepi, Bakalan, Jarak, Kujon, Tosari, Ngrangkah, Nglencoh, Tegalsruni, Temusari, Plalangan, Jrakah, Selo, interregional marker (Muntilan), Deles, Selokopo, Kepuhharjo and Pasarbubar tephra (Fig. 6.7). The most recognisable tephra units were included in the stratigraphic sections of Newhall et al. (2000) to link both stratigraphies. The Muntilan tephra has subsequently been correlated with the AD 1257 Samalas eruption on Lombok (Vidal et al. 2015).

6.2.1.3 Research in the Twenty-First Century

The Ph.D. thesis of Gertisser (2001) identified further stratigraphic marker horizons of moderate to large eruptions (Paten I, Paten II, Trayem, Jurangjero I, Jurangjero II tephras) that allowed tephra correlations from the south-eastern to the north-western sector of Merapi. A large number of radiocarbon dates extended the pyroclastic stratigraphy of Merapi back to 11,792 ± 90 ^{14}C y BP and challenged earlier views of a sector collapse of Old Merapi as young as 1900 ^{14}C y BP. Arguments against the latter included the recognition of a young dome-collapse PDC deposit on the eastern slopes of Merapi which suggested that the blockage of PDCs to the east—possibly caused by a westward directed sector collapse—became effective not until 1590 ± 40 ^{14}C y BP, or that by that time, the recent Merapi cone had already grown high enough for such currents to overflow the Somma rim. Some of the oldest dated deposits in the deeply incised valleys on the south-western flank hinted at the possibility of an early sector collapse more than 8380 ± 230 ^{14}C y BP. However, considering the results presented here, these deposits likely represent scattered outcrops of pre-sector collapse (Old Merapi) volcaniclastic units. The radiocarbon dates of Gertisser (2001) were published subsequently in a paper by Gertisser and Keller (2003a), which focused on the explosive activity of Merapi during the past 2000 years and the associated temporal evolution of the magma system.

Research carried out in more distal areas from Merapi in the Borobudur basin provided important new information about the geological history of Merapi. Murwanto (2004) showed that the long sequence of lacustrine deposits, interpreted to have formed by impoundment of Kali Progo to repeatedly establish an ancient Lake Borobudur, spanned at least 20,000 years from 22,040 ± 390 ^{14}C y BP. The timespan was subsequently extended with a maximum age of 31,430 ± 2070 ^{14}C y BP (Murwanto 2014), hinting indirectly at the occurrence of multiple debris avalanches or debris flows from Merapi which might have caused blockage of the Progo river (e.g. Newhall

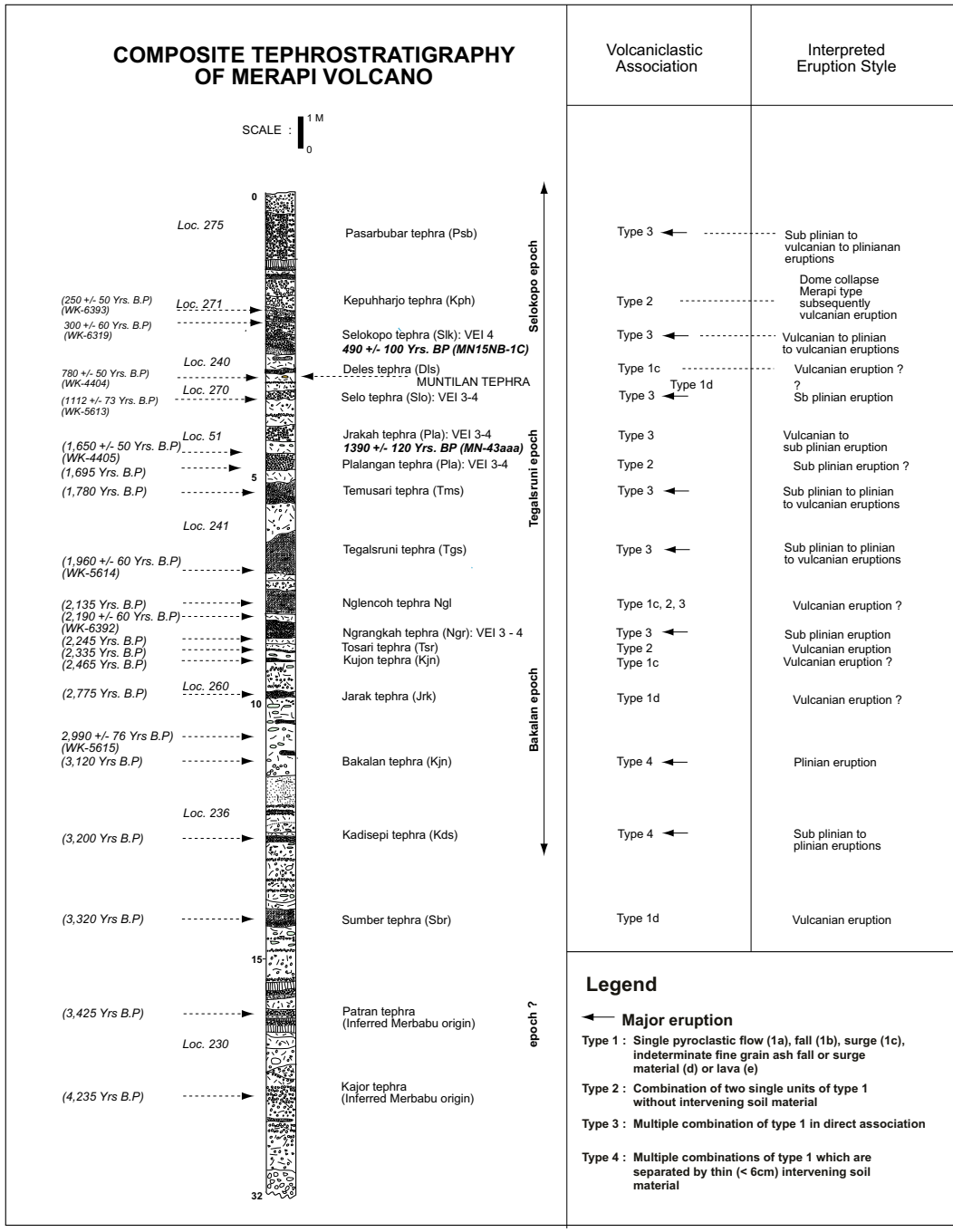

Fig. 6.7 Composite Late Holocene stratigraphy of Merapi volcano (after Andreastuti 1999; Andreastuti et al. 2000). Arrows point to the exact stratigraphic position where ^{14}C dates were obtained. Estimated dates, assuming a constant rate of soil formation, are shown in italic letters in brackets. Correlated ^{14}C dates from Newhall et al. (2000) are shown in bold italic letters. Key locations, the stratigraphic range of geochemically defined cycles, typical volcaniclastic associations and interpretation of eruptive styles are also shown (Andreastuti 1999)

et al. 2000). Gomez et al. (2010) analysed material from two drill cores near Candi Borobudur and related these to possible sector collapse events at ~ 115 ka or 119 ka, and at 31,040 ± 320 ^{14}C y BP. The source of the older event remained elusive at the time, while the younger event was linked to a collapse of Ancient Merapi (Berthommier 1990; Camus et al. 2000) or Proto-Merapi (Newhall et al. 2000).

To reassess the geological evolution of Merapi, Gertisser et al. (2012a) published stratigraphic field data, new radiocarbon ages and amongst the first ^{40}K/^{40}Ar and ^{40}Ar/^{39}Ar ages of the volcanic complex (Fig. 6.8). The latter suggested that construction of the Merapi volcanic complex began < 170 ka ago. According to the authors, two earliest (Proto-Merapi) volcanic edifices—Gunung Bibi (109 ± 60 ka), and Gunung Turgo and Gunung Plawangan (138 ± 3 ka; 135 ± 3 ka)—predate the main Merapi edifice. The construction of Old Merapi, a stratovolcano of basaltic andesite lavas and volcaniclastic rocks, began more than ~ 30 ka ago. The edifice was destroyed by one or, possibly, several sector collapses, the latest of which occurred some time after 4.8 ± 1.5 ka. The recent Merapi cone (New Merapi) started to grow afterwards and appears to have been almost continuously active, with periods of high eruption frequency interrupted by shorter intervals of apparently lower eruption frequency. The mostly basaltic andesite pyroclastic and epiclastic deposits of New Merapi cover the flanks of the entire volcanic complex, where they overlie similar deposits from eruptions of Old Merapi.

More recently, Bronto et al. (2014) discovered a large debris avalanche deposit in the Godean area in the Sleman Regency, approximately 30–35 km southwest of Merapi. The authors linked this deposit to a gigantic landslide of Merapi, although the age of the deposit and the associated sector collapse remained unconstrained. The authors estimated that the Godean debris

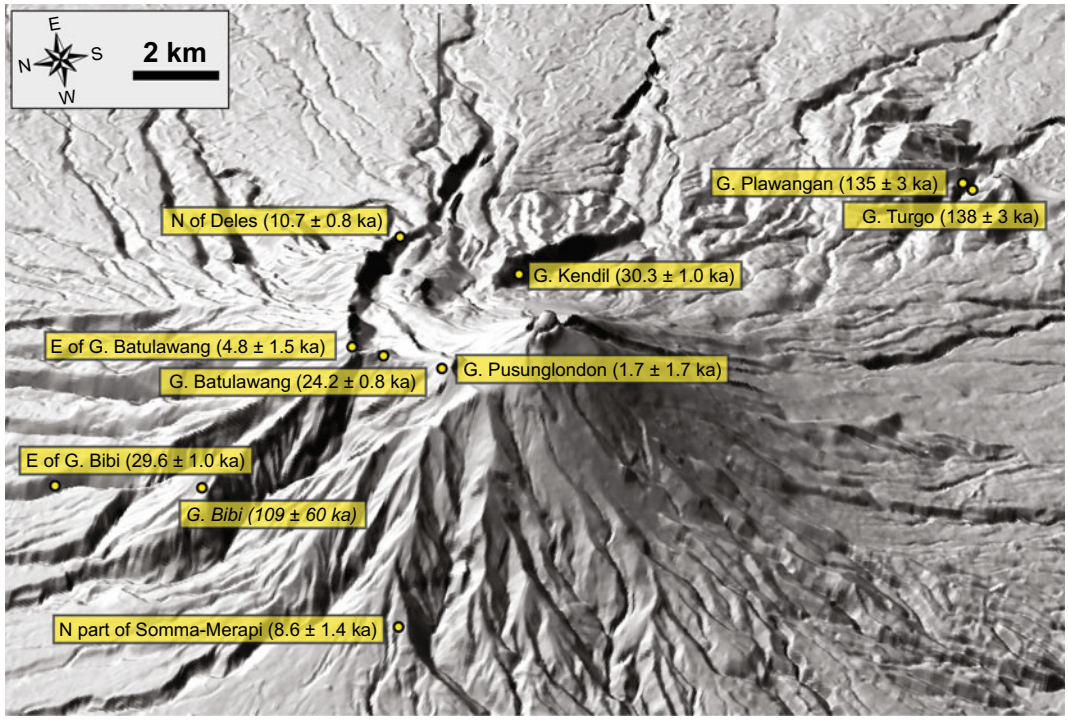

Fig. 6.8 Digital elevation model of Merapi showing the locations of lava samples dated using the ^{40}K/^{40}Ar and ^{40}Ar/^{39}Ar (shown in italic letters) techniques (Gertisser et al. 2012a). Digital elevation model courtesy of Carl Gerstenecker (TU Darmstadt, Germany)

avalanche, as it is called in Bronto et al. (2023, Chap. 7), has a volume of ~ 4.9–8.6 km^3 and covers an area of ~ 390 km^2. It is characterised by a hummocky topography, and jig-saw-fractured blocks of pyroclastic material, lava flows and reworked deposits. The deposit becomes lahar-like at greater distances of up to 50 km to the south of Merapi. This first recognition of a large-scale debris avalanche from Merapi (Bronto et al. 2014) represents a milestone in the study of the volcano that may help shed light on the long-standing issue of the occurrence of sector collapse(s) at Merapi, and the nature and timing of the destruction of Old Merapi (van Bemmelen 1949, 1956; del Marmol 1989; Berthommier 1990; Camus et al. 2000; Newhall et al. 2000; Gertisser et al. 2012a). These issues are discussed in Sect. 6.2.2.2 and in Bronto et al. (2023, Chap. 7).

Selles et al. (2015) reconstructed the geological and geomorphological evolution of Merapi based on a detailed characterisation of the lithofacies, and the temporal and spatial evolution of the volcaniclastic deposits on the eastern slopes of the volcanic complex. The authors recognised a small debris avalanche and debris flow fan, tentatively linked to the Mount St. Helens-type edifice collapse of Berthommier (1990) and Camus et al. (2000) at the end of the Middle Merapi stage. The deposit is characterised by a volume of 2.2–3.1 km^3 and covers an area of ~ 45 km^2 between 1000 and 400 m asl.

6.2.2 A Synthesis of the Geological History and Chronology of Merapi: Current Thinking

The synthesis of the geological history and chronology of Merapi presented here is centred on an updated version of the reinterpreted geological map of Wirakusumah et al. (1989), as presented in Gertisser et al. (2012a). A new version of this map, shown in Fig. 6.9 illustrates our current understanding of the geological evolution of Merapi, divided into eight main volcano-stratigraphic units, linked to three major evolutionary stages or temporal volcanic edifices that have existed throughout the lifespan of the volcanic complex: Proto-Merapi, Old Merapi and New Merapi. Unit 1 (Lava flows of Gunung Bibi) and Unit 2 (Lava flows of Gunung Turgo, Gunung Plawangan and Gunung Medjing) are grouped together as part of Proto-Merapi. Old Merapi comprises Unit 3 (Lava flows of the Somma-Merapi) and the older deposits of Units 4/5 (Holocene Pyroclastic Series). The younger deposits of Units 4/5 (Holocene Pyroclastic Series), Unit 6 (Young (post-Somma-Merapi) lava flows) and Units 7/8 (Recent and historical pyroclastic density current and lahar deposits; Lava domes of the recent episode) constitute the recent Merapi cone or New Merapi. The eight main volcano-stratigraphic units are described in more detail in Sect. 6.2.2.1; structural modifications and edifice collapse in the history of Merapi are covered in Sect. 6.2.2.2.

6.2.2.1 Volcano-Stratigraphic Units

The eight main volcano-stratigraphic units of Merapi described in this section partly overlap in time and are linked to the geological map presented in Fig. 6.9.

Lava flows of Gunung Bibi (Unit 1) Gunung Bibi is a morphologically distinct, heavily forested cone- or dome-shaped hill 3.5 km to the northeast of the summit of Merapi (Fig. 6.10a). It consists of highly weathered lava flows and breccias that resemble the surrounding lavas of the Somma-Merapi (Old Merapi) edifice. A scoria fall and associated PDC deposit found nearby may have originated from Gunung Bibi (Newhall et al. 2000). Exposures at Gunung Bibi are rare and the hill remains a poorly known part of the Merapi volcanic complex. Based on the only published $^{40}Ar/^{39}Ar$ date of 109 ± 60 ka on amphiboles (Gertisser et al. 2012a), Gunung Bibi is regarded as one of the oldest parts of Merapi. Despite the large uncertainty, which somewhat limits the value of this date, it is regarded more reliable than the earlier published $^{40}K/^{40}Ar$ whole-rock age of 670 ± 250 ka (Berthommier 1990; Camus et al. 2000) due to the common problem of inherited argon in whole-rock dating. It suggests that Gunung Bibi is < 170 ka old

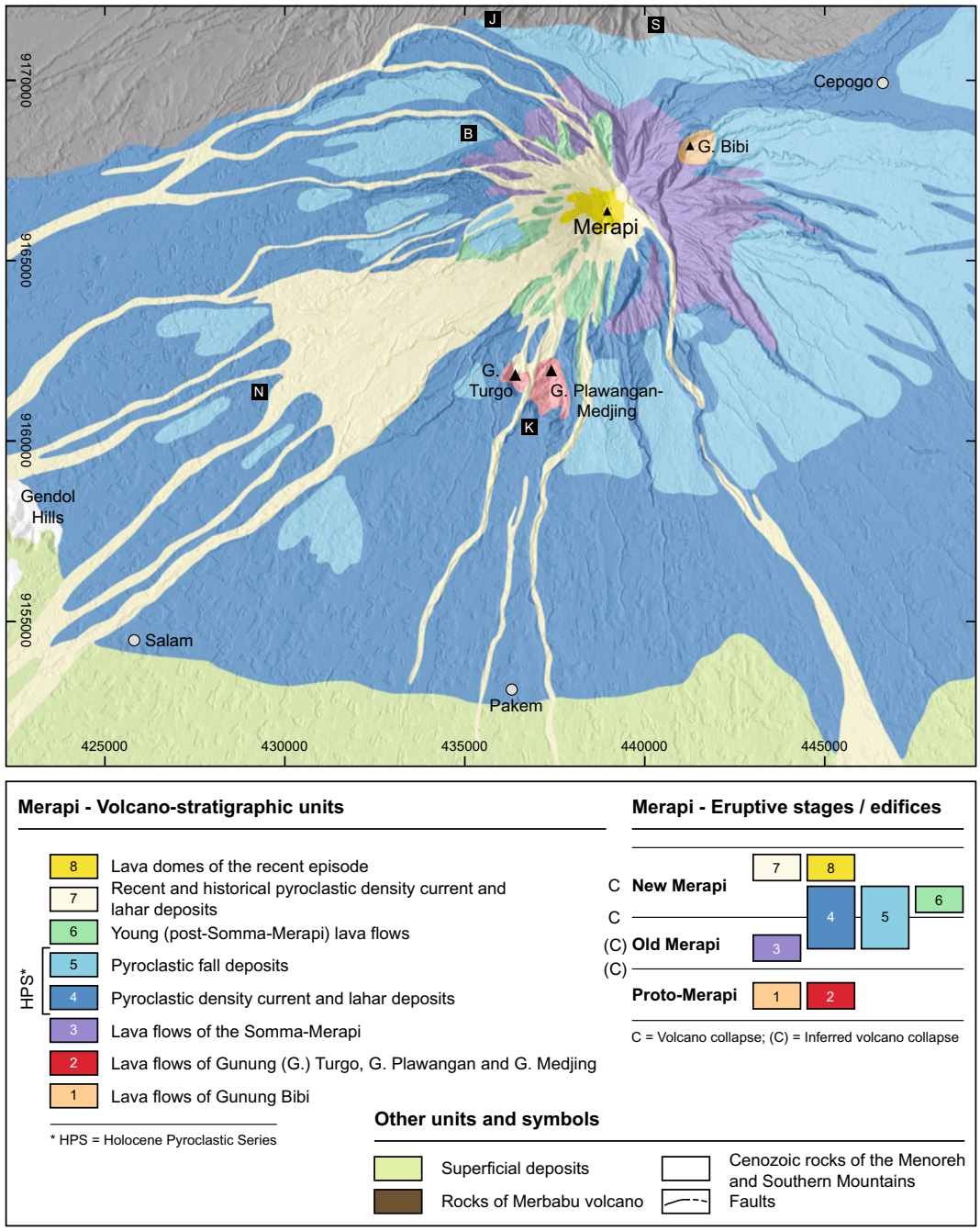

Fig. 6.9 Reinterpreted version of the geological map of Merapi (Wirakusumah et al. 1989), distinguishing eight main volcano-stratigraphic units linked to three main evolutionary stages or volcanic edifices—Proto-Merapi, Old Merapi and New Merapi. Yogyakarta is located to the south of the map area. Map coordinates are in UTM metres, displayed map symbols as in Fig. 6.1 (adapted and updated from Gertisser et al. 2012a)

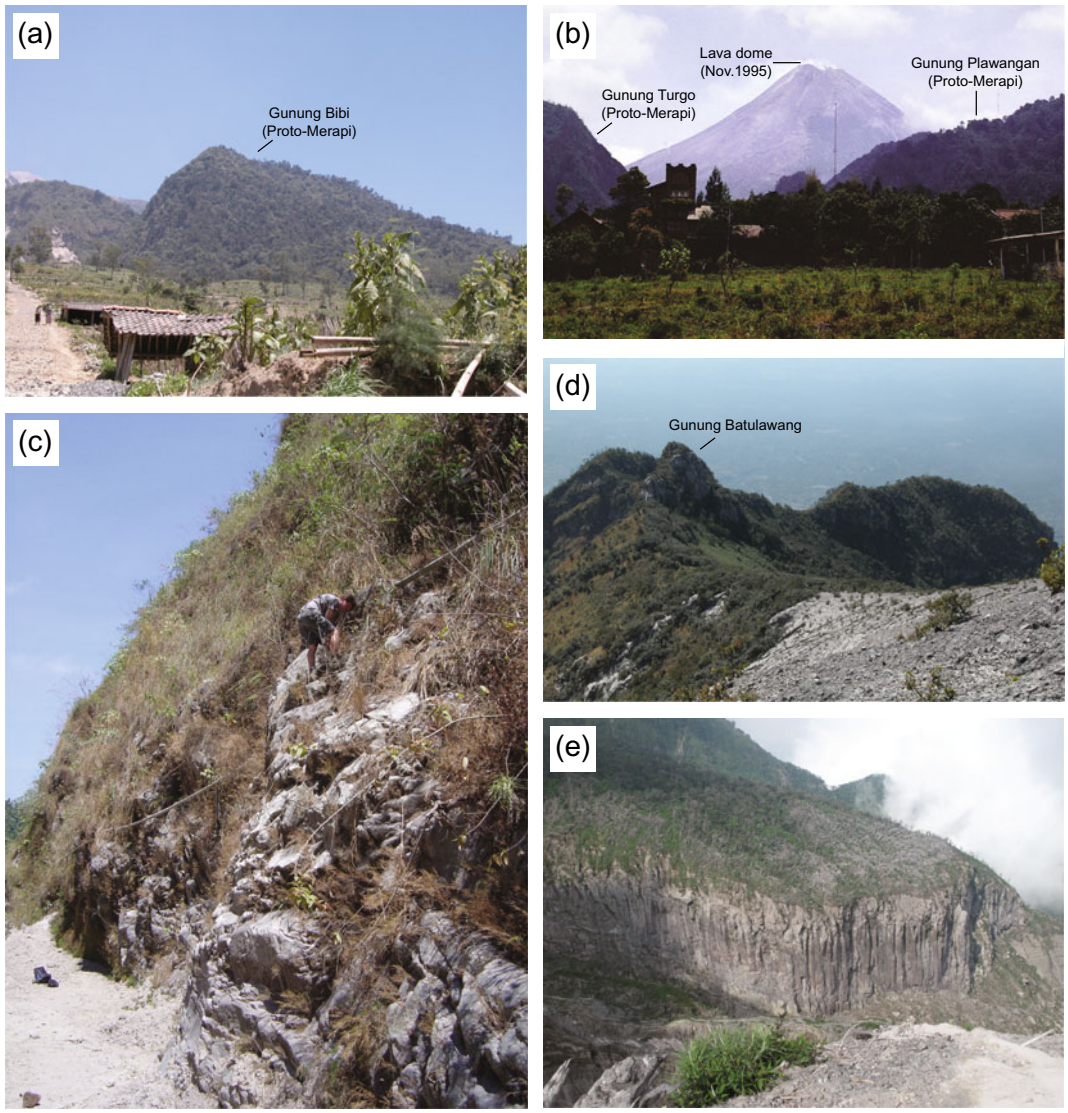

Fig. 6.10 Field photographs. **a** View of Gunung Bibi from the east. **b** Gunung Turgo and Gunung Plawangan, the erosional remnants of a Proto-Merapi edifice, as seen from the village of Kaliurang on Merapi's south slope. The active Merapi cone (New Merapi) is in the background. **c** The basaltic lava sequence exposed at the foot of Gunung Turgo in the Boyong river valley (Kali Boyong). **d** View from Gunung Pusunglondon across to Gunung Batulawang and the Somma-Merapi (Old Merapi). **e** Thick, columnar jointed basaltic andesite lava flow of the Somma-Merapi (Old Merapi) in the upper Kali Woro

and, therefore, substantially younger than the only other available numerical date implies. The date of 109 ± 60 ka (i.e. > ~ 50 ka) further indicates that Gunung Bibi predates the lava sequences of the Somma-Merapi (Old Merapi) edifice (see below), in contrast to earlier views that it may represent a volcanic plug (del Marmol 1989) or a vent that erupted through and built itself on the upper flank of the Somma-Merapi (Old Merapi) edifice (Newhall et al. 2000). Given the overlapping age range with Gunung Turgo and Gunung Plawangan as well as, by

inference, Gunung Medjing (see below), Gunung Bibi is regarded as an older, Proto-Merapi edifice (Gertisser et al. 2012a).

Lava flows of Gunung Turgo, Gunung Plawangan and Gunung Medjing (Unit 2) Based on two new $^{40}K/^{40}Ar$ groundmass ages of 138 ± 3 ka and 135 ± 3 ka (Gertisser et al. 2012a) for lava flows from the basal successions of Gunung Turgo and Gunung Plawangan exposed in the Boyong valley (Fig. 6.10b, c), the two hills are now considered significantly older than inferred by previous authors based on debatable U-Th ages (Berthommier 1990; Camus et al. 2000). Both hills are ascribed to Proto-Merapi in the sense of Newhall et al. (2000) to which, in this contribution, the lavas of a nearby hill, Gunung Medjing, are added (del Marmol 1989). In agreement with del Marmol (1989) and Newhall et al. (2000), these hills are interpreted as ruins of an ancient volcano rather than flank vents of Old Merapi (van Bemmelen 1949). The northward dip of the lava sequences towards the recent Merapi cone suggests that the hills may be slightly tilted mega- or Toreva-blocks, possibly related to sector collapse (Berthommier 1990; Camus et al. 2000; Newhall et al. 2000).

Lava flows of the Somma-Merapi (Unit 3) The thick succession of massive lava flows of the Somma-Merapi, exposed in the deeply incised valleys on the south-eastern, eastern and northern flanks of Merapi, and cut by the Kukusan fault, are part of Old Merapi (Fig. 6.10d, e). This succession constitutes the Batulawang Series of Berthommier (1990) and Camus et al. (2000). The beginning of Old Merapi was dated by Gertisser et al. (2012a) to > 30.3 ± 1.0 ka ($^{40}K/^{40}Ar$), based on the oldest date obtained for a lava flow at the base of Gunung Kendil (Fig. 6.8). The youngest date for a Somma-Merapi lava flow near the summit of Gunung Batulawang is 4.8 ± 1.5 ka ($^{40}K/^{40}Ar$) (Fig. 6.8; Gertisser et al. 2012a). The growth of the Somma-Merapi edifice therefore ended less than 4.8 ± 1.5 ka, a date that provides a maximum age limit of New Merapi. In total, the age range of the Somma-Merapi lava flow succession is presently constrained by six lava groundmass $^{40}K/^{40}Ar$ ages (Fig. 6.8; Gertisser et al. 2012a).

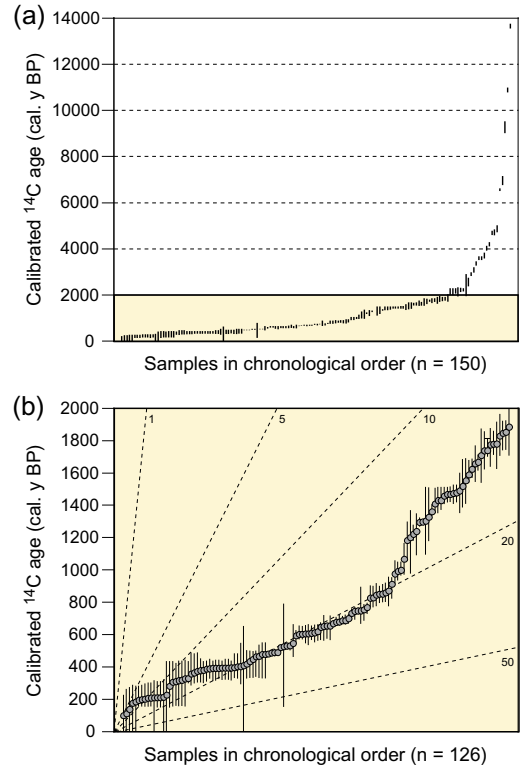

Fig. 6.11 The radiocarbon record of Merapi volcano (after Gertisser et al. 2012a). **a** Published radiocarbon dates plotted in chronological order (total number of analyses n = 150). All dates are shown as their maximum 1σ range in calibrated years BP (i.e., before 1950). **b** A close-up of figure (**a**) showing the subset of samples with calibrated ages < 2000 y BP (total number of analyses n = 126). Illustrated are the median probability and the maximum calibrated 1σ age range. The dashed lines indicate the gradients expected from the number of samples (as indicated) per 100 years. *Data sources* Andreastuti et al. (2000), Camus et al. (2000), Newhall et al. (2000), Gertisser and Keller (2003a) and Gertisser et al. (2012a)

Holocene Pyroclastic Series (Units 4 and 5) The pyroclastic and epiclastic deposits that cover the flanks of Merapi, constrained by ~ 150 radiocarbon ages to < 11,792 ± 90 ^{14}C y BP (Fig. 6.11), belong to both Old Merapi and New Merapi. This means they either pre- or post-date the latest of several sector collapses of Old Merapi that left the prominent horseshoe-shaped avalanche caldera or Somma rim open to the west, marking the end of the Old Merapi stage (del Marmol 1989; Berthommier 1990; Camus

et al. 2000; Newhall et al. 2000; Gertisser et al. 2012a). These deposits, collectively termed the Holocene Pyroclastic Series (Gertisser 2001; Gertisser and Keller 2003a, b; Gertisser et al. 2012a), comprise all prehistoric volcaniclastic deposits, including the Gumuk and Sambisari ashes of Berthommier (1990) and Camus et al. (2000), the volcaniclastic successions described in del Marmol (1989), Andreastuti (1999), Andreastuti et al. (2000), Newhall et al. (2000), and the deposits on Merapi's eastern flank described by Selles et al. (2015). On interfluve areas, the Holocene Pyroclastic Series comprises relatively thin PDC and reworked deposits, interbedded with numerous ash and lapilli fall layers and soil horizons. Prominent scoriaceous or pumiceous fall deposits, in many cases closely associated with PDC deposits, record large (VEI 3 and 4) sub-Plinian-type eruptions of Merapi during mid to late Holocene times (Andreastuti 1999; Andreastuti et al. 2000; Newhall et al. 2000; Gertisser 2001; Gertisser et al. 2012a). The sides of the valleys cut into the pyroclastic and epiclastic apron are dominated by thick sequences of intercalated valley-ponded PDC deposits, fluvial and laharic debris, and subordinate fall deposits and soils (Fig. 6.12a–c). Pyroclastic density current deposits include those of block-and-ash flows emplaced via dome collapse and other types that have been grouped according to dominant juvenile component lithology in the larger (lapilli to block size) clast range, including moderately vesicular breadcrust or cauliform-textured bombs, and moderately to highly vesicular, light grey pumiceous clasts (Fig. 6.13). These latter types were related to fountain to eruption column collapse from Vulcanian- to sub-Plinian-type eruptions (Gertisser et al. 2012a). The base of the Holocene Pyroclastic Series is defined by a palaeosol in the northern sector of Merapi which underlies a succession of pyroclastic deposits from, presumably, both Merapi and Merbabu, the volcano immediately north of Merapi (Gertisser 2001; Gertisser and Keller 2003a; Gertisser et al. 2012a). The oldest direct date for an explosive eruption of Merapi currently remains at 9630 ± 60 ^{14}C y BP (Newhall et al. 2000). This suggests that most of the lavas forming the bulk of the Old Merapi edifice are older and draped by pyroclastic and epiclastic deposits from dome-forming or explosive eruptions. In many of the deep river valleys in the southern to north-western sector of Merapi (Fig. 6.9), the volcaniclastic successions exposed in the valley walls and on adjacent interfluve areas also comprise deposits belonging to the Holocene Pyroclastic Series. They date back to 2260 ± 30 ^{14}C y BP around Kali Batang and Jurangjero/Kali Putih and, in other places, back to 3868 ± 47 ^{14}C y BP (Kajangkoso-Kali Senowo) and 4153 ± 37 ^{14}C y BP (Candi Asu-Kali Trising). Comparatively old pyroclastic deposits up to 3453 ± 33 ^{14}C y BP and, as mentioned previously, 8380 ± 230 ^{14}C y BP are also exposed inside the valleys of the Bedok and Bebeng rivers, respectively (Gertisser 2001; Gertisser and Keller 2003a; Gertisser et al. 2012a). Despite such sporadic exposures of older volcaniclastic deposits, most of the presently available radiocarbon ages are within the last 2000 years (Fig. 6.11), indicating that the older eruption record is fragmented and that older deposits are comparatively rare due to burial by younger deposits. The radiocarbon record reveals that over the last 2000 years, the volcanic activity at Merapi has been persistent, with 126 ages documented, averaging one eruption every 15.9 years, under the assumption that each radiocarbon date represents a single eruption (Gertisser et al. 2012a). However, given the likely case that some eruptions be absent from the geological record, as may particularly be the case for phreatic and dome-building eruptions, or under-reported due to erosion, reworking or burial, the average eruption frequency would be higher and closer to that observed since the beginning of the nineteenth century.

Young (post-Somma-Merapi) lava flows (Unit 6) This unit constitutes the young lava flows that crop out near the summit of Merapi around the Pasarbubar crater (Gunung Selokopo Ngisor, Gunung Selokop Duwur, Gunung Gadjah Mungkur, Gunung Pusunglondon), high on the south-western and western flanks (Gunung Dengkeng, Gunung Patuk Alap-alap), and further downslope in the Kuning and Gendol river


(a)

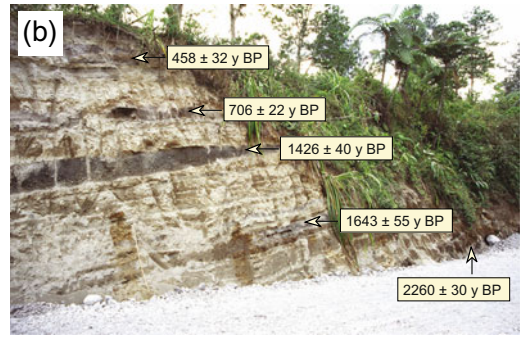
(b)
458 ± 32 y BP
706 ± 22 y BP
1426 ± 40 y BP
1643 ± 55 y BP
2260 ± 30 y BP

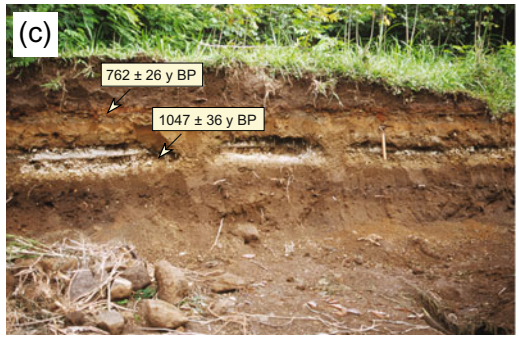
(c)
762 ± 26 y BP
1047 ± 36 y BP


(d)


(e)
G.Pusunglondon


(f)


(g)
> 250 ± 50 y BP
350 ± 40 y BP


(h)

◀ **Fig. 6.12** Field photographs. **a** Sequence of mainly thick pyroclastic density current (PDC) and epiclastic deposits exposed in the wall of the upper Kali Boyong north of Kaliurang. **b** Volcaniclastic succession at Jurangjero/Kali Putih on Merapi's southwest flank. The sequence, dated by the radiocarbon method, records more than 2000 years of intermittent explosive eruptions (Gertisser 2001; Gertisser et al. 2011). **c** Soil profile with intercalated widespread scoriaceous or pumiceous pyroclastic fall desposits near Krogowanan, approximately 11 km west-northwest of Merapi. The dated tephra layers correspond to the Trayem (older layer) and Jurangjero I (younger layer) tephras of Gertisser (2001) and Gertisser et al. (2012a). **d** Thick basaltic andesite lava flow forming the high point known as Gadjah Mungkur high on Merapi's north flank. **e** Gunung Pusunglondon, a young post-collapse cone near the summit of Merapi. **f** Basaltic andesite lava flows on the southeast side of Gunung Pusunglondon unconformably overlie the older lavas of the Somma-Merapi (Old Merapi). **g**. Massive young PDC deposits, separated by fluvially reworked deposits, on Merapi's south flank in a quarry west of Kali Opak near the Merapi golf course. Both PDC deposits are widespread on Merapi's south flank. The lower PDC deposits may be from a historical or prehistoric eruption. The radiocarbon dates are from Gertisser et al. (2012b). **h** Deeply incised, valley-confined 1954 PDC deposits in Kali Apu

valleys (Fig. 6.12d–f). Preliminary satellite image analysis also suggests the presence of prehistoric lava domes, such as on Merapi's upper NNW slope, which may be grouped into this unit (S. Bronto Personal Communication 2020). Based on the youngest age of the older Somma-Merapi lava flow succession, the lava sequences of this unit are considered younger than 4.8 ± 1.5 ka (Fig. 6.8). They constitute the Gadjah Mungkur series of Berthommier (1990) and Camus et al. (2000), a sequence of lavas unaffected by, and therefore younger than the Kukusan fault, which we, in accordance with Berthommier (1990) and Camus et al. (2000), interpret as a structure related to sector collapse. As such, these lava sequences are part of New Merapi. A poorly constrained $^{40}K/^{40}Ar$ date of 1.7 ± 1.7 ka for a lava flow from Gunung Pusunglondon and another zero age for a flow from Gunung Gadjah Mungkur (Gertisser et al. 2012a) are suggestive of the young ages of these lavas compared to those of the Somma-Merapi (Old Merapi) east of the Kukusan fault, although many of these lavas are not yet dated.

Recent and historical pyroclastic density current and lahar deposits (Unit 7) and lava domes of the recent episode (Unit 8) Given the difficulty of identifying the products of historical eruptions in the field, due to similarity of field characteristics, poor preservation potential, extensive reworking of primary deposits or lack of radiometric ages, the boundary between the youngest deposits of the Holocene Pyroclastic Series and the deposits of historical to recent eruptions have remained difficult to determine in places (Fig. 6.12g). In general, the historical to recent volcaniclastic deposits consist of PDC and related deposits that are comparable to those of the Holocene Pyroclastic Series (units 4 and 5 above) and dominate the successions in the southern, western and north-western sectors up to 10 km (or occasionally more) from the summit (Figs. 6.12g, h and 6.14). In exceptional cases, PDCs reached up to 16 km from source (e.g. in 2010; Subandriyo et al. 2023, Chap. 12) and possibly further. In general, however, at greater distances downstream, the volcaniclastic successions are dominated by lahar and fluvial deposits in and around the main river valleys. The lava dome complex at the summit of Merapi (Fig. 6.15a) constitutes domes extruded after AD 1786 (Camus et al. 2000) within the larger Pasarbubar crater. Reconstructions and maps of the dome complex were presented by del Marmol (1989), Berthommier (1990), Innocenti et al. (2013b) and Solikhin et al. (2015), among others. A schematic sketch map of the summit area and lava dome complex after the 2010 eruption (Solikhin et al. 2015) is shown in Fig. 6.15b. With a few possible exceptions, eccentric vents and flank eruptions are unknown in the historical eruption record of Merapi (Fig. 6.16), which suggests that there have been 29 eruptions or eruptive episodes in the nineteenth century (average of one eruption every 3.4 years) and 25 eruptions or eruptive episodes in the twentieth century (average of one eruption every 4 years). Most of the 78 historical eruptions or eruptive

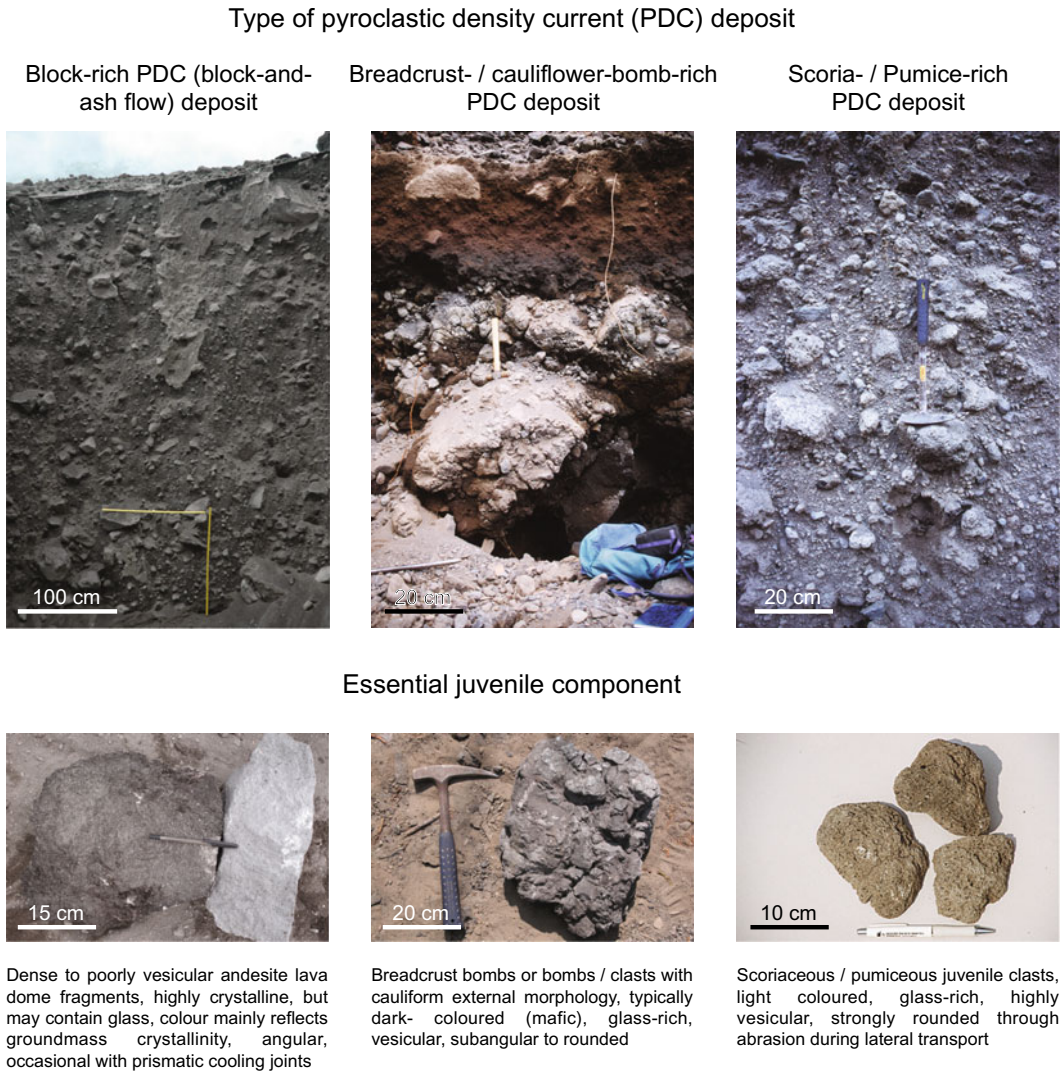

Fig. 6.13 Different types of pyroclastic density current deposits identified in the prehistoric and historical to recent geological record of Merapi based on the dominant juvenile component they contain. Inferred flow generation mechanisms are also indicated (modified after Gertisser 2012a)

episodes were of VEI 1-3, with VEI 2 eruptions being most common. They erupted from central vents in Merapi's summit region, and produced lava domes or flows, explosions and PDCs. Approximately 20 eruptions or eruptive episodes caused damage to infrastructures and fatalities, and 15 events produced syn- and/or post-eruptive lahars. It has been proposed that there was a shift in the style of activity from the nineteenth to the twentieth century, with explosive eruptions and some associated PDCs during the 1800s having been larger than any eruptions and PDCs

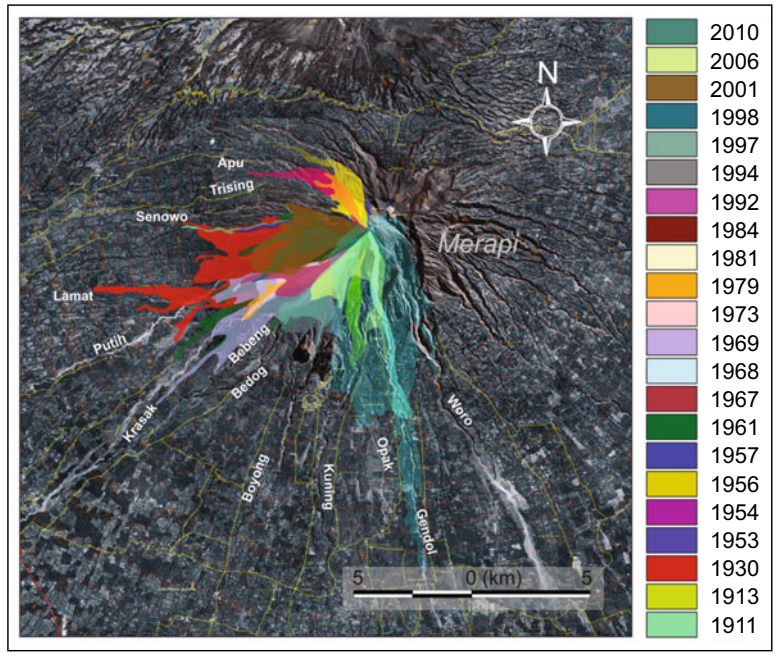

Fig. 6.14 Distribution of pyroclastic density currents of Merapi between 1911 and 2010. Map courtesy of I.G.M. A. Nandaka, Balai Penyelidikan dan Pengembangan Teknologi Kebencanaan Geologi (BPPTKG), Geological Agency of Indonesia

produced in the twentieth century (Newhall et al. 2000; Voight et al. 2000). However, such a pattern is less discernible from Fig. 6.16, and the large-magnitude eruption in 2010, which was preceded by a typical dome-forming eruption in 2006 and followed by a series of predominantly phreatic eruptions between 2012 and 2014 and in 2018, and renewed effusive (dome-forming) activity from 2018 onward (Global Volcanism Program 2013; Nandaka et al. 2023, Chap. 18; Fig. 6.17), shows that the size and intensity of eruptions at Merapi can change at relatively short timescales.

6.2.2.2 Structural Evolution and Volcano Collapse

Ever since the postulation of a collapse of the western flank of Merapi by van Bemmelen (1949, 1956), the issues of major structural modifications of the volcano and edifice collapse have remained debated topics. While there are still open questions about both the exact nature and timing of such events in Merapi's history, there has been significant progress since van Bemmelen's pioneering work. Evidence for edifice collapse at Merapi (Fig. 6.9) comes from (1) the structure of the volcanic edifice, such as the presence of a segmented horseshoe-shaped crater, Somma rim or avalanche caldera that may have formed by one or more collapses, (2) indirectly from impoundment of Kali Progo west-southwest of Merapi to form lake deposits of an ancient, recurring Lake Borobudur, (3) analysis of rocks retrieved from drill cores in the Borobudur basin, and (4) the recognition of landslide or debris avalanche deposits, including the recent discovery of the Godean debris avalanche deposit, a large debris avalanche deposit in the Godean and surrounding area southwest and south of Merapi by Bronto and co-workers (e.g. Djumarma et al. 1986; del Marmol 1989; Wirakusumah et al. 1989; Berthommier 1990; Camus et al. 2000; Newhall et al. 2000; Gomez et al. 2010; Gertisser et al. 2012a; Bronto et al. 2014, 2023, Chap. 7; Murwanto 2014).

The earliest, and in many respects, least constrained volcano collapse may have occurred at the Proto-Merapi stage, leaving behind the prominent hills of Gunung Turgo, Gunung Plawanagan and Gunung Medjing on Merapi's south flank (Berthommier 1990; Camus et al. 2000; Newhall et al. 2000). To date, no deposits

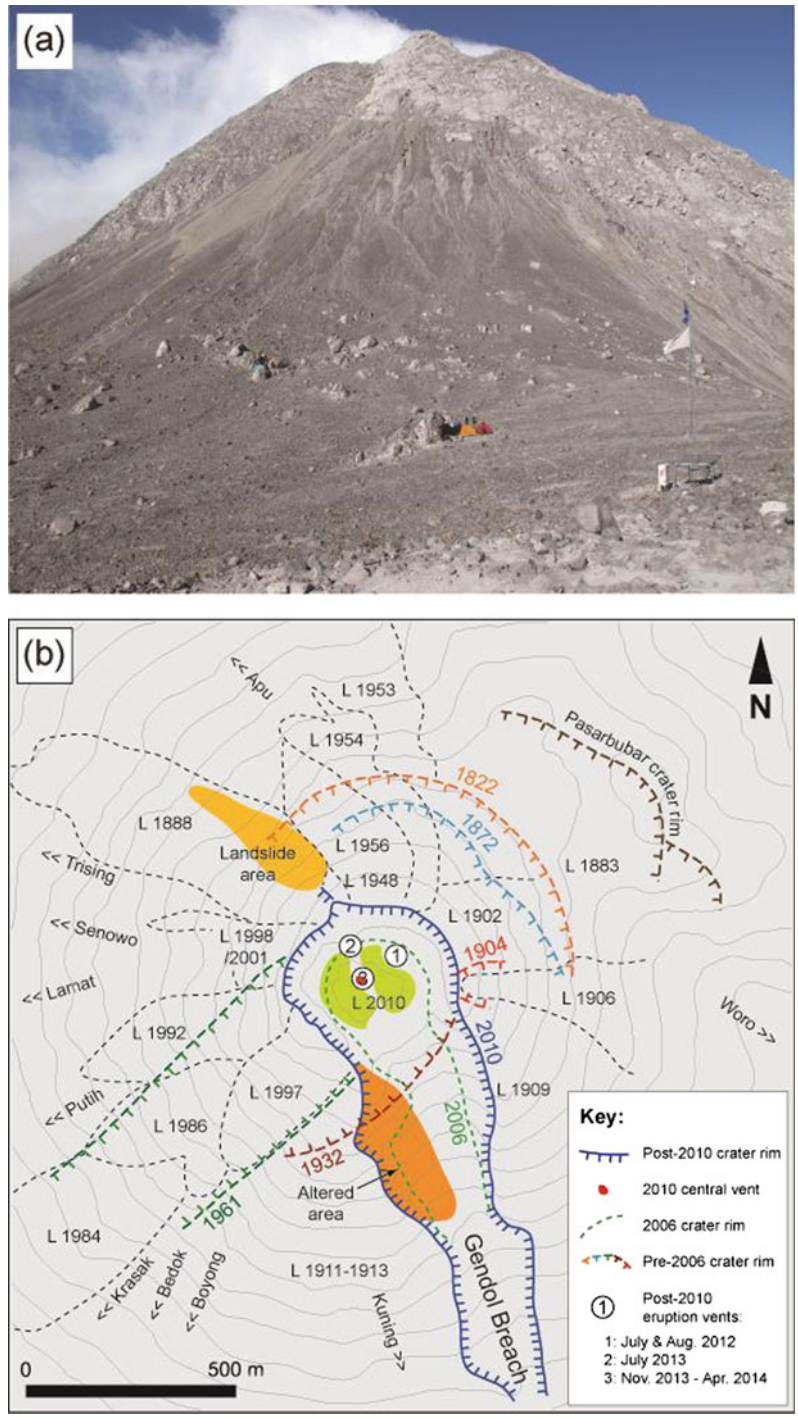

Fig. 6.15 **a** The lava dome complex at the summit of Merapi above the plateau of the Pasarbubar crater (photo taken in August 2011). **b** Schematic sketch map of the Merapi summit area and lava dome complex after the 2010 eruption (after Solikhin et al. 2015)

of such a collapse are known. Considering the ages of 138 ± 3 ka and 135 ± 3 ka for the basal lavas of Gunung Turgo and Gunung Plawangan (Gertisser et al. 2012a), it is possible that these hills are the source of mafic volcaniclastic material or blocks retrieved from drill cores in

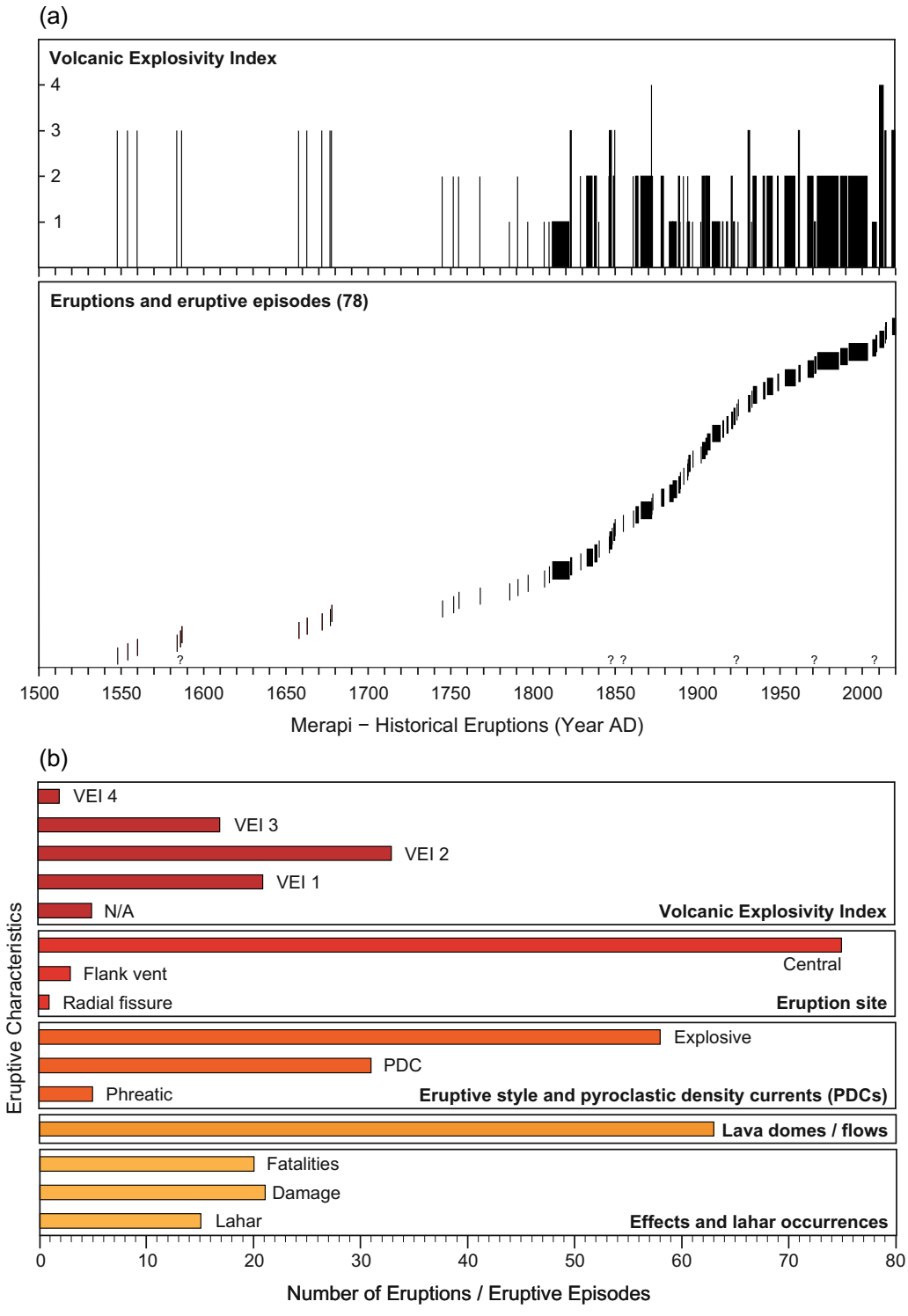

Fig. 6.16 Record of historical eruptions and eruptive episodes of Merapi compiled with data from Siebert et al. (2011) and the Global Volcanism Program (2013). The earliest historical observations date from AD 1584. **a** Eruptions and eruptive episodes and their Volcanic Explosivity Index (VEI) designation (Newhall and Self 1982). The two VEI 4 eruptions are those in 1872 and 2010. **b** Eruptive characteristics: VEI, eruption site, eruptive style and occurrence of pyroclastic density currents, and effects and lahar occurrences

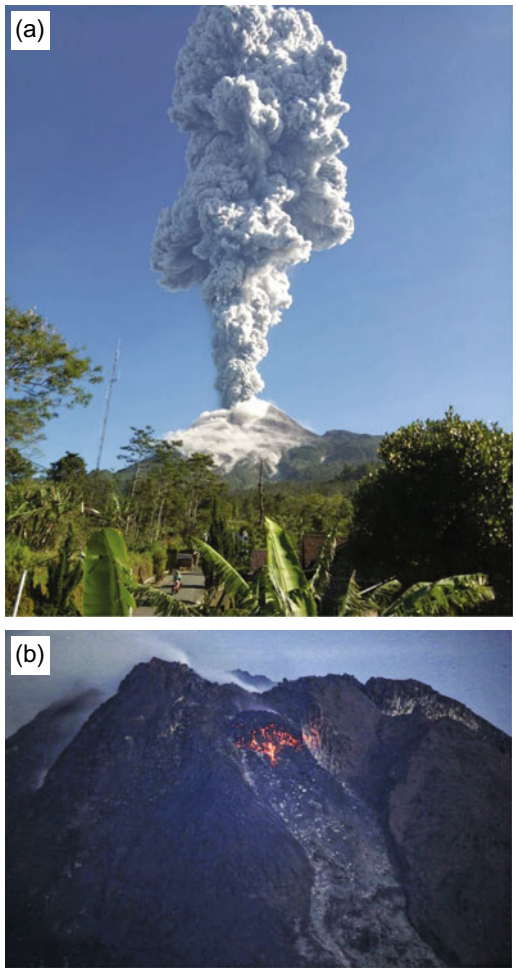

Fig. 6.17 Eruptive activity of Merapi after the 2010 eruption. **a** Ash plume rising at least 6 km above the summit during a short-lived phreatic explosion on 1 June 2018. **b** Lava dome in the western part of the summit as seen on 17 February 2021. The dome was first observed at the surface on 4 January 2021, marking the beginning of a new effusive eruption phase. *Photo credit* BPPTKG—CVGHM, Geological Agency of Indonesia

the southern part of the Borobudur basin, dated at 119 ± 2 ka or 115 ± 2 ka (Gomez et al. 2010). If correct, this would imply that the Proto-Merapi edifice, which comprises Gunung Turgo, Gunung Plawanagan and Gunung Medjing, existed until at least 115 ± 2 ka, after which it may have collapsed to generate a debris avalanche or debris flow that transported material from the edifice to the Borobudur basin. This interpretation differs from that of Bronto et al. (2023, Chap. 7) and must be considered with caution, given (1) that the reported basaltic rocks at the respective depth(s) in the drill cores (see Table 2 in Gomez et al. 2010) could have possibly originated from either Merapi (Gunung Turgo, Gunung Plawanagan and Gunung Medjing) or Merbabu, and (2) a lack of more detailed petrological, geochemical and chronological investigations of the retrieved drill core material.

The post-Proto Merapi complex may have collapsed multiple times. Several volcano collapses can be linked to Old Merapi, leaving the pronounced avalanche caldera on the eastern and northern side of the volcano, and generating debris avalanches from edifice failure to the west (Newhall et al. 2000). The oldest date of 31,430 ± 2070 ^{14}C y BP for black lacustrine clay from an ancient Lake Borobudur (Murwanto 2014; Bronto et al. 2023, Chap. 7), which coincides with an age of 31,040 ± 320 ^{14}C y BP for dark grey volcanic ash in a drill core located at the confluence between the Elo and Progo river (Gomez et al. 2010), may hint at a collapse early in the evolution of Old Merapi, which, according to the latest dates, started to grow more than 30.3 ± 1.0 ka ago (Gertisser et al. 2012a). Younger dates from the long sequence of lacustrine deposits in the alluvial plain of Borobudur (Murwanto 2014; Bronto et al. 2023, Chap. 7), including a preliminary age of 3430 ± 50 ^{14}C y BP given by Newhall et al. (2000), may signify impoundment of Kali Progo by rapidly emplaced debris avalanches from Merapi, although we cannot exclude the possibility that they reflect other times in the history of Lake Borobudur not necessarily related to new blockages. Debris avalanche deposits associated with such events are not known at present. A younger and latest collapse of Old Merapi is widely considered to be the main Somma rim forming event, although the nature and date of this event have remained strongly debated (see Sect. 6.2.1 and Bronto et al. 2023, Chap. 7). We speculate that the Godean debris avalanche (Bronto et al. 2023,

Chap. 7) could possibly be related to this inferred major event in Merapi's geological history, although a lack of direct age constraints of the associated deposits precludes a definitive answer at present. This contrasts with Bronto et al. (2023, Chap. 7), who argue that the Godean debris avalanche is significantly older, linking it to the oldest of three collapse structures identified through satellite image analysis that separate Merapi into four evolutionary stages.

Volcano collapses have also affected New Merapi. Whether the youngest dates (660 ± 110 and 420 ± 50 ^{14}C y BP; Newhall et al. 2000; Bronto et al. 2023, Chap. 7) of lacustrine deposits from an earlier Lake Borobudur reflect a debris avalanche event from Merapi is poorly substantiated at present. However, a relatively small collapse did affect the New Merapi cone some time after 1130 ± 50 ^{14}C y BP (Newhall et al. 2000). This partial collapse event was the only one identified directly by a debris avalanche deposit, until the discovery of the much larger Godean debris avalanche (Bronto et al. 2014, 2023, Chap. 7). The deposit in Kali Boyong, exposed on the valley floor following the 1994 eruption, consists of megaclasts of brecciated lava clasts with typical jigsaw cracks and pyroclastic material in a finer grained matrix. From its limited exposure, no inferences could be made about the volume or extent of the event, although it is regarded a much smaller event compared with the latest collapse of Old Merapi (Newhall et al. 2000).

Like other steep-sided stratovolcanoes, New Merapi appears to have been affected by multiple larger or smaller flank or sector collapses throughout its lifespan. During the recent and historical period, small collapses of the uppermost, hydrothermally altered and weakened edifice, or older lava domes from the summit dome complex, have accompanied some of the eruptions. The collapsed material, however, has often been incorporated in PDCs of these eruptions rather than distinct debris avalanche deposits. Breaches at the top of the volcano or in the crater wall are a direct result of explosive activity or such collapses, removing small portions of the uppermost volcanic edifice (e.g. Voight et al. 2000). The latest of these small collapses occurred during the 2006 and 2010 eruptions. Removal of part of the summit rim on 4 June 2006 led to a shift in the direction of dome-collapse PDCs from the southwest to the south during the 2006 eruption (Charbonnier and Gertisser 2008; Ratdomopurbo et al. 2013). Explosive activity and retrogressive summit collapses during the peak of the large-magnitude 2010 eruption on 5 November 2010 generated high-energy PDCs (Komorowski et al. 2013) and significantly enlarged the 'Gendol breach', which acted as the main pathway for subsequent rockfalls and dome-collapse PDCs, particularly in the later stages of the 2010 eruption and in 2019–2020, following another period of dome growth (Global Volcanism Program 2019, 2020). Small collapses of older parts of the summit are a potential future hazard that requires careful attention (Bronto et al. 2023, Chap. 7).

6.3 Compositional Variations of the Eruptive Products of Merapi

6.3.1 Rock Types and Classification

For the purpose of this chapter, 718 whole-rock major element analyses from the literature (Bahar 1984; Bardintzeff 1984; del Marmol 1989; Berthommier 1990; Boudon et al. 1993; Andreastuti, 1999; Andreastuti et al. 2000; Camus et al. 2000; Gertisser 2001; Gertisser and Keller 2003a, b; Debaille et al. 2006; Gertisser et al. 2012a; Chadwick et al. 2013; Preece 2014; this study) were grouped into the eight main volcano-stratigraphic units, and the major evolutionary stages or volcanic edifices of Merapi, based on information on sample location, sampled unit and/or sample age. Selected whole-rock data are presented in Tables 6.1 and 6.2; the complete dataset, including sample allocation to volcano-stratigraphic units, is available from the corresponding author upon request. Overall, the

Table 6.1 Selected whole rock major element oxide (wt.%) and trace element (ppm) data for Merapi

Unit[a]	1	2	2	2	3	3	3	3
Geochemical affinity[b]	MK	HK	HK	HK	MK	MK	MK	MK
Sample	M96-175	M95-028	M96-050	M96-052	M95-026	M96-056	M96-071	M98-047
SiO_2	56.49	50.20	50.37	50.30	55.50	55.41	56.60	55.58
TiO_2	0.72	1.03	1.09	0.92	0.78	0.76	0.73	0.79
Al_2O_3	18.71	19.78	18.68	19.17	18.33	18.69	18.75	18.45
Fe_2O_3*	7.45	9.53	10.12	9.90	8.33	8.07	7.51	7.79
MnO	0.17	0.13	0.14	0.17	0.17	0.18	0.16	0.17
MgO	2.58	3.19	4.28	4.91	3.41	3.17	2.26	2.56
CaO	8.09	9.72	9.26	10.24	8.44	8.43	8.01	8.08
Na_2O	3.59	3.19	3.18	3.11	3.43	3.59	4.00	3.67
K_2O	1.59	1.97	1.83	1.41	1.71	1.67	1.72	1.88
P_2O_5	0.29	0.28	0.28	0.21	0.21	0.22	0.24	0.32
LOI	0.71	1.14	1.40	−0.08	0.10	0.29	0.49	1.03
Total	100.40	100.16	100.62	100.26	100.41	100.47	100.49	100.33
Ba	428	474	584	437	451	454	430	434
Ce	38.2	23.3	28.7	19.4	29.1	28.2	31.7	38.0
Co	14.6	31.0	28.1	29.3	21.4	19.1	13.3	17.0
Cr	10.4	124.1	34.3	49.0	11.2	6.2	7.1	5.9
Dy	3.77	2.88	3.49	2.57	2.94	3.14	3.25	3.56
Er	2.31	1.69	1.99	1.49	1.59	1.72	1.67	1.94
Eu	1.43	1.10	1.33	0.94	1.00	1.19	1.14	1.34
Gd	4.13	3.15	3.91	2.69	3.03	3.43	3.31	4.03
Hf	2.77	1.67	1.93	1.31	2.01	2.31	2.35	2.64
Ho	0.739	0.606	0.723	0.527	0.544	0.616	0.680	0.737
La	18.9	11.6	14.3	10.0	14.4	14.4	15.3	19.2
Lu	0.366	0.249	0.331	0.227	0.281	0.326	0.302	0.325
Mo	0.68	0.74	0.93	0.57	0.82	0.89	0.70	1.12
Nb	4.49	2.02	2.42	1.52	2.63	2.95	3.62	4.65
Nd	20.0	12.1	15.5	10.6	13.7	14.7	15.6	18.7
Ni	b.d	43.1	16.4	19.0	4.5	2.1	2.0	2.7
Pb	25.4	16.6	18.3	14.9	14.8	15.3	18.3	17.3
Pr	4.78	2.84	3.57	2.48	3.32	3.43	3.68	4.51
Rb	37.8	23.9	36.2	20.9	46.1	38.3	42.7	47.7
Sm	4.22	3.10	3.82	2.65	3.06	3.33	3.58	4.35
Sr	529	568	467	642	496	519	519	520
Ta	0.38	0.15	0.20	0.12	0.21	0.23	0.30	0.36
Tb	0.603	0.473	0.557	0.403	0.469	0.513	0.476	0.592
Th	5.68	4.91	5.46	4.21	6.27	5.52	5.87	6.16
Tm	0.326	0.258	0.297	0.243	0.254	0.299	0.262	0.343
U	1.35	0.84	1.08	0.62	1.31	1.16	1.29	1.53
V	151	331	298	316	243	213	150	189
Y	22.4	18.0	21.1	16.3	17.9	20.9	20.1	21.1
Yb	2.11	1.61	1.98	1.47	1.70	1.87	1.91	2.09
Zr	114	64	68	48	88	92	102	113

(continued)

Table 6.1 (continued)

Unit[a]	3	4/5	4/5	4/5	4/5	4/5	4/5	4/5
Geochemical affinity[b]	MK	MK	MK	MK	MK	HK	HK	HK
Sample	M98-107	M96-073	M96-137	M96-163	M98-0532	M96-075	M96-102	M96-164
SiO_2	55.70	54.50	54.12	51.40	54.39	53.87	51.87	51.86
TiO_2	0.69	0.86	0.80	0.73	0.82	0.71	0.81	0.84
Al_2O_3	18.54	18.85	18.77	21.46	18.59	18.87	20.44	19.31
Fe_2O_3*	7.44	8.28	8.47	7.56	7.87	8.13	8.24	8.48
MnO	0.15	0.20	0.18	0.17	0.19	0.19	0.20	0.20
MgO	2.28	2.75	3.17	2.56	2.68	3.03	2.47	3.02
CaO	8.04	8.50	8.75	7.69	8.28	8.55	8.86	9.30
Na_2O	3.97	3.77	3.61	3.09	3.81	3.43	3.35	3.36
K_2O	1.73	1.71	1.61	1.25	1.77	2.04	1.74	1.82
P_2O_5	0.24	0.28	0.27	0.25	0.27	0.29	0.31	0.29
LOI	1.14	0.30	0.38	4.24	1.77	1.06	1.63	1.46
Total	99.90	100.00	100.14	100.40	100.45	100.17	99.91	99.93
Ba	458	478	445	411	439	525	364	477
Ce	41.1	35.3	33.5	31.5	33.6	38.0	33.4	36.0
Co	22.2	16.3	18.7	18.3	16.6	17.1	22.9	18.9
Cr	7.2	5.6	5.5	6.2	3.3	9.2	6.0	24.5
Dy	3.85	3.90	3.55	3.25	3.71	3.62	4.48	3.86
Er	2.30	2.29	2.18	1.96	2.17	2.15	2.52	2.14
Eu	1.42	1.40	1.39	1.18	1.44	1.33	1.40	1.35
Gd	4.29	4.20	3.89	3.73	4.29	3.85	4.74	4.17
Hf	2.66	2.54	2.45	2.23	2.74	2.23	2.88	2.21
Ho	0.805	0.845	0.749	0.718	0.769	0.780	0.926	0.791
La	20.0	16.5	16.1	15.6	16.3	18.7	16.3	18.0
Lu	0.338	0.385	0.349	0.339	0.371	0.358	0.416	0.358
Mo	1.11	0.93	1.12	0.95	1.00	1.14		1.04
Nb	4.62	4.17	3.65	3.38	4.12	3.31	4.35	2.92
Nd	19.3	17.6	18.0	16.4	18.1	18.1	20.0	18.9
Ni	5.2	1.6	1.6	1.7	2.8	2.3	7.0	3.3
Pb	15.7	13.0	19.6	15.1	14.7	19.6	14.9	18.9
Pr	4.91	4.41	4.16	4.00	4.20	4.38	4.552	4.53
Rb	49.0	42.5	40.6	38.7	44.0	50.3	24.6	45.2
Sm	4.40	4.22	4.24	3.92	4.12	4.01	4.72	4.68
Sr	573	532	552	533	547	570	533	611
Ta	0.36	0.34	0.31	0.25	0.31	0.27	0.31	0.22
Tb	0.622	0.624	0.577	0.536	0.615	0.584	0.759	0.600
Th	6.20	5.92	5.98	5.35	5.07	7.61	5.27	7.33
Tm	0.330	0.382	0.353	0.322	0.358	0.345	0.391	0.341
U	1.42	1.29	1.28	1.06	1.34	1.57	1.06	1.35
V	239	200	199	194	197	193	259	224
Y	22.3	24.1	22.3	21.2	24.6	22.1	25.0	23.4
Yb	2.10	2.24	2.16	2.00	2.34	2.12	2.54	2.06
Zr	112	107	99	95	115	90	104	90

(continued)

Table 6.1 (continued)

Unit[a]	4/5	4/5	4/5	4/5	4/5	4/5	4/5	4/5
Geochemical affinity[b]	HK	HK	HK	HK	HK	HK	HK	HK
Sample	M96-167	M97-021	M97-031	M97-0392	M97-053	M97-077	M97-0781	M98-030
SiO_2	54.41	52.85	55.62	52.86	54.12	52.45	53.24	52.13
TiO_2	0.75	0.88	0.71	0.87	0.74	0.78	0.75	0.78
Al_2O_3	18.72	18.57	18.63	18.80	18.92	18.96	19.35	19.02
Fe_2O_3*	8.31	9.09	7.37	8.78	8.19	8.89	8.31	8.49
MnO	0.18	0.18	0.19	0.19	0.19	0.20	0.20	0.20
MgO	2.94	3.51	2.37	3.20	2.91	3.27	2.82	2.80
CaO	8.39	9.41	7.79	8.94	8.49	9.18	8.88	8.72
Na_2O	3.57	3.36	3.80	3.48	3.47	3.32	3.43	3.39
K_2O	2.30	1.98	2.38	2.14	2.15	1.91	2.03	1.99
P_2O_5	0.27	0.25	0.25	0.24	0.30	0.31	0.32	0.31
LOI	0.16	0.42	1.34	0.55	1.08	0.91	0.73	2.07
Total	99.98	100.49	100.45	100.05	100.56	100.18	100.05	99.90
Ba	533	531	602	515	512	457	486	291
Ce	36.2	33.1	40.4	31.6	36.2	35.7	38.6	37.0
Co	20.0	23.6	16.9	21.9	18.8	19.2	18.8	11.3
Cr	8.3	12.6	9.2	8.9	6.6	5.7	6.0	2.4
Dy	3.26	3.56	3.54	3.41	3.30	3.54	3.68	4.82
Er	1.95	1.92	2.00	2.01	1.98	2.08	2.13	2.73
Eu	1.14	1.31	1.37	1.31	1.27	1.30	1.31	1.53
Gd	3.36	3.58	3.49	3.37	3.70	3.69	3.84	5.13
Hf	2.13	2.06	2.45	2.12	2.01	2.17	2.58	3.95
Ho	0.678	0.741	0.767	0.701	0.722	0.739	0.785	1.006
La	18.7	16.8	20.3	15.6	18.4	17.9	18.8	16.9
Lu	0.326	0.312	0.352	0.345	0.325	0.339	0.360	0.467
Mo	1.16	0.83	1.26	1.19	0.97	0.92	0.98	
Nb	2.77	2.85	3.27	2.73	2.85	3.18	3.55	6.28
Nd	17.1	17.0	18.6	16.2	16.8	18.3	19.1	23.4
Ni	2.3	4.6	3.0	2.9	1.4	0.1	0.1	2.2
Pb	15.7	24.3	13.8	18.2	17.6	16.7	19.6	21.3
Pr	4.08	4.07	4.74	3.91	4.40	4.27	4.63	5.288
Rb	58.1	49.4	64.5	48.7	52.7	44.1	48.0	20.5
Sm	3.93	4.17	4.40	4.15	4.19	4.27	4.70	5.39
Sr	600	555	614	569	586	588	624	544
Ta	0.20	0.21	0.25	0.20	0.21	0.22	0.26	0.47
Tb	0.519	0.568	0.526	0.606	0.570	0.581	0.615	0.832
Th	6.91	6.56	8.91	6.68	6.86	6.94	8.26	8.18
Tm	0.304	0.322	0.319	0.358	0.282	0.337	0.348	0.428
U	1.44	1.37	1.71	1.49	1.22	1.22	1.56	1.11
V	229	249	186	272	207	205	206	152
Y	22.7	22.5	22.3	22.4	22.6	22.5	23.3	26.9
Yb	1.93	2.02	2.17	2.10	1.99	2.01	2.10	2.84
Zr	89	83	99	85	88	89	94	144

(continued)

Table 6.1 (continued)

Unit[a]	4/5	4/5	4/5	6	6	7/8	7/8	7/8
Geochemical affinity[b]	HK	HK	HK	HK	HK	HK	HK	HK
Sample	M98-031	M98-066	M98-096	M07-001	M07-044	M95-011	M96-142	M97-068
SiO_2	51.70	53.06	53.29	54.77	53.23	52.88	55.88	51.85
TiO_2	0.84	0.81	0.78	0.84	0.87	0.80	0.69	0.87
Al_2O_3	18.77	18.97	18.64	18.68	18.21	18.61	19.05	18.53
Fe_2O_3*	8.38	8.95	8.55	7.88	9.30	9.32	7.45	9.65
MnO	0.20	0.20	0.20	0.18	0.19	0.20	0.18	0.21
MgO	3.09	3.23	3.22	2.59	3.05	3.50	2.44	3.90
CaO	9.23	9.23	8.86	8.32	8.96	9.39	8.13	9.58
Na_2O	3.35	3.41	3.45	3.86	3.75	3.30	3.76	3.20
K_2O	1.90	2.05	2.05	1.92	1.98	2.00	2.25	1.98
P_2O_5	0.26	0.30	0.29	0.28	0.25	0.29	0.31	0.29
LOI	2.49	0.27	0.81	−0.13	−0.17	0.07	0.24	0.31
Total	100.21	100.48	100.14	99.18	99.61	100.35	100.37	100.36
Ba	307	506	535	*476*	*455*	439	522	431
Ce	33.8	36.4	36.5	*35.7*	*36.2*	34.5	39.0	34.6
Co	13.0	20.4	19.8	*15.5*	*24.4*	21.6	14.2	27.8
Cr	2.5	4.9	9.7			11.7	8.2	16.0
Dy	4.49	3.77	4.07	*4.04*	*4.06*	3.46	3.88	3.45
Er	2.49	2.12	2.21	*2.3*	*2.54*	2.11	2.32	1.93
Eu	1.45	1.37	1.40	*1.18*	*1.24*	1.34	1.38	1.36
Gd	4.77	3.96	4.00	*4.54*	*4.12*	4.13	4.20	3.65
Hf	3.62	2.24	2.32	*3*	*2.6*	2.15	2.74	2.14
Ho	0.932	0.732	0.747	*0.88*	*0.76*	0.708	0.837	0.724
La	14.8	18.4	19.0	*16.3*	*18*	17.2	20.2	17.3
Lu	0.431	0.323	0.338	*0.400*	*0.350*	0.325	0.379	0.330
Mo		1.05	1.03	*0.7*	*0.6*	1.05	1.22	0.92
Nb	5.63	3.10	3.25	*4.3*	*4.5*	3.30	4.06	2.94
Nd	21.0	18.8	19.1	*16.2*	*14.2*	17.8	19.9	18.0
Ni	2.1	3.1	4.1	*1.3*	*2.3*	3.1	0.8	2.6
Pb	20.0	18.5	18.9	*3.5*	*2.6*	15.7	19.8	14.8
Pr	4.736	4.24	4.37	*4.24*	*4.47*	4.18	4.79	4.28
Rb	20.7	47.4	50.8	*42.3*	*42.2*	46.8	52.4	45.7
Sm	4.97	4.37	4.27	*3.95*	*3.73*	4.34	4.57	4.33
Sr	531	565	584	*564.2*	*594.6*	600	546	603
Ta	0.41	0.24	0.25	*0.4*	*0.3*	0.23	0.34	0.21
Tb	0.773	0.595	0.636	*0.63*	*0.62*	0.588	0.622	0.627
Th	7.14	6.77	6.68	*5*	*5.9*	7.23	8.04	6.16
Tm	0.395	0.361	0.340	*0.38*	*0.32*	0.314	0.386	0.318
U	1.09	1.51	1.46	*1.3*	*1.2*	1.29	1.43	1.02
V	169	220	211	*196*	*284*	222	156	249
Y	24.7	22.1	22.3	*23.8*	*20.6*	23.0	23.9	22.8
Yb	2.59	2.16	2.12	*2.2*	*2.63*	2.22	2.35	2.01
Zr	133	87	91	*108*	*107*	86	107	83

[a] Volcano-stratigraphic unit (see text and Fig. 6.9); [b] Geochemical affinity: MK = medium-K; HK = high-K. Other symbols and abbreviations: Fe_2O_3* = total Fe as Fe_2O_3; b.d. = below detection. Data sources: Gertisser (2001), Gertisser and Keller (2003a, b), Handley et al. (2011, 2014), Gertisser et al. (2012a) and previously unpublished data by the authors (shown by italic font), produced in the same laboratories and with the same methods as described in Gertisser (2001), Gertisser and Keller (2003a, b) and Handley et al. (2011, 2014)

Table 6.2 Whole rock isotopic data for Merapi

Unit[a]	Geochemical affinity[b]	Sample	$^{87}Sr/^{86}Sr$	$^{143}Nd/^{144}Nd$	$^{208}Pb/^{204}Pb$	$^{207}Pb/^{204}Pb$	$^{206}Pb/^{204}Pb$	$^{176}Hf/^{177}Hf$	$\delta^{18}O$ (‰ SMOW)
1	MK	M96-175	0.705105	0.512752	*39.070*	*15.674*	*18.740*	0.283185	*+7.7*
2	HK	M95-028	0.705793	0.512729	*39.219*	*15.703*	*18.823*	0.283146	*+6.4*
2	HK	M96-050	0.705539	0.512742	*39.189*	*15.693*	*18.807*	0.283160	*+7.7*
3	MK	M95-026	0.705260	0.512727	39.130	15.693	18.769	0.283146	+6.4
3	MK	M96-056	0.705275	0.512765	39.170	15.709	18.771	0.283131	+6.6
3	MK	M98-047	0.705014	0.512712	39.110	15.689	18.740	0.283144	+6.9
3	MK	M98-107	0.705169	0.512722	39.215	15.715	18.781	0.283144	+6.9
4/5	MK	M96-073	0.705392	0.512774	39.134	15.692	18.755	0.283157	+6.3
4/5	MK	M96-137	0.705277	0.512758	39.139	15.695	18.759	0.283148	+6.8
4/5	MK	M96-163	0.705155	0.512754					+8.3
4/5	MK	M98-0532	0.705353	0.512759				0.283160	+7.3
4/5	HK	M96-102	0.705515	0.512753					+6.9
4/5	HK	M96-167	0.705696	0.512701	39.117	15.684	18.766		+6.0
4/5	HK	M97-021	0.705741	0.512712	39.125	15.685	18.769	0.283138	+6.7
4/5	HK	M97-031	0.705625	0.512711	39.098	15.678	18.760	0.283141	+7.0
4/5	HK	M97-0392	0.705663	0.512714	39.130	15.688	18.763	0.283137	+6.2
4/5	HK	M97-053	0.705658	0.512678					+7.0
4/5	HK	M98-030	0.705704	0.512732					+7.1
4/5	HK	M98-031	0.70554	0.512746				0.283141	+7.5
4/5	HK	M98-066	0.705826	0.512675	39.175	15.699	18.780		+6.6
4/5	HK	M98-096	0.705643	0.512686	39.156	15.697	18.771	0.283147	+6.5
6	HK	M07-001	*0.70536*	*0.512774*					
6	HK	M07-044	*0.705284*						
7/8	HK	M95-011	*0.705687*	*0.512695*					
7/8	HK	M96-142	0.705737	0.512723	39.195	15.714	18.773	0.283128	+6.7
7/8	HK	M97-068	0.705711	0.512671	39.141	15.694	18.763	0.283128	+6.3

[a] Volcano-stratigraphic unit (see text and Fig. 6.9); [b] Geochemical affinity: MK = medium-K; HK = high-K. Data sources: Gertisser (2001), Gertisser and Keller (2003a, b), Handley et al. (2011, 2014), Gertisser et al. (2012a) and previously unpublished data by the authors (shown by italic font), produced in the same laboratories and with the same methods as described in Gertisser (2001), Gertisser and Keller (2003a, b) and Handley et al. (2011, 2014)

lavas and pyroclastic rocks that constitute the eight main volcano-stratigraphic units display notable mineralogical, geochemical and isotopic variations, with variations in whole rock SiO_2 content between 48.3 and 61.4 wt% (recalculated to 100 wt%, volatile-free). In the chemical classification using TAS (total alkali–silica diagram) (Le Maitre et al. 2002; Fig. 6.18a), the Merapi rocks straddle the boundary between basalt/trachybasalt, basaltic andesite/basaltic trachyandesite and andesite/trachyandesite. Variations in K_2O content (Fig. 6.18b) divide the eruptive products of Merapi into medium-K and high-K types (Le Maitre et al. 2002). In the classic K_2O versus SiO_2 classification of Peccerillo and Taylor (1976), these types correspond to the calc-alkaline and high-K calc-alkaline suite of rocks, respectively. Basaltic andesite/basaltic trachyandesite (high-K basaltic andesite) is by far the dominant rock type of Merapi, which may therefore be classed as a basaltic andesite volcano. Basalt/trachybasalt (high-K basalt) and andesite/trachyandesite (high-K andesite) are subordinate.

Merapi lavas, including recent domes (e.g. 1984, 1994, 1998, 2006, 2010), and pyroclastic rocks may contain a range of igneous inclusions, including mafic and felsic plutonic fragments and co-magmatic, occasionally highly crystalline, enclaves (e.g. del Marmol 1989; Chadwick et al. 2013; Troll et al. 2013a; van der Zwan et al. 2013; Preece, 2014; Troll and Deegan 2023, Chap. 8), which range from 40.2 to 53.4 wt% SiO_2 and 48.8–55.0 wt% SiO_2 (recalculated to 100 wt%, volatile-free), respectively (Chadwick et al. 2013; Preece 2014).

Material derived from the subvolcanic crustal basement is frequently found as thermally metamorphosed (calc-silicate) xenoliths, less abundant metasedimentary or volcaniclastic rock fragments, and rare xenoliths of buchite (pyrometamorphic, glass-rich rock) within the eruptive products (Clocchiatti et al. 1982; del Marmol 1989; Berthommier 1990; Camus et al. 2000; Gertisser 2001; Gertisser and Keller 2003b; Chadwick et al. 2007, 2013; Deegan et al. 2010, 2023, Chap. 10; Troll et al. 2012, 2013a, b; Whitley et al. 2019, 2020; Whitley 2020).

6.3.2 Mineralogy and Petrography

6.3.2.1 Mineralogical and Petrographical Characteristics

Merapi volcanic rocks contain variable amounts of plagioclase, clinopyroxene, orthopyroxene, olivine, titanomagnetite and amphibole as major (> 5 vol%) or minor (1–5 vol%) mineral phases. Apatite is a common accessory phase (< 1 vol %). Rare chrome spinel occurs as inclusions in some olivine crystals, and similarly uncommon pyrrhotite has been identified within titanomagnetite, amphibole and clinopyroxene hosts. Alkali feldspar, cristobalite and biotite occur in the groundmass of a few Merapi samples (e.g. Bahar 1984; del Marmol 1989; Berthommier 1990; Andreastuti 1999; Camus et al. 2000; Hammer et al. 2000; Gertisser 2001; Gertisser and Keller 2003a, b; Deegan et al. 2010; Preece et al. 2013, 2016; Preece 2014; Peters et al. 2017; Li et al. 2021). Irrespective of the potassium content, and reflecting the relative restricted range of whole rock SiO_2 compositions, the mineralogical characteristics of the Merapi rocks are often similar, although differences between the basaltic, and basaltic andesitic to andesitic rock types are notable (Fig. 6.19).

Lavas and scoriaceous and pumiceous clasts in volcaniclastic deposits (Fig. 6.20) exhibit porphyritic textures with phenocryst contents typically up to ~ 60% of the total rock volume (e.g. Bahar 1984; del Marmol 1989; Berthommier 1990; Camus et al. 2000; Gertisser 2001). Phenocrysts (> 0.3 mm), microphenocrysts (0.03–0.3 mm) and crystal clots (glomerocrysts) are enclosed within a fine-grained or glassy groundmass (< 0.03 mm). The latter gives rise to a vitrophyric texture in quickly cooled magmas or lavas. In many cases, small, lath-shaped plagioclase microlites, which have grown before complete solidification of the quenched magmas or lavas, lead to a hyalopilitic texture. In more viscous lavas, the plagioclase microlites may be flow-aligned.

In all Merapi volcanic rocks, plagioclase and clinopyroxene are ubiquitous and typically dominate the phenocryst assemblage, with

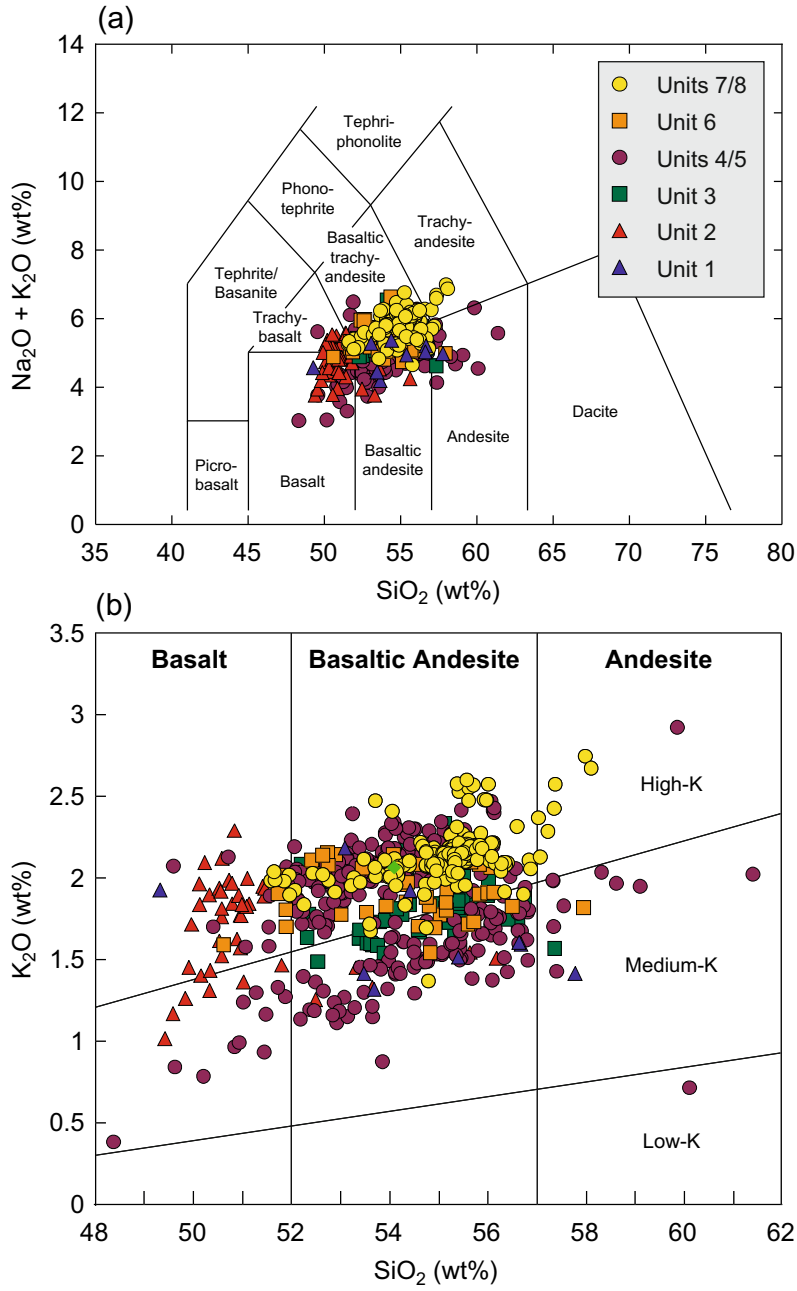

Fig. 6.18 **a** Total alkali versus SiO_2 (TAS) and **b** K_2O versus SiO_2 classification diagrams (Le Maitre et al. 2002) for Merapi lavas and pyroclastic rocks. All analyses are recalculated to 100 wt%, free of volatiles. Symbols (key as in Fig. 6.9): Unit 1 = Lava flows of Gunung Bibi; Unit 2 = Lava flows of Gunung Turgo, Gunung Plawangan and Gunung Medjing; Unit 3 = Lava flows of the Somma-Merapi; Units 4 and 5 = Pyroclastic deposits of the Holocene Pyroclastic Series; Unit 6 = Young (post-Somma-Merapi) lava flows; Units 7 and 8 = Recent and mostly historical pyroclastic density current and lahar deposits as well as lava domes of the recent episode. *Data Sources* Bahar (1984), Bardintzeff (1984), del Marmol (1989), Berthommier (1990), Boudon et al. (1993, Andreastuti (1999), Andreastuti et al. (2000), Camus et al. (2000), Gertisser (2001), Gertisser and Keller (2003a, b), Debaille et al. (2006), Gertisser et al. (2012a), Chadwick et al. (2013), Preece (2014) and this study

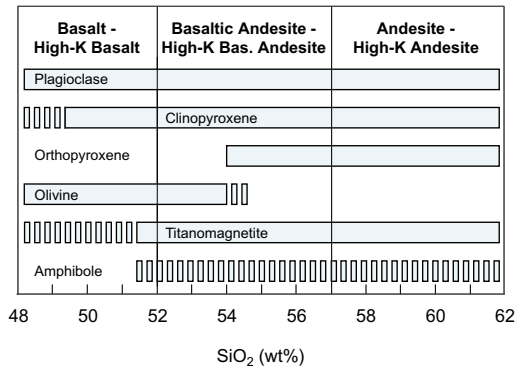

Fig. 6.19 Typical major and minor phenocryst and microphenocryst phases for Merapi lavas and pyroclastic rocks (after del Marmol 1989; Gertisser 2001)

plagioclase always prevailing (e.g. Bahar 1984; del Marmol 1989; Berthommier 1990; Gertisser 2001). In the basaltic rocks, especially those of Gunung Turgo, Gunung Plawangan and Gunung Medjing (Fig. 6.20b), olivine may appear as a major mineral phase and can replace clinopyroxene as a common phenocryst phase alongside plagioclase (del Marmol 1989). Therefore, clinopyroxene phenocrysts can be rare or even absent in the oldest basaltic lavas of Merapi, a phenomenon that was also observed in a lava flow located in Kali Kuning at the foot of Gunung Plawangan (del Marmol 1989). In the basaltic rocks of the younger periods, plagioclase and clinopyroxene dominate over olivine, which occurs as an accessory phase in some samples but is often absent in the lavas of the Somma-Merapi. Orthopyroxene occurs at the expense of olivine as phenocrysts or microphenocrysts in more SiO_2-rich volcanic rocks only and is an important index mineral to distinguish basaltic from basaltic andesitic and andesitic rock types. Occasionally, phenocrysts or microphenocrysts of olivine and orthopyroxene coexist in rocks with 52–55 wt% SiO_2. In relatively rare cases, both olivine and orthopyroxene are absent, resulting in basaltic andesite or andesite with only clinopyroxene. Except for the basalts of Gunung Turgo, Gunung Plawangan and Gunung Medjing, amphibole may occur as an accessory, minor or major mineral phase (Fig. 6.20). Titanomagnetite is the only primary magmatic Fe–Ti oxide phase in the Merapi rocks. It is usually more abundant in the younger and more SiO_2-rich eruptive products and occurs only sporadically and as a minor phase in the basalts of Gunung Turgo, Gunung Plawangan and Gunung Medjing. Apatite is present as an accessory phase in nearly all Merapi volcanic rocks where it occurs as microphenocryst or as inclusion in plagioclase, pyroxene or amphibole. Furthermore, rare Cr-spinel has been observed as inclusions in olivine in the basalts of Gunung Turgo, Gunung Plawangan and Gunung Medjing (del Marmol 1989; Gertisser 2001). The groundmass mineral assemblages in the microcrystalline rock varieties are dominated by plagioclase, clinopyroxene, orthopyroxene and titanomagnetite, although alkali feldspar, cristobalite and biotite have been described in a few samples, with cristobalite also occasionally filling pore space (Hammer et al. 2000; Gertisser 2001; Costa et al. 2013; Preece et al. 2013, 2016). Glomerocrysts, consisting of plagioclase, clinopyroxene, minor amounts of orthopyroxene or, alternatively, olivine, titanomagnetite and, in some cases, amphibole, are often present in the Merapi rocks. Brownish glass may occur in interstitial spaces between larger crystals giving rise to an intersertal texture.

Igneous inclusions in the Merapi lavas consist of highly crystalline basaltic andesites, comagmatic enclaves, plutonic crystalline rocks, often characterised by a magmatic cumulate texture, and amphibole megacrysts up to several centimetres in length (del Marmol 1989; Camus et al. 2000; Chadwick et al. 2013; Troll et al. 2013a; van der Zwan et al. 2013; Preece 2014; Peters et al. 2017; Troll and Deegan 2023, Chap. 8). The light grey dense igneous inclusions in the 2010 lava dome are akin to the highly crystalline basaltic andesite inclusions. They were interpreted as fragments of a plug of cooled, rigid magma that resided at shallow depth within the magmatic system and was partially re-heated, fragmented and incorporated into the juvenile 2010 magma (Preece 2014; Preece et al. 2016; Subandriyo et al. 2023, Chap. 12). The igneous inclusions ubiquitously contain plagioclase, pyroxene and titanomagnetite, almost always amphibole, which can be a major

mineral phase in some inclusions, and various proportions of glass or groundmass depending on inclusion type (Camus et al. 2000; Chadwick et al. 2013; Troll et al. 2013a). Preece (2014) additionally identified alkali feldspar, cristobalite and biotite in the light grey inclusion material in the 2010 eruptive products.

The abundant calc-silicate xenoliths in the Merapi lavas were grouped into magmatic skarns, which contain evidence of formation within the magma, and exoskarns, which represent fragments of crystalline, metamorphosed wall-rocks (Deegan et al. 2010; Whitley et al. 2019, 2020; Whitley 2020). They are often dominated by wollastonite and diopside but may also contain plagioclase, augite, ferrian aluminian diopside or augite (fassaite), hedenbergite, tremolite, grossular-andradite or uvarovite garnet, quartz, magnetite, chromite, spinel, melilite, epidote, leucite, biotite, apatite, titanite, scapolite, prehnite, bustamite, cuspidine, fluorite, spurrite and a wadalite-phase, amongst others. Traces of texturally distinct calcite were also observed in several of the samples. In addition, magmatic skarns may contain Ca-enriched glass, which is largely absent in the exoskarn xenoliths (Clocchiatti et al. 1982; Kerinec 1982; Camus et al. 2000; Chadwick et al. 2007, 2013; Deegan et al. 2010, 2023, Chap. 10; Troll et al. 2012, 2013a, b; Preece 2014; Whitley et al. 2019, 2020; Whitley 2020). Buchites contain abundant (> 70 vol%) quartz or other SiO_2 polymorphs with interstitial glass around the crystal borders, and minor small interstitial clinopyroxene, plagioclase and wollastonite (Whitley 2020; Whitley et al. 2020).

6.3.2.2 Mineral Textures and Compositions

Detailed descriptions of mineral textures and compositions at Merapi, including extensive datasets of mineral analyses, can be found in unpublished Ph.D. theses (e.g. Bahar 1984; del Marmol 1989; Andreastuti 1999; Berthommier 1990; Gertisser 2001; Preece 2014; Whitley 2020); other accounts are given in published work (e.g. Camus et al. 2000; Hammer et al. 2000; Gertisser and Keller 2003a, b; Chadwick et al. 2007, 2013; Costa et al. 2013; Nadeau et al. 2013; Preece et al. 2013, 2014, 2016; van der Zwan et al. 2013; Erdmann et al. 2014; Deegan et al. 2016; Peters et al. 2017; Whitley et al. 2000). The range of mineral (phenocryst and microphenocryst) compositions in the lavas and pyroclastic rocks of the main volcano-stratigraphic units are summarised below together with the main mineral textural characteristics. A subset of representative analyses is shown in Fig. 6.21.

Feldspar (Fig. 6.21a) is always present in the Merapi volcanic rocks as phenocrysts, microphenocrysts, inclusions in pyroxene and amphibole, and groundmass microlites; it is also a main constituent of crystal aggregates or glomerocrysts. Phenocrysts and microphenocrysts are ubiquitously plagioclase up to a few millimetres in size. Larger plagioclase crystals (up to 6 mm long), which are typically zoned, multiply twinned and fractured, and contain melt inclusions arranged in certain crystal zones, are occasionally found in the oldest basaltic lavas of Gunung Turgo, Gunung Plawangan and Gunung Medjing. This plagioclase type may be recognised in younger Merapi rocks as crystals, so-called antecrysts, that are typically smaller, complexly zoned, broken, rounded and mantled by more albitic feldspar (del Marmol 1989). Overall, plagioclase crystals at Merapi may be euhedral, rounded or resorbed, broken, twinned or sieve-textured, and frequently contain inclusions of brown glass and other minerals. They can be unzoned, but commonly display normal, reverse or oscillatory zoning. In rare cases, plagioclase phenocrysts may have rims of alkali feldspar

Fig. 6.20 Photomicrographs of volcanic rocks from the main volcano-stratigraphic units of Merapi (cf. Fig. 6.9). **a** Lava block of Gunung Bibi (Unit 1). **b** Lava flow of Gunung Plawangan (Unit 2). **c** Old Merapi lava flow near Deles (Unit 3). **d** Clast in PDC deposit in Kali Juweh in the north-western sector of Merapi (Unit 4). **e** Scoriaceous or pumiceous clast from the sub-Plinian Jurangjero I tephra (Gertisser 2001; Gertisser et al. 2012a) (Unit 5). ▶ **f** Selokopo lava (Unit 6). **g** Breadcrust bomb from young PDC deposit on Merapi's south flank (Unit 7). **h** 1994 lava dome (Unit 8). Abbreviations: Am = amphibole; Pl = plagioclase; Cpx = clinopyroxene; Ol = olivine; Mag = magnetite; V = vesicles; rr = reaction (breakdown) rim around amphibole

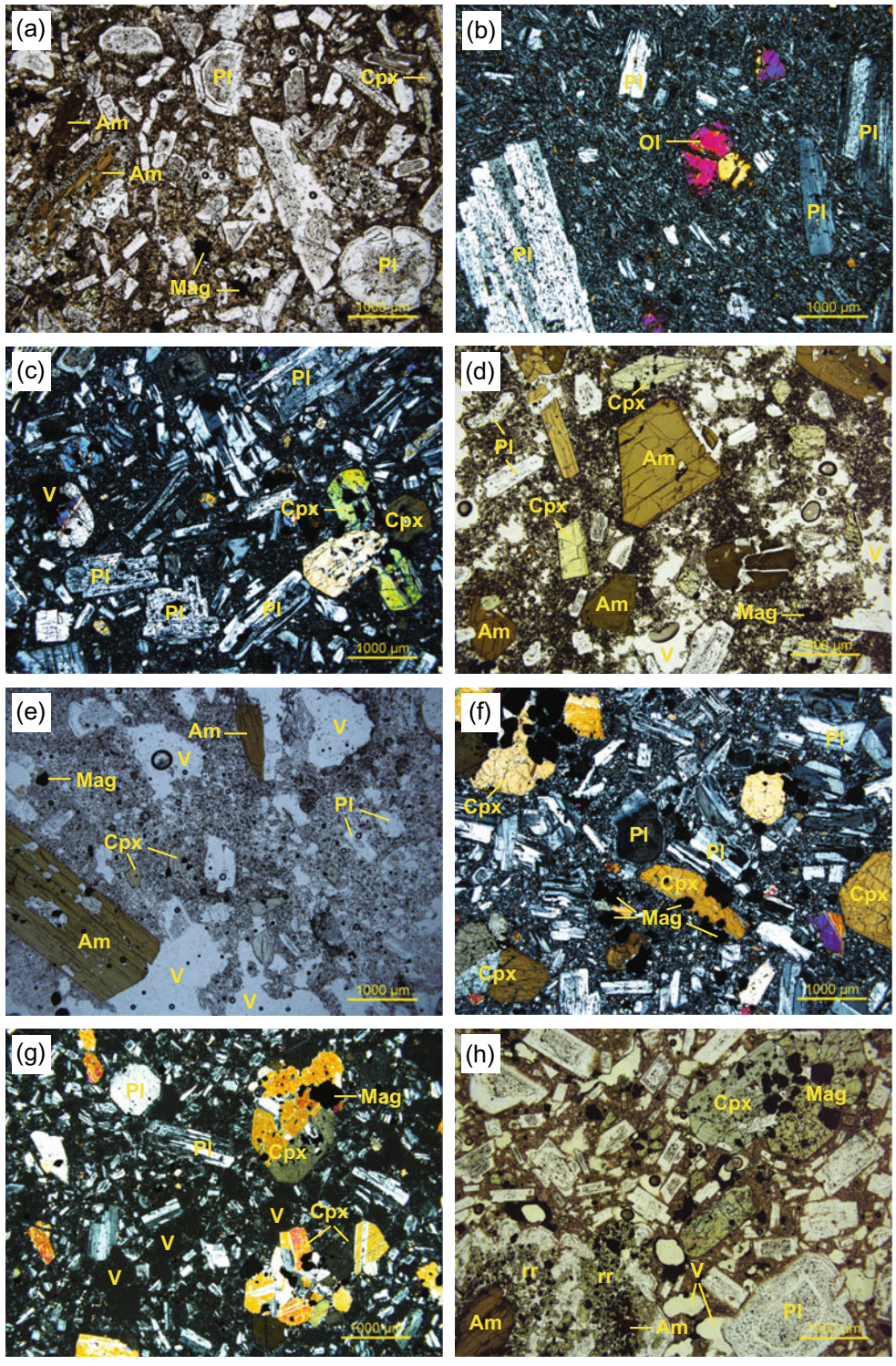
(a)
Pl
Cpx
Am
Am
Mag
Pl
1000 µm
(b)
Pl
Ol
Pl
Pl
Pl
1000 µm
(c)
Pl
V
Cpx
Cpx
Pl
Pl
Pl
1000 µm
(d)
Cpx
Pl
Am
Cpx
V
Am
Am
Mag
V
(e)
Am
V
V
Mag
Pl
Cpx
Am
V
V
1000 µm
(f)
Pl
Cpx
Pl
Pl
Cpx
Cpx
Mag
Cpx
1000 µm
(g)
Pl
Mag
Pl
Cpx
V
Cpx
V
V
1000 µm
(h)
Cpx
Mag
rr
rr
V
Am
Am
Pl

(Camus et al. 2000). Overall, plagioclase phenocryst and microphenocryst compositions range from An_{25} to An_{96} (del Marmol 1989; Andreastuti 1999; Camus et al. 2000; Preece 2014), with variations within a single sample and individual crystals up to 60 mol% and more than 40 mol% anorthite (An), respectively (Gertisser 2001). In some samples, clear and inclusion-free plagioclase phenocrysts are characterised by large homogeneous, anorthite-rich cores (> ~ An_{90}) and thin rims of more albitic compositions. Such crystals typically constitute only a small proportion of the plagioclase population of a sample but may occur in the basaltic and more evolved rock types, spanning the entire geological history from the oldest units through to the recent eruptive products (del Marmol 1989; Gertisser 2001; Chadwick et al. 2007, 2013; Preece 2014). A rare group of mostly fairly albitic (An_{55-60}), untwined, inclusion-free and anhedral crystals up to 0.5 mm in size is present primarily in the basalts (del Marmol 1989). Plagioclase microlites are generally more albitic in composition than phenocrysts and microphenocrysts (Camus et al. 2000), however they may contain up to ~ 84 mol% An (Preece 2014). In some of the recent dome rocks and pyroclastic material, plagioclase microlites are often mantled by alkali element-rich rims of anorthoclase and more K-rich alkali feldspar (sanidine) with up to 58 mol.% orthoclase (Camus et al. 2000; Hammer et al. 2000; Preece 2014; Preece et al. 2023, Chap. 9).

Clinopyroxene (Fig. 6.21b) occurs in essentially all Merapi volcanic rocks as phenocrysts, microphenocrysts and groundmass microlites. Phenocrysts are typically euhedral to subhedral, unzoned or only weakly zoned with continuous changes in composition, and often host silicate melt (glass) inclusions, as well as inclusions of magnetite, plagioclase and apatite (Gertisser 2001; Preece 2014). Some clinopyroxenes are discontinuously zoned with abrupt compositional changes between core regions and outer zones. In a few samples, clinopyroxene can be found as overgrowth rims on earlier formed orthopyroxene crystals. The clinopyroxene phenocrysts of Merapi are augite (< 45 mol% wollastonite (Wo)) and diopside (> 45 mol% Wo) with a range of $Wo_{39-51}En_{34-50}Fs_{4-19}$, following the classification scheme of Morimoto (1988) (Fig. 6.21b). Al_2O_3 concentrations vary between 0.4 and 8.9 wt%; magnesium numbers (Mg# = 100 × Mg/Mg + Fe^{2+} (molar)) between 73 and 85 (Andreastuti 1999; Camus et al. 2000; Gertisser 2001; Costa et al. 2013; Preece 2014; Deegan et al. 2016). High-Al compositions, which may also be enriched in Cr, occur as corroded, xenocrystic cores in abruptly zoned clinopyroxene crystals (Gertisser 2001). Clinopyroxene microphenocrysts and microlites analysed in the 2010 eruptive products are also usually augite and diopside ($Wo_{40-50}En_{35-45}Fs_{13-21}$), with 0.8–7.6 wt% Al_2O_3 and Mg# 65–81, with most between Mg# 70–80 (Preece 2014). However, several crystals with higher Fe content also occur and are classed as hedenbergite ($Wo_{49-50}En_{8-21}Fs_{29-41}$), with 1.2–2.6 wt% Al_2O_3 and Mg# 19–47 (Fig. 6.21b). These crystals were exclusively found in the 2001 dome rocks near a calc-silicate xenolith (Preece 2014).

Orthopyroxene phenocrysts and microphenocrysts (Fig. 6.21b) are homogeneous in composition or slightly normally zoned with higher Fe/Mg ratios towards the rims. With an overall compositional range of $En_{60-71}Fs_{26-36}Wo_{1-8}$, they may be classified as enstatite or, if the Wo component exceeds 5 mol%, formally as pigeonite in the Morimoto (1988) scheme (Gertisser 2001; Preece 2014). The Mg# of the orthopyroxenes varies between 66 and 76 and is always lower than that of clinopyroxenes in the same sample (Gertisser 2001).

Fig. 6.21 Mineral (phenocryst and microphenocryst) compositions in volcanic rocks from the main volcanostratigraphic units of Merapi. **a** Feldspars (Ab-An-Or). **b** Pyroxenes (Wo-En-Fs) and olivine (Fo-Fa). **c** Amphiboles: (Mg/Mg + Fe^{2+}) versus Si (pfu) plot for calcic amphiboles in the classification scheme of Leake et al. (1997); Cl (per formula unit; pfu) versus F (pfu) in Merapi amphiboles. **d** Homogeneous and exsolved titanomagnetites in the system Fe^{2+}–Fe^{3+}–Ti. **e** Cr-rich spinels and titanomagnetite in lavas from Gunung Turgo, Gunung Plawangan and Gunung Medjing in the system Cr–Al–Fe^{3+}. Symbols keyed to Fig. 6.9. *Data Source* Gertisser (2001) ▶

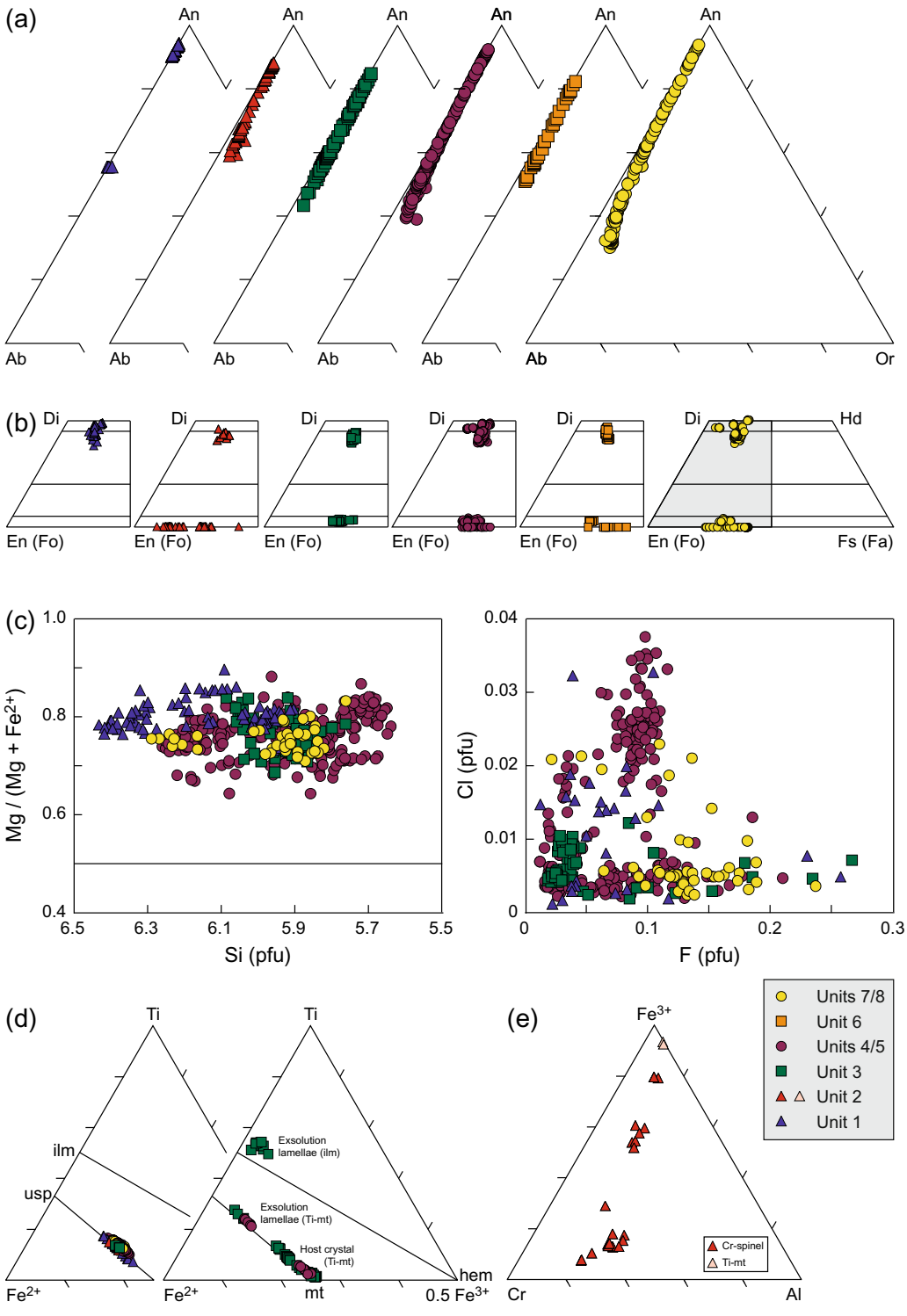
(a)
An
An
An
An
An
An
Ab
Ab
Ab
Ab
Ab
Ab
Or
(b)
Di
Di
Di
Di
Di
Di
Hd
En (Fo)
En (Fo)
En (Fo)
En (Fo)
En (Fo)
En (Fo)
Fs (Fa)
(c)
1.0
0.8
0.6
0.4
Mg / (Mg + Fe2+)
6.5
6.3
6.1
5.9
5.7
5.5
Si (pfu)
0.04
0.03
0.02
0.01
0
Cl (pfu)
0
0.1
0.2
0.3
F (pfu)
(d)
Ti
Ti
ilm
usp
Exsolution lamellae (ilm)
Exsolution lamellae (Ti-mt)
Host crystal (Ti-mt)
Fe2+
Fe2+
mt
hem
0.5 Fe3+
(e)
Fe3+
Cr-spinel
Ti-mt
Cr
Al
Units 7/8
Unit 6
Units 4/5
Unit 3
Unit 2
Unit 1

Olivine phenocrysts and microphenocrysts (Fig. 6.21b) have forsterite (Fo) contents ranging from 56 to 88 mol%. Olivines with more than 80 mol% Fo are largely restricted to the basalts of Gunung Turgo, Gunung Plawangan and Gunung Medjing, where they occur as individual crystals or, more often, in crystal clots, while the more Fe-rich olivines (< Fo 65) are found in the younger eruptive products (del Marmol 1989; Gertisser 2001; Camus et al. 2000). In rare cases, phenocrysts exhibit reaction rims of orthopyroxene. Olivine is either unzoned or normally zoned with gradational changes from Mg-rich cores to more Fe-rich rims, and variations in Fo content up to 20 mol% in individual crystals. In the Gunung Turgo, Gunung Plawangan and Gunung Medjing basalts, zoned crystals with Mg-rich cores (Fo ~ 87–88) and thin, Fe-rich rims (Fo ~ 70) occur together with randomly distributed, unzoned olivines of Fo ~ 70 (del Marmol 1989; Gertisser 2001). The high-Mg olivine crystals or crystal cores are interpreted as xenocrysts that crystallised from a near-primary basaltic melt and were subsequently incorporated into a more differentiated magma.

Amphibole (Fig. 6.21c) in the Merapi volcanic rocks occurs as phenocrysts and microphenocrysts but is absent in the groundmass. It can be a major constituent of glomerocrysts and magmatic cumulate inclusions, and is found occasionally as megacrysts up to several centimetres long (e.g. Peters et al. 2017; Troll and Deegan 2023, Chap. 8). Euhedral amphiboles in equilibrium with the surrounding melt typically occur in pumiceous or scoriaceous clasts from pyroclastic fall or PDC deposits associated with larger explosive eruptions (Gertisser 2001; Gertisser et al. 2011), although fresh amphiboles without or with only minimal breakdown textures also occur in some recent dome lavas, e.g. in the 2010 lava dome (Preece 2014). Where amphibole is not in contact with glass, such as in magmatic cumulates, it also lacks a reaction rim. In most Merapi volcanic rocks, however, amphibole crystals are surrounded by reaction rims composed of small plagioclase, pyroxene (or olivine) and titanomagnetite, corresponding to the gabbroic type of Garcia and Jacobson (1979). In several lava samples, amphibole breakdown rims of the black type occur, i.e. those without plagioclase (Garcia and Jacobson 1979). In cases where the amphibole has completely reacted, only amphibole relicts or pseudomorphs composed of titanomagnetite remain. The gabbroic type is considered as a result of slow magma ascent from depth during effusive eruptions, whereas the black type is thought to originate from oxidation, dehydrogenation and cooling during or after lava or dome extrusion. Compositionally, all Merapi amphiboles are calcic amphiboles (Leake et al. 1997), which, depending on the assumed ferric iron content, can be classified as either magnesiohastingsite ($Al^{VI} < Fe^{3+}$) or pargasite ($Al^{VI} > Fe^{3+}$) (Camus et al. 2000; Gertisser 2001; Preece 2014; Peters et al. 2017; Fig. 6.21c). Crystals are either homogeneous in composition or, occasionally, normally or reversely zoned, with rims containing either lower or higher Mg/Fe ratios than the cores. Where zoning is present, it can be either continuous or characterised by abrupt compositional changes. Core-rim variations are also observed with respect to Al_2O_3, which ranges from 10.3 to 14.3 wt% in total. The Mg# of the amphiboles varies between 57 and 84 (Gertisser 2001; Preece 2014). Available data for Cl and F concentrations in Merapi amphiboles suggest the presence of both Cl- and F-dominated varieties (Gertisser 2001; Fig. 6.21c).

Titanomagnetite microphenocrysts or inclusions in plagioclase, pyroxene and amphibole (Fig. 6.21d) are typically anhedral or irregularly shaped. They span a wide compositional range in ulvöspinel content between 12 and 85 mol%, although compositions are often more uniform in specific rock types (del Marmol 1989; Camus et al. 2000; Gertisser 2001; Preece 2014). Titanomagnetite is always present in moderate amounts in the basaltic andesites, whereas it is relatively rare, and occasionally absent, in the basalts of Gunung Turgo, Gunung Plawangan and Gunung Medjing (del Marmol 1989; Gertisser 2001). In some samples, titanomagnetite shows lamellar exsolution, a feature that is prevalent in the lavas of the Somma-Merapi and the recent domes, but commonly absent in the

products of larger explosive eruptions. In addition to these exsolved titanomagnetites, a homogeneous population may occur in the same samples, although perhaps more often, exsolution can affect all titanomagnetite crystals (Gertisser 2001; Preece 2014). Most exsolution lamellae are of the trellis type that consist of ilmenite lamellae parallel to the {111} planes of the titanomagnetite host and result from slow cooling of the lavas below the solidus with accompanying oxidation (Buddington and Lindsley 1964; Haggerty 1993). Rarely, exsolution of a spinel phase of the magnetite-ulvöspinel solid solution series occurs (Gertisser 2001; Fig. 6.21d).

Cr-spinel (Fig. 6.21e) forms rare inclusions in some of the Mg-rich (Fo ~ 87–88 mol%) olivines in the basaltic lavas of Gunung Turgo, Gunung Plawangan and Gunung Medjing. The Cr-spinels contain variable concentrations of Cr_2O_3 (6.0–44.4 wt%), Al_2O_3 (4.5–16.5 wt%), Fe_2O_3 (10.5–55.9 wt%) and MgO (2.3–11.4 wt %), with corresponding notable variations in molar Cr/(Cr + Al), Al/(Al + Cr + Fe^{3+}), Fe^{3+}/(Al + Cr + Fe^{3+}) and Mg/(Mg + Fe^{2+}) (Gertisser 2001), and a large compositional spread in a ternary Fe^{3+}–Cr–Al diagram (Fig. 6.21e).

Apatite is present as anhedral inclusions within clinopyroxene, plagioclase and amphibole phenocrysts, and rarely as groundmass microlites. Apatite in the 2010 eruptive products contain 0.4–1.4 wt% Cl, 1.1 to 5.4 wt% F and 0.4–1.0 wt% H_2O (Preece 2014; Li et al. 2021).

Biotite has been noted as a late crystallising phase of likely magmatic origin in the light grey inclusion material of the 2010 lava dome (Preece 2014). Costa et al. (2013) also noted the presence of biotite in 2010 samples. Biotite contains between 11.9 and 15.6 wt% FeO, with Mg# between 63 and 70. Fluorine and Cl vary between 0.5 and 3.8 wt% and 0.1–0.3 wt%, respectively (Preece 2014).

Cristobalite also occurs in the inclusions in the 2010 dome rocks where it fills small vesicles and is pervasive within the groundmass, often with 'fish-scale' cracked morphology or a microbotryoidal texture (Preece 2014). However, cristobalite is not restricted to this lithology and has previously been noted as vesicle infill in several lava samples of the Somma-Merapi and some lava dome clasts in PDC deposits of the Holocene Pyroclastic Series (Gertisser 2001). Analyses from the 2010 samples (Preece 2014) show that cristobalite contains small amounts of Al_2O_3 (up to 1.73 wt%) and Na_2O (up to 0.99 wt%).

6.3.3 Major and Trace Element Compositions

Whole-rock variation diagrams of selected major and trace elements vs SiO_2 for Merapi are shown in Fig. 6.22. In general, the rocks of medium-K and high-K character, identified in Fig. 6.18b, do not display significant differences in major element oxides other than K_2O. Discernible trends can be observed for most if not all major element oxides with SiO_2, although the data for some elements are rather scattered. Overall, TiO_2, Fe_2O_3*, MgO and CaO abundances decrease with increasing SiO_2 content, while Na_2O, despite considerable scatter, and Na_2O increases. Unusually low Na_2O concentrations are found in some samples of the Holocene Pyroclastic Series (HPS) and are thought to reflect low-temperature alteration of volcanic glass by meteoric water mobilising and removing sodium. The Al_2O_3 content of the rocks always exceeds 16 wt% and is scattered without any systematic correlation with SiO_2. Extremely high Al_2O_3 contents (> 21 wt%) occur only in highly altered samples with > 2.5 wt% loss on ignition (LOI) (Gertisser 2001; Gertisser and Keller 2003b). The trace element variations with SiO_2 are generally more scattered than the major element data but systematic trends are nevertheless apparent. Concentrations of incompatible trace elements, such as the large ion lithophile elements (LILE) Rb and Ba, increase systematically with increasing SiO_2 content, and the variations of these elements mirror that of K_2O, with higher Rb and Ba concentrations in the more K_2O-rich rocks. In accordance with other high field strength elements (HFSE), Zr increases systematically with increasing SiO_2 content, with some samples of the HPS plotting above the main Merapi trend.

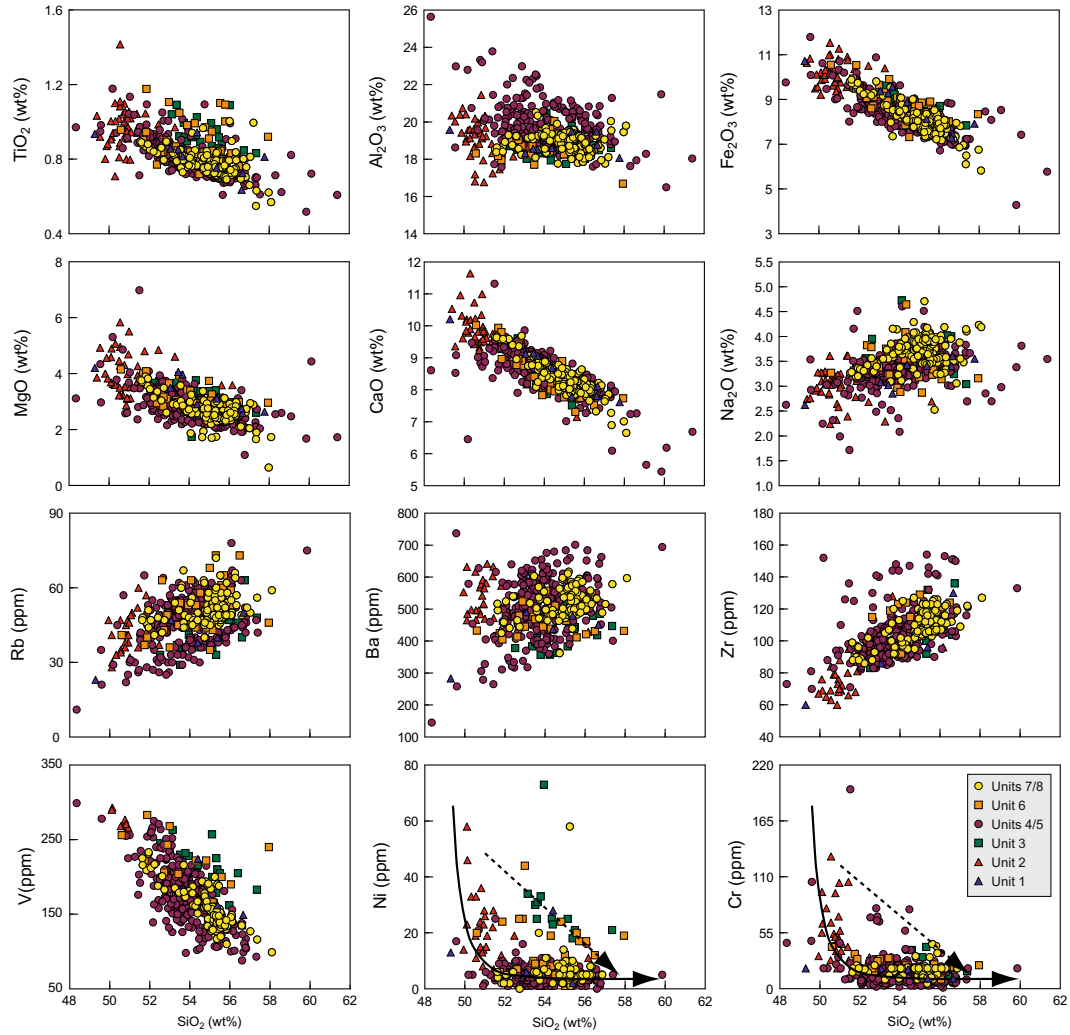

Fig. 6.22 Selected major and trace element variation diagrams vs SiO_2 for the Merapi volcanic suite. Major element analyses are normalised to 100 wt%, free of volatiles. General fractional crystallisation trends (solid line) and magma mixing trends (dashed line) are shown in the Ni versus SiO_2 and Cr versus SiO_2 diagrams. Symbols keyed to Fig. 6.9. *Data Sources* as in Fig. 6.18

Among the transition elements, V shows near-linear negative correlation with SiO_2, whereas both Ni and Cr display a main curvilinear trend of strongly decreasing abundance in the basalt range that becomes less pronounced in the more SiO_2-rich rock types. Additionally, some samples of intermediate composition display anomalously high Cr and Ni contents and follow a linear trend of decreasing Ni and Cr abundances with increasing SiO_2 content. It should be noted, however, that the lowest concentrations of both elements are at the analytical level of detection.

The trace element patterns of the Merapi volcanic rocks normalised to N-MORB are those typical of magmas from subduction-related tectonic settings. They are all remarkably similar, with enrichment in LILE, U and Th, a pronounced Pb peak in many samples and moderate enrichment in light rare earth elements (LREE) relative to the heavy rare earth elements (HREE) and the

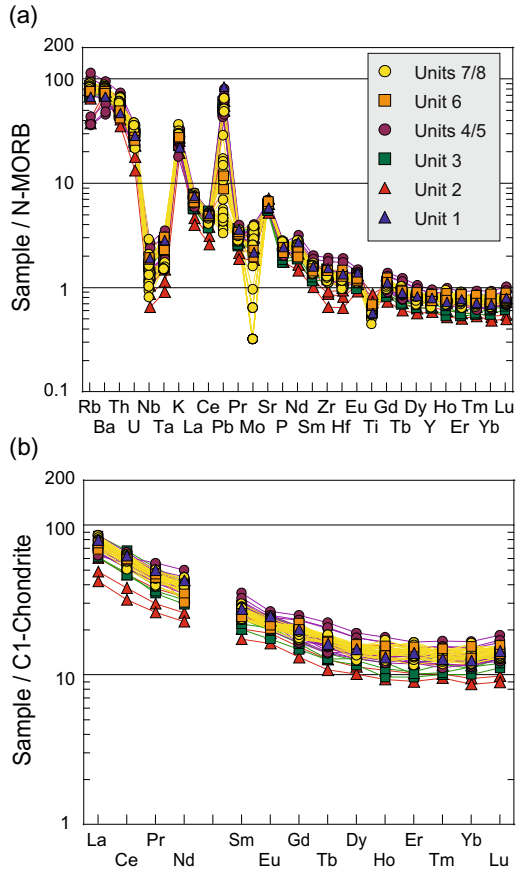

Fig. 6.23 **a** N-MORB-normalised trace element and **b** chondrite-normalised REE patterns for Merapi lavas and pyroclastic rocks. The normalising values are from Sun and McDonough (1989). Symbols keyed to Fig. 6.9. *Data Sources* Gertisser (2001), Gertisser and Keller (2003a, b), Handley et al. (2011); Gertisser et al. (2012a, b, c), Preece (2014) and this study

high field strength elements (HFSE). The elements Nb, Ta and Ti form distinct negative troughs in the trace element patterns, as does Mo in a few samples. In all rocks, the HREE are slightly depleted relative to N-MORB (Fig. 6.23a).

In a chondrite-normalised REE diagram (Fig. 6.23b), the Merapi volcanic rocks exhibit similar patterns, with fractionated LREE and relatively flat or slightly concave up HREE patterns, a typical feature of subduction-related volcanic rocks. However, there is a general lack of a pronounced Eu anomaly in all samples, or only a small negative or positive EU anomaly present ((Eu/Eu* = 0.85–1.07). LREE (La) enrichment ranges from 42 to 86 times chondritic values, with $(La/Sm)_N$ = 1.9–3.4 and $(La/Yb)_N$ = 4.1–7.0. Middle rare earth elements (MREE) and HREE show unfractionated patterns ($(Gd/Yb)_N$ = 1.3–1.7), generally within 9–25 times chondritic values.

6.3.4 Isotopic Compositions

6.3.4.1 Radiogenic Isotopes

Sr, Nd, Hf and Pb isotopic ratios exist for whole rock samples spanning the entire geological history of Merapi, as well as a small number of magmatic minerals, plutonic inclusions, calc-silicate xenoliths and limestones from the local upper crust.

The $^{87}Sr/^{86}Sr$ ratios of the Merapi volcanic rocks (lavas and pyroclastic rocks) display significant variations between 0.70480 and 0.70594, while $^{143}Nd/^{144}Nd$ ratios range from 0.51267 to 0.51280 (Whitford 1975a, b; Whitford et al. 1981; White and Patchett 1984; del Marmol 1989; McDermott and Hawkesworth 1991; Gertisser 2001; Turner and Foden 2001; Woodhead et al. 2001; Gertisser and Keller 2003b; Debaille et al. 2006; Handley et al. 2011, 2014, 2018; this study). Systematic differences in Sr and Nd isotopic ratios are most pronounced between the rocks of medium-K and high-K type, with the latter typically characterised by higher $^{87}Sr/^{86}Sr$ and lower $^{143}Nd/^{144}Nd$ (Gertisser 2001; Gertisser and Keller 2003b). Variations in Sr and Nd isotopic ratios with whole rock SiO_2 content are negligible. $^{87}Sr/^{86}Sr$ ratios (0.70568–0.70627) of plagioclase phenocrysts in recent Merapi volcanic rocks may exceed those of the whole rocks (Chadwick et al. 2007; Troll and Deegan 2023, Chap. 8). Plutonic xenoliths have a comparatively narrow range of $^{87}Sr/^{86}Sr$ (0.70529–0.70575) and $^{143}Nd/^{144}Nd$ (0.51257–0.51272), largely within the range of the volcanic rocks. Generally higher $^{87}Sr/^{86}Sr$ (0.70567–0.70787) and lower $^{143}Nd/^{144}Nd$ (0.51215–0.51272) are reported for calc-silicate xenoliths, including xenolith-hosted plagioclase crystals, and the

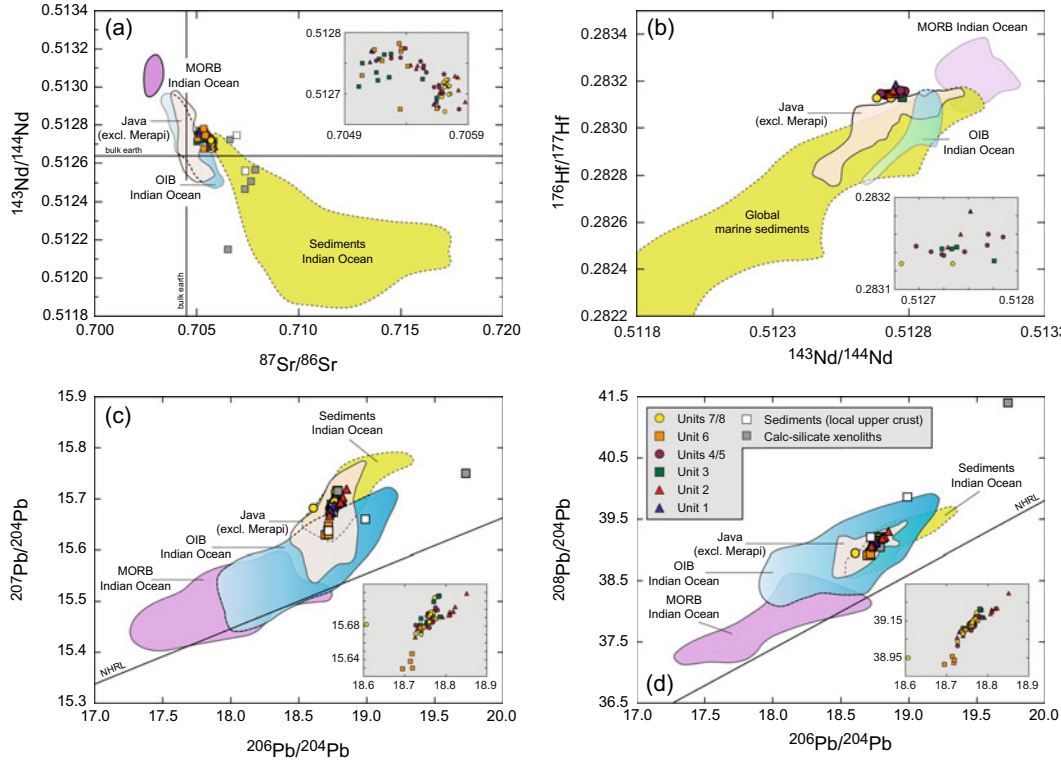

Fig. 6.24 Radiogenic isotope geochemistry of the main volcano-stratigraphic units of Merapi in relation to Indian Ocean MORB and OIB, volcanic rocks from Java and Indian Ocean marine sediments. Where available, isotopic data of sediments from the local upper crust and calc-silicate xenoliths in the Merapi lavas are also shown. **a** $^{143}Nd/^{144}Nd$ versus $^{87}Sr/^{86}Sr$ diagram. For *Data Sources*, see Gertisser et al. (2003b). Additional Sr and Nd isotopic data for Merapi are from Debaille et al. (2006), Handley et al. (2011, 2014, 2018) and this study; further calc-silicate xenolith data are from Chadwick et al. (2013). **b** $^{176}Hf/^{177}Hf$ versus $^{143}Nd/^{144}Nd$ diagram. The Merapi Hf isotopic data displayed are from Handley et al. (2011). For *Data Sources* for the Indian Ocean MORB and OIB fields in Hf–Nd space, see Gertisser et al. (2012c). The Java field was compiled with data from White and Patchett (1984), Woodhead et al. (2001) and Handley et al. (2007, 2008, 2011). **c**, **d** $^{207}Pb/^{204}Pb$ and $^{208}Pb/^{204}Pb$ versus $^{206}Pb/^{204}Pb$ diagram. NHRL denotes the Northern Hemisphere Reference Line. Symbols of volcano-stratigraphic units keyed to Fig. 6.9. For *Data Sources*, see Gertisser et al. (2003b). Additional Pb isotopic data for Merapi are from Debaille et al. (2006) and Handley et al. (2014); further calc-silicate xenolith data from Chadwick et al. (2013)

local upper crust (Gertisser 2001; Gertisser and Keller 2003b; Chadwick et al. 2007, 2013; Troll et al. 2013a, b; Troll and Deegan 2023, Chap. 8). In the $^{143}Nd/^{144}Nd$ versus $^{87}Sr/^{86}Sr$ diagram (Fig. 6.24a), the Merapi eruptive products are broadly negatively correlated and form a cluster below the field for mid-ocean ridge basalt (MORB). The Merapi data plot between the field for MORB and sediments from the Indian Ocean, partly overlap the field of Indian Ocean island basalts and are displaced to somewhat higher $^{87}Sr/^{86}Sr$ at similar $^{143}Nd/^{144}Nd$ values compared with many Javanese volcanoes. The upper crustal basement beneath Merapi and calc-silicate xenoliths plot near the unradiogenic end of the Sr isotopic spectrum of the Indian Ocean sediments, while $^{143}Nd/^{144}Nd$ is more scattered.

Hf isotopic data are available for a smaller whole rock sample set, with $^{176}Hf/^{177}Hf$ showing a compositional range between 0.28304 and 0.28319 (White and Patchett 1984; Woodhead et al. 2001; Handley et al. 2011) and no systematic variations with whole rock SiO_2 or K_2O content. In Hf–Nd isotopic space (Fig. 6.24b),

the Merapi rocks have amongst the highest Hf isotopic ratios of all Javanese volcanoes, plot near to, but are distinct from, the Indian Ocean MORB and OIB fields, and also fall outside the published range for global marine sediments.

$^{206}Pb/^{204}Pb$, $^{207}Pb/^{204}Pb$ and $^{208}Pb/^{204}Pb$ range from 18.601 to 18.851, 15.607 to 15.736 and 38.621 to 39.300, respectively (Whitford 1975a, b; del Marmol 1989; McDermott and Hawkesworth 1991; Gertisser 2001; Turner and Foden 2001; Woodhead et al. 2001; Gertisser and Keller 2003b; Debaille et al. 2006; Handley et al. 2014). In contrast to the Sr and Nd isotopic ratios, there are no apparent systematic variations in Pb isotopic ratios between rocks of medium-K and high-K type and with indices of magmatic differentiation (Gertisser 2001; Gertisser and Keller 2003b). Ratios of $^{206}Pb/^{204}Pb$ (18.706–18.849), $^{207}Pb/^{204}Pb$ (15.654–15.695) and $^{208}Pb/^{204}Pb$ (39.041–39.178) of plutonic xenoliths lie within the range of the volcanic rocks (Chadwick et al. 2013; Troll and Deegan 2023, Chap. 8). Calc-silicate xenoliths and the local upper crust show more pronounced variations in $^{206}Pb/^{204}Pb$ (18.720–19.728), $^{207}Pb/^{204}Pb$ (15.660–15.750) and $^{208}Pb/^{204}Pb$ (39.043–41.440) (Gertisser 2001; Gertisser and Keller 2003b; Chadwick et al. 2013; Troll and Deegan 2023, Chap. 8). Well-defined positive correlations can be observed in diagrams of $^{207}Pb/^{204}Pb$ and $^{208}Pb/^{204}Pb$ versus $^{206}Pb/^{204}Pb$ (Fig. 6.24c, d), where the Merapi data plot near and beyond the radiogenic $^{206}Pb/^{204}Pb$ end of the Indian Ocean MORB field. $^{207}Pb/^{204}Pb$ and $^{208}Pb/^{204}Pb$ ratios for Merapi are higher than typical Indian Ocean MORB values, and within the range of Java volcanic rocks and Indian Ocean marine sediments, which generally overlap with the field of the Merapi eruptive products in plots of $^{207}Pb/^{204}Pb$ and $^{208}Pb/^{204}Pb$ vs $^{206}Pb/^{204}Pb$. The Merapi rocks plot well above the Northern Hemisphere Reference Line (NHRL) and close to or within the field of Indian Ocean OIB field in diagrams of $^{207}Pb/^{204}Pb$ and $^{208}Pb/^{204}Pb$ versus $^{206}Pb/^{204}Pb$, respectively. Calc-silicate xenoliths and the local upper crust overlap with the field of the Merapi eruptive products or plot towards more radiogenic Pb isotopic compositions, although $^{207}Pb/^{204}Pb$ values only marginally exceed those of the Merapi volcanics.

6.3.4.2 Oxygen Isotopes

A total of 44 whole rock oxygen isotope analyses are currently available for Merapi (Gertisser 2001; Gertisser and Keller 2003b; Troll et al. 2013a, b; Handley et al. 2014; Drignon et al. 2016). These are complemented by oxygen isotope data for magmatic crystals, plutonic and crustal xenoliths as well as sediments of the local upper crust (Gertisser 2001; Gertisser and Keller 2003b, Troll et al. 2013a; Deegan et al. 2016, 2021, 2023, Chap. 10; Whitley et al. 2019, 2020; Whitley 2020; Troll and Deegan 2023, Chap. 8).

$\delta^{18}O$ values in the basalt to andesite whole rocks range from + 6.0‰ to + 8.3‰ (SMOW) (Gertisser 2001; Gertisser and Keller 2003b). These values exceed typical mantle and basaltic oceanic crust values ($\delta^{18}O$ = + 5.37 to + 5.81‰ (SMOW), average of 5.50‰; Eiler et al. 2000). Gertisser (2001) and Gertisser and Keller (2003b) observed the highest $\delta^{18}O$ values in pumiceous rocks and proposed that this reflects an increase in $\delta^{18}O$ by low-temperature alteration via hydration and oxygen exchange between the glassy groundmass and meteoric water. More recently, however, whole rock $\delta^{18}O$ values as high as + 8.3‰ have also been measured in recent, unaltered basaltic andesites (Troll et al. 2013a). A similar range in oxygen isotope ratios was observed in medium-K and high-K rock varieties (Gertisser 2001; Gertisser and Keller 2003b). $\delta^{18}O$ values of phenocrysts range from + 4.6‰ to + 7.9‰ and 4.3‰ to + 8.1‰ for plagioclase and pyroxene, respectively (Troll et al. 2013a; Borisova et al. 2016; Deegan et al. 2016, 2021; Troll and Deegan 2023, Chap. 8). Such values correspond to melt $\delta^{18}O$ values of up to + 7.7‰ ($\delta^{18}O_{plag}$ (melt)) and up to + 8.4‰ (($\delta^{18}O_{pyx}$ (melt)), assuming mineral-melt fractionation factors of + 0.2 for plagioclase and −0.3 for pyroxene (Harris et al. 2005 and references therein). Plutonic xenoliths have $\delta^{18}O$ between + 6.5‰ to + 6.8‰, well within the range of the basaltic to andesitic whole rocks. Plagioclase and pyroxene within these xenoliths

display a narrow $\delta^{18}O$ range from + 5.4‰ to + 5.8‰ and 6.0‰ to + 6.2‰, respectively (Troll et al. 2013a; Troll and Deegan 2023, Chap. 8). Limestones from the local upper crust are characterised by $\delta^{18}O$ between + 18.9 and + 24.5, while calc-silicate xenoliths in the Merapi lavas generally have lower $\delta^{18}O$ between + 10.4‰ to + 14.2‰ (Gertisser 2001; Gertisser and Keller 2003b; Troll et al. 2013a), as a result of magma-carbonate interaction (e.g. Deegan et al. 2023, Chap. 10).

6.3.4.3 Uranium Series Isotopes

Disequilibria between short-lived radionuclides of the uranium decay chain are powerful indicators of magmatic processes and their timescales (e.g. Bourdon et al. 2003). Short-lived uranium series isotopes were measured relatively frequently in Merapi whole rocks and in a few plagioclase crystals, mostly, but not exclusively, in recent eruptive products. Here, we summarise published ^{238}U–^{230}Th–^{226}Ra isotope data for Merapi (Gill and Williams 1990; McDermott and Hawkesworth 1991; Condomines and Sigmarsson 1993; Gauthier and Condomines 1999; Turner and Foden 2001; Condomines et al. 2005; Handley et al. 2018).

Most of the Merapi whole rock samples, as well as the few plagioclase separates analysed (Handley et al. 2018), show uranium excesses [($^{238}U/^{230}Th$] activity ratios > 1), typical of subduction-related volcanic rocks. However, a small number of samples, including a clinopyroxene and a magnetite separate analysed, display small Th excesses [($^{238}U/^{230}Th$] activity ratios < 1) (Gill and Williams 1990; Condomines et al. 2005; Turner and Foden 2001). ($^{230}Th/^{232}Th$) activity ratios range from 0.627 to 0.821, with some of the higher whole rock values coming from earlier studies which were mostly produced by alpha spectrometry (Fig. 6.25a). The vast majority of Merapi whole rock samples and plagioclase separates are also characterised by excess radium [($^{226}Ra/^{230}Th$] activity ratios > 1), with most samples showing ($^{226}Ra/^{230}Th$) ratios between 3.0 and 3.4. The plagioclase separates from the 2006 and 2010 eruptions show similar ($^{226}Ra/^{230}Th$) ratios of 3.5–3.7, slightly higher than the whole rocks (Handley et al. 2018). Whole rock Ra excesses comparable to those of the 2006 and 2010 eruptions are observed in other historical and recent eruptions (Gill and Williams 1990; Gauthier and Condomines 1999; Condomines et al. 2005), while significantly lower Ra excesses, or even small Th excesses, are reported for some older whole rock samples (Turner and Foden 2001; Condomines et al. 2005) (Fig. 6.25b).

6.4 Magma Genesis and Magmatic Differentiation at Merapi

A broad petrogenetic model for Merapi involves the generation of primary magmas by partial melting of a heterogenous, Indian Ocean MORB-like mantle source, metasomatised by slab-derived fluid and melt components of the Sunda arc subduction system, followed by complex magmatic differentiation processes during magma storage and ascent through the crust that have led to systematic geochemical variations, as detailed in the following sections.

6.4.1 Magma Generation

The generation of primary Merapi magmas in the mantle, the geochemical and isotopic characteristics of the mantle source and the nature of subducted slab-derived components have been the subject of numerous studies, including those of Whitford (1975a, b), Whitford and Nicholls (1976), Whitford et al. (1979, 1981), White and Patchett (1984), McDermott and Hawkesworth (1991), Gertisser (2001), Turner and Foden (2001), Woodhead et al. (2001), Gertisser and Keller (2003b), Debaille et al. (2006) and Handley et al. (2011, 2014, 2018), Deegan et al. (2016, 2021).

The mantle source of the Merapi magmas is thought to be similar to that of Indian Ocean mid-ocean ridge basalts (MORB), overprinted by slab-derived components that have caused heterogeneous changes in the geochemical and isotopic composition of the mantle wedge

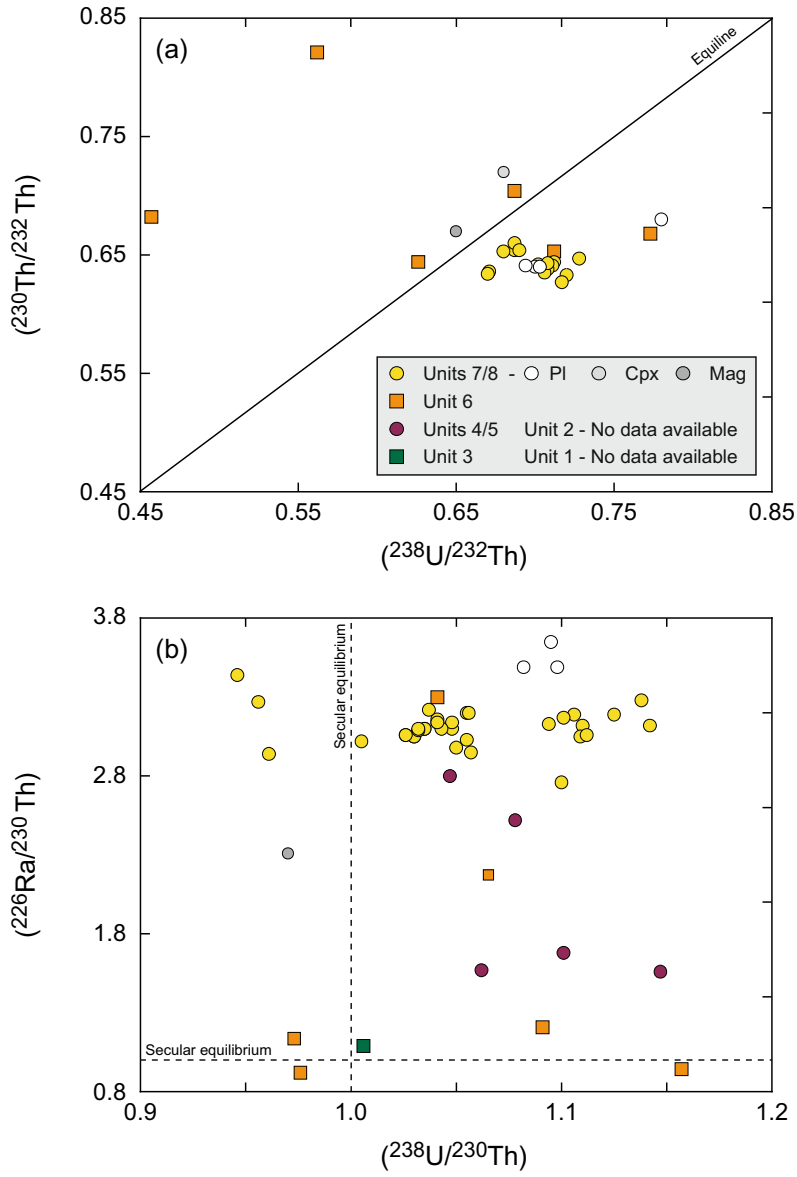

Fig. 6.25 **a** ($^{238}U/^{232}Th$) versus ($^{230}Th/^{232}Th$) equiline diagram and **b** ($^{226}Ra/^{230}Th$) versus ($^{238}U/^{230}Th$) plot for Merapi whole-rocks (coloured symbols) and some mineral separates (Pl = plagioclase, Cpx = clinopyroxene; Mag = magnetite). Symbols keyed to Fig. 6.9. *Data Sources* Gill and Williams (1990), McDermott and Hawkesworth (1991), Condomines and Sigmarsson (1993), Gauthier and Condomines (1999), Turner and Foden (2001), Condomines et al. (2005) and Handley et al. (2018)

beneath the volcano. This is illustrated in Fig. 6.24, where the displacement of Merapi (and other Javanese volcanoes) from the field of Indian Ocean MORB field in terms of Sr, Nd, Pb and Hf isotopic ratios has been related mainly to mantle source contamination (Gertisser 2001; Gertisser and Keller 2003b; Handley et al. 2011, 2014). Both fluids from the subducted mafic oceanic lithosphere and a subducted Indian Ocean sediment component have been identified in the mantle source of the Merapi magmas based on trace element compositions and ratios as well as isotopic characteristics (del Marmol 1989; Gertisser 2001; Gertisser and Keller 2003b; Handley et al. 2011; Deegan et al. 2021). These include the LREE-enriched REE patterns, elevated LILE/HFSE, LREE/HFSE and Th/HFSE ratios compared with MORB, the negative Nb–Ta and Ti anomalies in multi-element normalised diagrams (Fig. 6.23a) and the Sr, Nd, Hf and Pb isotopic compositions (Fig. 6.24) that indicate the presence of a crustal component in the

Merapi magmas. This is further illustrated in the $\delta^{18}O$ versus $^{87}Sr/^{86}Sr$ diagram (Fig. 6.26), where the Merapi whole rock data plot in a narrow range towards the more radiogenic end of the Java field and are shifted from the MORB field to higher $^{87}Sr/^{86}Sr$. These features can be explained by variable degrees of mantle source contamination by a crustal component and suggest that a small percentage of sediment addition to the mantle wedge is sufficient to generate the Sr isotopic characteristics of primary magmas at Merapi (Gertisser 2001; Gertisser and Keller 2003b), a model that is consistent with oxygen isotopic compositions of Merapi pyroxenes (Deegan et al. 2021). Indicators of fluid addition from the slab to the mantle source also include the observed disequilibria between short-lived radionuclides of the uranium decay chain in the Merapi eruptive products (Fig. 6.25). Most of the whole rock samples analysed (Gill and Williams 1990; Gauthier and Condomines 1999; Turner and Foden 2001; Condomines et al. 2005; Handley et al. 2018) show both uranium and radium excesses. These values may be used to constrain the timescales of slab dehydration to < 375,000 years and < 8000 years for the $^{238}U/^{230}Th$ and $^{226}Ra/^{230}Th$ disequilibria to be preserved. Gertisser (2001) and Gertisser and Keller (2003b) argued that the contrasts between the geochemical and radiogenic isotope (e.g. $^{87}Sr/^{86}Sr$) compositions of medium-K and high-K rock types, together with the similar oxygen isotope ratios within both suites can be reconciled with a model of variable source enrichment by subducted

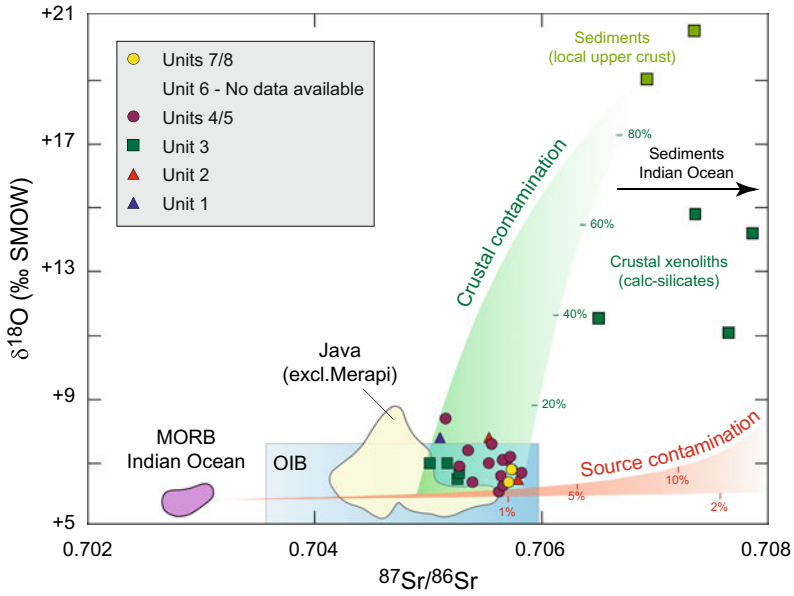

Fig. 6.26 $\delta^{18}O$ versus $^{87}Sr/^{86}Sr$ isotope diagram for Merapi whole rocks, Indian Ocean MORB and OIB, other volcanic rocks from Java, local upper crustal rocks, Merapi calc-silicate xenolits and Indian Ocean marine sediments, visualising the effects of both contamination of the mantle source (source contamination) and magma contamination in the crust (crustal contamination) on magmatic compositions at Merapi. Because of higher Sr concentrations in the crustal component than in the mantle source, source contamination produces mixing curves that are strongly concave upward reflecting large changes in $^{87}Sr/^{86}Sr$ ratios at nearly constant $\delta^{18}O$ values produced by relatively small amounts of contamination. By contrast, crustal contamination of magmas with initial Sr concentrations higher than those in the assimilated crustal material, more strongly affects $\delta^{18}O$ values than Sr isotope ratios (James 1981). Percentages of sediment or crust added are indicated along the mixing curves (after Gertisser and Keller 2003b). For *Data Sources*, see Gertisser et al. (2003b). The Java field has been updated with data from Handley et al. (2010); additional calc-silicate data are from Chadwick et al. (2013). Symbols keyed to Fig. 6.9. *Data Sources* for Merapi Sr isotopic data as in Fig. 6.24

sedimentary material (cf. Fig. 6.26). In their model, a slightly larger contribution from sediment-derived aqueous fluids and partial melts to the source of the high-K type compared to the medium-K magmas may account for the trace element and isotopic contrasts between the two suites, a compositional gap that coincides with the transition from the normal to the anomalous calc-alkaline association of the Sunda arc (Whitford 1975b). The contamination of a MORB-like mantle with sediments from the subducted slab has also been considered as an important process affecting the geochemical composition of the mantle source of other Quaternary volcanoes from Java and the Sunda arc in general (e.g. Turner and Foden 2001; Handley et al. 2010, 2014).

6.4.2 Magma Storage Conditions and Magmatic Differentiation

Magma storage conditions and magmatic differentiation processes affecting primary mantle-derived magmas during transfer through the crust and storage in crustal reservoirs were discussed in Bahar (1984), del Marmol (1989), Berthommier (1990), Andreastuti (1999), Gertisser (2001), Gertisser and Keller (2003a) and Handley et al. (2014, 2018) based on the geochemical and isotopic compositions of lavas and pyroclastic rocks and their constituent minerals. Additional studies addressed these issues using crystal isotope stratigraphy (e.g. Chadwick et al. 2007; Borisova et al. 2016; Peters et al. 2017), igneous inclusion petrology (e.g. Chadwick et al. 2013; Troll et al. 2013a; van der Zwan et al. 2013), melt inclusion studies (e.g. Nadeau et al. 2013; Preece et al. 2014), quantitative textural analysis (e.g. Innocenti et al. 2013a, b; van der Zwan et al. 2013), thermobarometry and thermodynamic modelling (e.g. Gertisser 2001; Chadwick et al. 2013; Costa et al. 2013; Nadeau et al. 2013; Erdmann et al. 2014; Preece et al. 2014, 2016; Deegan et al. 2016), phase equilibrium experiments (e.g. Erdmann et al. 2016) and detailed investigations of crustal xenoliths (e.g. Deegan et al. 2010; Borisova et al. 2013; Whitley et al. 2019, 2020; Whitley 2020). These aspects are discussed in detail in Troll and Deegan (2023, Chap. 8), Deegan et al. (2023, Chap. 10) and Preece et al. (2023, Chap. 9) and therefore only a brief synopsis is provided here.

A consensus appears to emerge of the existence of complex crustal magma storage system beneath Merapi, where magmas are stored in magma storage zones or reservoirs at different levels throughout the crust from around the crust-mantle boundary at ~ 25 km depth (Katili 1975) to less than a kilometre below the summit of the volcano, where the magma system is interpreted to consist of highly interconnected magma reservoirs (Preece et al. 2014; Troll and Deegan 2023, Chap. 8). The presence of amphiboles without reaction rims in pumiceous or scoriaceous clasts from explosive eruptions and crystals with no or relatively thin breakdown rims in some of the recent and Holocene lava dome components indicate that magmas feeding these eruptions rise quickly through these near-surface magma reservoirs outside the amphibole stability field (Gertisser 2001; Gertisser et al. 2011; Chadwick et al. 2013; Costa et al. 2013; Preece et al. 2013; Preece 2014; Peters et al. 2017). Most lava domes, however, contain amphiboles with thick reaction rims indicative of temporary magma storage at shallow depth, slow magma ascent or a combination of both (Gertisser 2001; Gertisser et al. 2011; Costa et al. 2013; Preece et al. 2013; Preece 2014). Later studies on rock samples from recent eruptions corroborated these ideas, adding evidence from groundmass textural variations (Preece et al. 2013, 2016, 2023, Chap. 9; Preece 2014), clinopyroxene diffusion timescales (Costa et al. 2013) as well as ^{210}Pb isotopic data that indicate less efficient degassing related to faster magma ascent and vice versa (Handley et al. 2018). Mineral chemical data and phase equilibria based on the quartz–ulvøspinel–ilmenite–fayalite (QUILF) algorithm (Andersen et al. 1993) suggest magmatic temperatures between ~ 920 and 1050 °C and oxygen fugacities (fO_2) for the Merapi magmas between 0.6 and 2.2 logarithmic units above the FMQ oxygen buffer (Gertisser 2001), a

range not unusual for subduction-related volcanic rocks. These values are like those derived from amphibole compositions (Erdmann et al. 2014). Melt inclusion studies imply magmatic H_2O contents, based on the volatiles-by-difference method (e.g. Devine et al. 1995), of up to 6.4 wt % (Gertisser 2001), and between 0.2 and 4.8 wt % H_2O based on direct analysis of pyroxene-hosted melt inclusions by secondary ion mass spectrometry and attenuated total reflectance micro-Fourier transform infrared spectroscopy (Preece et al. 2014). The highest H_2O contents are preserved in melt inclusions from explosive eruption products rather than from dome lavas (Gertisser 2001; Preece et al. 2014).

Strong evidence for polybaric fractional crystallisation, magma replenishment and associated magma mixing or mingling, crystal mush remobilisation, crystal recycling and crustal contamination as important processes of magmatic differentiation is provided by petrological, geochemical and isotopic data. The forsteritic olivines and their inclusions of Cr-spinel in the basaltic lavas from Gunung Turgo, Gunung Plawangan and Gunung Medjing document the earliest stages of differentiation of primary, mantle-derived magmas at Merapi (del Marmol 1989; Gertisser 2001). Crystallisation at high pressure of Cr-spinel, Mg-rich olivine and Al-rich clinopyroxene before eruption of the most primitive Merapi magmas is regarded as an important process that determines the behaviour of ferromagnesian elements such as Ni and Cr in the residual melt and ultimately controls the relatively low concentrations of these elements in the least differentiated Merapi magmas (del Marmol 1989; Gertisser 2001). Continued fractional crystallisation is considered a feasible process in the evolution of magmas of both medium-K and high-K character, which were interpreted to represent discrete magma series or magma differentiation trends from distinct parental magmas (Gertisser 2001; Gertisser and Keller 2003b). Support for this interpretation comes from (1) the overall increase of the alkalies, LILE and HFSE, and the decrease of TiO_2, Fe_2O_3*, CaO, MgO and ferromagnesian trace elements with increasing SiO_2 (Fig. 6.22), and (2) systematic changes in modal mineralogy, such as the occurrence of olivine as a major constituent exclusively in the basalts, the appearance of orthopyroxene at the expense of olivine in more evolved rock types, the increasing abundance of titanomagnetite with increasing SiO_2, and often late-stage crystallisation of amphibole. Collectively, the combined geochemical and petrographical characteristics indicate that magmatic differentiation at Merapi involves fractional crystallisation of a plagioclase-dominated mineral assemblage that includes clinopyroxene, olivine, orthopyroxene, titanomagnetite, amphibole and apatite. The absence of clinopyroxene in some of the basalts of Gunung Turgo, Gunung Plawangan and Gunung Medjing may suggest that olivine and plagioclase crystallisation precedes that of clinopyroxene (del Marmol 1989). Despite the important role of plagioclase fractionation, no significant Eu anomaly is observed in the Merapi rocks (Fig. 6.23b), likely due to the oxidised nature of the Merapi magmas (Gertisser 2001). The slightly concave up HREE patterns observed in some samples hint at amphibole fractionation at depth. Crystal clots and plutonic crystalline inclusions provide snapshots of these fractional crystallisation processes and provide unequivocal evidence for deep amphibole crystallisation, amphibole-bearing cumulate formation in the lower crust and crystal mush (cumulate) remobilisation (e.g. Chadwick et al. 2013; Erdmann et al. 2014; Peters et al. 2017; Troll and Deegan 2023, Chap. 8).

While fractional crystallisation appears to be a dominant magmatic differentiation process, there is compelling evidence for magma replenishment and associated mixing and mingling processes, typically accompanied by crystal recycling. These include the presence of complexly zoned crystals, in particular plagioclase and clinopyroxene (e.g. del Marmol 1989; Gertisser 2001; Chadwick et al. 2007; Borisova et al. 2016), mixed or bimodal mineral compositions (e.g. Erdmann et al. 2014) and clinopyroxene overgrowth rims around orthopyroxene (e.g. Gertisser 2001). Features of incomplete magma mixing or magma mingling, such as the presence of banded

pumiceous or scoriaceous clasts, exist but are less frequent (del Marmol 1989; Gertisser 2001; Gertisser and Keller 2003a; Troll et al. 2013a). Replenishment and mixing of primitive and more evolved magmas at Merapi may be responsible for intermediate compositions in the basaltic andesite range, characterised by Ni an Cr concentrations that are higher than those expected from fractional crystallisation (Fig. 6.22). The cyclical variations and gradual shifts towards more mafic compositions in the young tephra sequences of the Holocene Pyroclastic Series as well as during the historical to recent eruptions may therefore reflect magma mixing or mingling processes; these may result from continuous or periodic supply of primitive magma to a shallower magma storage zone, and progressive changes in the volume of intruding primitive to evolved magma residing at a shallower level (Gertisser and Keller 2003a). The relative monotony of magma compositions since the mid-twentieth century may imply the existence of a continuously active, small-volume, steady state magma reservoir where fractional crystallisation, magma recharge and eruption have been well balanced for erupting magmas to be essentially uniform in composition (Gertisser and Keller 2003a; Troll and Deegan 2023, Chap. 8).

Contamination and assimilation of crustal rocks during magma storage and ascent through the crustal basement at Merapi is best exemplified by the presence of predominantly calc-silicate crustal xenoliths in the eruptive products (Clocchiatti et al. 1982; del Marmol 1989; Camus et al. 2000; Gertisser and Keller 2003b; Chadwick et al. 2007, 2013; Deegan et al. 2010, 2023, Chap. 10; Troll et al. 2012, 2013a, b; Whitley et al. 2019, 2020; Whitley 2020). Magma-crust interaction is interpreted to be responsible for some of the isotopic variations within the Merapi suite, particularly the elevated $\delta^{18}O$ values up to 8.3‰ of Merapi compared to mantle values and above the MORB-sediment mixture in $\delta^{18}O$ versus $^{87}Sr/^{86}Sr$ space (Fig. 6.26), which can be reconciled by contamination of the parental magmas of the medium-K and high-K series rocks with crustal material compositionally similar to the calcareous sediments of the local upper crust. Such a model is further supported by elevated oxygen isotopic compositions of pyroxenes relative to mantle values and inferred source contamination trends (Deegan et al. 2021), and evidence from carbon and uranium-series isotopes (Berthommier 1990; Handley et al. 2018; Whitley et al. 2019; Whitley 2020). However, crustal contamination by a classic assimilation and fractional crystallisation (AFC) process (DePaolo 1981) or bulk crustal contamination during the evolution of the Merapi magmas appears to be negligible, as, for example, Sr, Nd and Pb isotopic ratios remain relatively unchanged or vary unsystematically with increasing SiO_2 content in both medium-K and high-K series rocks (Gertisser and Keller 2003b).

6.4.3 Magmatic Evolution of Merapi: Temporal Geochemical Variations

The geochemical evolution of Merapi through time was described by Bahar (1984), del Marmol (1989), Berthommer (1990), Andreastuti (1999), Andreastuti et al. (2000), Camus et al. (2000), Gertisser (2001), Gertisser and Keller (2003a, b) and Gertisser et al. (2012a). First order observations include (1) long-term geochemical variations over the much of the life-span of the volcano, such as the general tendency of increasing SiO_2 content from the lavas of Gunung Turgo, Gunung Plawangan and Gunung Medjing to the younger units of the volcanic complex (Bahar 1984; del Marmol 1989; Berthommer 1990; Camus et al. 2000; Gertisser 2001; Gertisser and Keller, 2003a, b; Gertisser et al. 2012a), and the transition from an older medium-K to a younger high-K series (Andreastuti 1999; Gertisser 2001; Gertisser and Keller 2003a, b; Gertisser et al. 2012a); (2) medium-term variations over timescales up to several thousands of years, where cyclical trends of increasing and decreasing SiO_2 content through time were identified (Bahar 1984; del Marmol 1989; Berthommier 1990; Andreastuti 1999; Camus et al. 2000; Gertisser 2001;

Gertisser and Keller 2003a); and (3) short-term variations that occur within a single eruption or eruption cycle, such as those during larger Holocene eruptions (Andreastuti 1999) or during the historical to recent period (del Marmol 1989; Berthommier 1990; Andreastuti 1999; Andreastuti et al. 2000; Camus et al. 2000; Gertisser 2001; Gertisser and Keller 2003a).

The compositional variation of the eruptive products (K_2O vs. SiO_2 classification diagram; Le Maitre et al. 2002) of the main volcano-stratigraphic units is illustrated in Fig. 6.27. Most units, including, for example, the lava flows of Gunung Bibi (Unit 1), show considerable variations in SiO_2 and/or K_2O content, comprising medium-K and high-K type compositions or are dominated by high-K compositions only. Basaltic andesitic rocks are most common in all volcano-stratigraphic units except for the lava flows of Gunung Turgo, Gunung Plawangan and Gunung Medjing (Unit 2), which are, for the most part, basalts of both medium-K and high-K type, but also comprise a few basaltic andesites of medium-K variety (del Marmol 1989). Most whole-rock geochemical analyses exist for the Holocene Pyroclastic Series (Units 4 and 5), which comprises the extensive volcaniclastic apron on the flanks of Merapi apart from the recent and historical pyroclastic density current and lahar deposits (Unit 7). Samples of the Holocene Pyroclastic Series range from basaltic to andesitic compositions, and variations in K_2O content clearly divide its eruptive products into medium-K and high-K types (Gertisser 2001; Gertisser and Keller 2003a, b; Gertisser et al. 2012a). Based on their stratigraphic and chronological data, the authors showed that the volcaniclastic deposits younger than ~ 1900 ^{14}C y BP are distinctly more K-rich than the older deposits of the Holocene Pyroclastic Series, with the transition from medium-K to high-K type coinciding with the inferred date of the sector collapse at the end of the Old Merapi stage, as proposed by Newhall et al. (2000). The compositional change was attributed to deep processes at the magma source (Gertisser and Keller 2003b), leaving a temporal link between this collapse event and the high-K magmas that erupted since ~ 1900 ^{14}C y BP unexplored. Similar shifts in magma compositions have been observed at other volcanoes such as Colima (Crummy et al. 2014), Bezymianny (Davydova et al. 2018), Stromboli (Francalanci et al. 2013) and Taranaki, a volcano that mirrors the geochemical variations observed at Merapi (Hatherton and Dickenson 1969; Stewart et al. 1996). Where these coincide with major structural modifications of the volcano, it was inferred that edifice instabilities were caused by injection of deep and compositionally distinct magma, or that edifice collapse led to subsequent changes in the composition of erupted magma through modifications of the architecture of the crustal magma plumbing systems. Such modifications may lead to enhanced decompression, opening of the system and increased magma flux rates, affect magma storage, ascent and differentiation processes, and provide a viable avenue for future structural, geochronological and petrological research at Merapi.

Based on their data, Gertisser (2001), Gertisser and Keller (2003a, b) and Gertisser et al. (2012a) included the lava flows of the Somma-Merapi (Unit 3) in their 'medium-K series', but the additional data presented here (Bahar 1984; del Marmol 1989; Berthommier 1990; Camus et al. 2000; Debaille et al. 2006) suggest that Somma-Merapi lavas contain higher K rock types also. By contrast, the picture of two distinct magmatic series and a shift from older medium-K to younger eruptive products of high-K type during the Late Holocene remains valid (Andreastuti 1999; Gertisser, 2001; Gertisser and Keller 2003a, b; Gertisser et al. 2012a). The young (post-Somma-Merapi) lava flows (Unit 6), the recent and historical pyroclastic density current and lahar deposits (Unit 7) and the lava domes of the recent episode (Unit 8) characteristically comprise volcanic products of high-K type, although subtle K_2O variations at a given SiO_2 content are apparent within the rocks of high-K affinity.

Furthermore, crude cyclical variations with systematic shifts in whole rock SiO_2 content have been identified in the young tephra sequences of the Holocene Pyroclastic Series

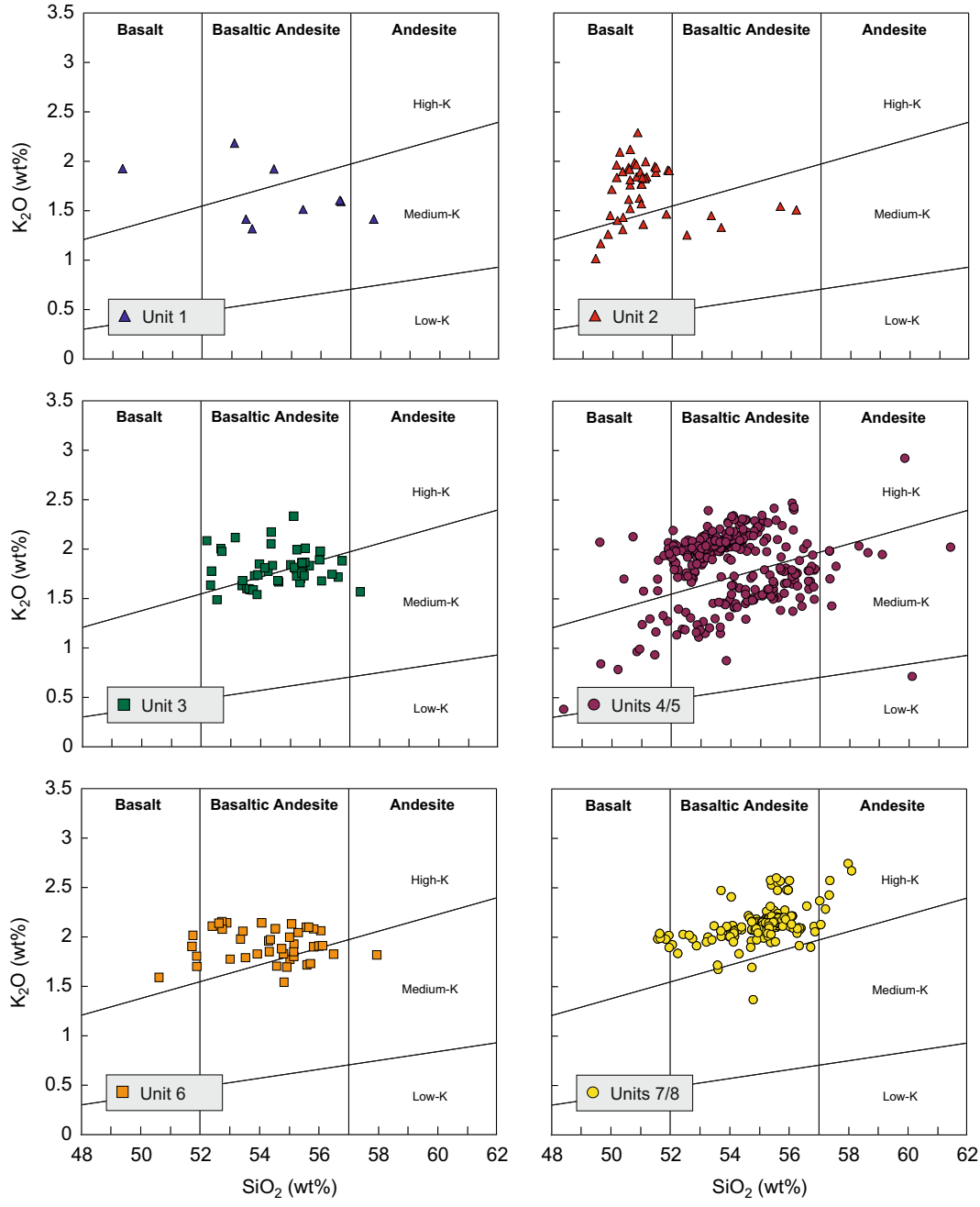

Fig. 6.27 K_2O versus SiO_2 variation diagrams (Le Maitre et al. 2002) for the main volcano-stratigraphic units of Merapi. Symbols keyed to Fig. 6.9. *Data Sources* as in Fig. 6.18

from as far back as ~ 3000 years ago. These are characterised by periods of decreasing SiO_2 content with changes from basaltic andesite (56–57 wt% SiO_2) to basalt (51–53 wt% SiO_2), alternating with shorter periods of more abrupt SiO_2 increases. Trends towards more mafic compositions were recognised also within the historical to recent eruptions during the

nineteenth and early twentieth century, while magma compositions have remained largely uniform, and near the upper limit of the total whole rock SiO_2 range of Merapi, since the mid-twentieth century (Andreastuti 1999; Gertisser 2001; Gertisser and Keller 2003a).

6.5 Summary

Based on the available chronological data, the construction of the basalt to basaltic andesite volcanic complex of Merapi began after 170 ka. Remnants of the oldest parts of Merapi, Proto-Merapi, are preserved at Gunung Bibi, as well as at Gunung Turgo, Gunung Plawangan and Gunung Medjing. The main volcanic complex consists of an older edifice, Old Merapi, and the presently active stratocone, New Merapi. The evolution of Merapi has been governed by multiple gravitational sector collapses of various scales affecting the edifices of Proto-, Old and New Merapi. A major sector collapse or several successive sector collapses of Old Merapi produced the prominent remnant avalanche caldera open to the west, which has been subsequently filled by the growth of New Merapi. The eruptive products of Merapi are predominantly basaltic andesite. Basaltic and andesitic rock types are subordinate, although the lavas of Gunung Turgo, Gunung Plawangan and Gunung Medjing are principally basaltic. Variations in K_2O content divide the Merapi rocks into medium-K and high-K types. Geochemical and isotopic characteristics are consistent with a two-stage petrogenetic model, where primary magmas of both medium-K and high-K affinity are derived from a heterogenous, Indian Ocean MORB-like mantle source metasomatised by components derived from the subducted oceanic slab and sediment cover. Magmas are subsequently modified during transfer through the crust by complex magmatic differentiation processes, including polybaric fractional crystallisation, magma replenishment followed by magma mixing or mingling, crystal mush remobilisation, crystal recycling and contamination by carbonate rocks of the local upper crust. Since $\sim$ 1900 ^{14}C y BP, all lavas and pyroclastic rocks of Merapi are of the high-K type. Cyclical geochemical variations with systematic shifts in whole rock SiO_2 content have been identified in the Late Holocene to recent eruptive products, but magma compositions have remained broadly uniform since the mid-twentieth century.

Acknowledgements We gratefully acknowledge our colleagues from the Center of Volcanology and Geological Hazard Mitigation (CVGHM) and the Merapi Volcano Observatory (BPPTKG) in Yogyakarta for their generosity and support while conducting research at Merapi. Fieldwork at Merapi wouldn't have been possible without the generous help of our local guides and drivers, including Sutisna, Dedi, Budi, Sony, Biyanto and many others, who are gratefully acknowledged here. This synthesis has benefitted from stimulating discussions with many colleagues over many years, including Brent Alloway, Sutikno Bronto, Guy Camus, Alain Gourgaud, Antonius Ratdomopurbo, Dewi Sri Sayudi, Lothar Schwarzkopf, Ian Smith, Valentin Troll, Pierre Vincent and Barry Voight. Ian Smith and Valentin Troll are thanked for their constructive reviews and helpful suggestions.

References

Andersen DJ, Lindsley DH, Davidson PM (1993) QUILF: a Pascal program to assess equilibria among Fe–Mg–Mn–Ti-oxides, pyroxenes, olivine and quartz. Comput Geosci 19:1333–1350

Andreastuti SD (1999) Stratigraphy and geochemistry of Merapi Volcano, Central Java, Indonesia: implication for assessment of volcanic hazards. PhD Thesis, University of Auckland, Auckland, New Zealand

Andreastuti SD, Alloway BV, Smith IEM (2000) A detailed tephrostratigraphic framework at Merapi Volcano, Central Java, Indonesia: implications for eruption predictions and hazard assessment. J Volcanol Geotherm Res 100:51–67

Bahar I (1984) Contribution à la connaissance du volcanisme indonésien: le Merapi (Centre Java); cadre structural, pétrologie, géochimie et implications volcanologiques. PhD Thesis, Université des Sciences et Techniques du Languedoc, Montpellier, France

Bardintzeff JM (1984) Merapi Volcano (Java, Indonesia) and Merapi-type nuée ardente. Bull Volcanol 47:433–446

Berthommier PC (1990) Etude volcanologique du Merapi (Centre-Java). Téphrostratigraphie et chronologie – produits éruptifs. PhD Thesis, Université Blaise Pascal, Clermont-Ferrand, France

Borisova AY, Martel C, Gouy S, Pratomo I, Sumarti S, Toutain J-P, Bindeman IN, de Parseval P, Metaxian J-P, Surono, (2013) Highly explosive 2010 Merapi

eruption: evidence for shallow-level crustal assimilation and hybrid fluid. J Volcanol Geotherm Res 261:193–208

Borisova AY, Gurenko AA, Martel C, Kouzmanov K, Cathala A, Bohrson WA, Pratomo I, Sumarti S (2016) Oxygen isotope heterogeneity of arc magma recorded in plagioclase from the 2010 Merapi eruption (Central Java, Indonesia). Geochim Cosmochim Acta 190:13–34

Boudon G, Camus G, Gourgaud A, Lajoie J (1993) The 1984 nuée ardente deposits of Merapi volcano, Central Java, Indonesia: stratigraphy, textural characteristics, and transport mechanisms. Bull Volcanol 55: 327–342

Bourdon B, Henderson GM, Lundstrom CC, Turner SP (eds) (2003) Uranium-series Geochemistry. Min Soc Am, Rev Mineral Geochem (Vol. 52)

Bronto S, Ratdomopurbo A, Asmoro P, Adityarani M (2014) Longsoran rakasa Gunung Api Merapi Yogyakarta – Jawa Tengah (Gigantic landslides of Merapi volcano, Yogyakarta – Central Java). J Geol Sumb Min 15:165–183

Bronto S, Rahardjo W, Asmoro P, Ratdomopurbo A, Adityarani M, Permatasari A (2023) The godean debris avalanche deposit from a sector collapse of Merapi volcano. In: Gertisser R, Troll VR, Walter TR, Nandaka IGMA, Ratdomopurbo A (eds) Merapi volcano—geology, eruptive activity, and monitoring of a high-risk volcano. Springer, Berlin, Heidelberg, pp 195–231

Buddington AF, Lindsley DH (1964) Iron-titanium oxide minerals and synthetic equivalents. J Petrol 5:310–357

Camus G, Gourgaud A, Mossand-Berthommier P-C, Vincent PM (2000) Merapi (Central Java, Indonesia): an outline of the structural and magmatological evolution, with a special emphasis to the major pyroclastic events. J Volcanol Geotherm Res 100:139–163

Chadwick JP, Troll VR, Ginibre C, Morgan D, Gertisser R, Waight TE, Davidson JP (2007) Carbonate assimilation at Merapi Volcano, Java, Indonesia: insights from crystal isotope stratigraphy. J Petrol 48:1793–1812

Chadwick JP, Troll VR, Waight TE, van der Zwan FM, Schwarzkopf LM (2013) Petrology and geochemistry of igneous inclusions in recent Merapi deposits: a window into the sub-volcanic plumbing system. Contrib Mineral Petrol 165:259–282

Charbonnier SJ, Gertisser R (2008) Field observations and surface characteristics of pristine block-and-ash flow deposits from the 2006 eruption of Merapi Volcano, Java, Indonesia. J Volcanol Geotherm Res 177:971–982

Clocchiatti R, Joron JL, Kerinec F, Treuil M (1982) Quelques données préliminaires sur la lave du dôme actuel du volcan Mérapi (Java, Indonésie) et sur ses enclaves. CR Acad Sci Paris 295:817–822

Condomines M, Sigmarsson O (1993) Why are so many arc magmas close to ^{238}U–^{230}Th radioactive equilibrium? Geochim Cosmochim Acta 57:4491–4497

Condomines M, Gauthier PJ, Tanguy JC, Gertisser R, Thouret JC, Berthommier P, Camus G (2005) ^{226}Ra or $^{226}Ra/Ba$ dating of Holocene volcanic rocks: application to Mt. Etna and Merapi volcanoes. Earth Planet Sci Lett 230:289–300

Costa F, Andreastuti S, Bouvet de Maisonneuve C, Pallister JS (2013) Petrological insights into the storage conditions, and magmatic processes that yielded the centennial 2010 Merapi explosive eruption. J Volcanol Geotherm Res 261:209–235

Crummy JM, Savov IP, Navarro-Ochoa C, Morgan DJ, Wilson M (2014) High-K Mafic Plinian Eruptions of Volcán de Colima, Mexico. J Petrol 55:2155–2192

Davydova VO, Yu P, Plechov VD, Shcherbakov AB, Perepelov (2018) High-K basaltic trachyandesite xenoliths in pyroclastic deposits from the Bezymianny volcano (Kamchatka). Russ Geol Geophys 59:1087–1099

Debaille V, Doucelance R, Weis D, Schiano P (2006) Multi-stage mixing in subduction zones: Application to Merapi volcano (Java island, Sunda arc). Geochim Cosmochim Acta 70:723–741

Deegan FM, Troll VR, Freda C, Misiti V, Chadwick JP, McLeod CL, Davidson JP (2010) Magma-carbonate interaction processes and associated CO_2 release at Merapi volcano, Indonesia: insights from experimental petrology. J Petrol 51:1027–1051

Deegan FM, Troll VR, Gertisser R, Freda C (2023) Magma-carbonate interaction at Merapi volcano, Indonesia. In: Gertisser R, Troll VR, Walter TR, Nandaka IGMA, Ratdomopurbo A (eds) Merapi volcano—geology, eruptive activity, and monitoring of a high-risk volcano. Springer, Berlin, Heidelberg, pp 291–321

Deegan FM, Whitehouse MJ, Troll VR, Budd DA, Harris C, Geiger H, Hålenius U (2016) Pyroxene standards for SIMS oxygen isotope analysis and their application to Merapi volcano, Sunda arc, Indonesia. Chem Geol 447:1–10

Deegan FM, Whitehouse MJ, Troll VR, Geiger H, Jeon H, le Roux P, Harris C, van Helden M, González-Maurel O (2021) Sunda arc mantle source $\delta^{18}O$ value revealed by intracrystal isotope analysis. Nat Commun 12:3930

DePaolo DJ (1981) Trace element and isotopic effects of combined wallrock assimilation and fractional crystallization. Earth Planet Sci Lett 53:189–202

Devine JD, Gardner JE, Brack HP, Layne GD, Rutherford MJ (1995) Comparison of microanalytical methods for estimating H_2O contents of silicic volcanic glasses. Am Mineral 80:319–328

del Marmol MA (1989) The petrology and geochemistry of Merapi Volcano, Central Java, Indonesia. PhD Thesis, The Johns Hopkins University, Baltimore, USA

Djumarma A, Bronto S, Bahar I, Suparban F, Sukhyar R, Newhall C, Holcomb RT, Banks NG, Torley R, Lockwood JP, Tilling RI, Rubin M, del Marmol MA (1986) Did Merapi volcano (Central Java) erupt catastrophically in 1006 A.D.? Abstract, IAVCEI Internat Volcanol Congr 1986, Rotorua, New Zealand

Drignon MJ, Bechon T, Arbaret L, Burgisser A, Komorowski J-C, Martel C, Yaputra R (2016) Preexplosive conduit conditions during the 2010 eruption of Merapi volcano (Java, Indonesia). Geophys Res Lett 43:11595–11602

Erdmann S, Martel C, Pichavant M, Kushnir A (2014) Amphibole as an archivist of magmatic crystallization conditions: problems, potential, and implications for inferring magma storage prior to the paroxysmal 2010 eruption of Mount Merapi. Indonesia. Contrib Mineral Petrol 167:1016

Erdmann S, Martel C, Pichavant M, Bourdier J-L, Champallier R, Komorowski J-C, Cholik N (2016) Constraints from Phase Equilibrium Experiments on Pre-eruptive Storage Conditions in Mixed Magma Systems: a Case Study on Crystal-rich Basaltic Andesites from Mount Merapi, Indonesia. J Petrol 57:535–560

Eiler JM, Schiano P, Kitchen N, Stolper EM (2000) Oxygen-isotope evidence for recycled crust in the sources of mid-ocean-ridge basalts. Nature 403:530–534

Francalanci L, Lucchi F, Keller J, De Astis G, Tranne CA (2013) Eruptive, volcano-tectonic and magmatic history of the Stromboli volcano (north-eastern Aeolian archipelago). In: Lucchi F, Peccerillo A, Keller J, Tranne CA, Rossi PL (eds) The Aeolian Islands Volcanoes. Geol Soc London Mem 37:397–471

Garcia MO, Jacobson SS (1979) Crystal clots, amphibole fraction and the evolution of calc-alkaline magmas. Contrib Mineral Petrol 69:319–327

Gauthier PJ, Condomines M (1999) ^{210}Pb-^{226}Ra radioactive disequilibria in recent lavas and radon degassing: inferences on the magma chamber dynamics at Stromboli and Merapi volcanoes. Earth Planet Sci Lett 172:111–126

Gertisser R (2001) Gunung Merapi (Java, Indonesien): Eruptionsgeschichte und magmatische Evolution eines Hochrisiko-Vulkans. PhD Thesis, Albert-Ludwigs-Universität Freiburg, Freiburg, Germany

Gertisser R, Keller J (2003a) Temporal variations in magma composition at Merapi Volcano (Central Java, Indonesia): magmatic cycles during the past 2,000 years of explosive activity. J Volcanol Geotherm Res 123:1–23

Gertisser R, Keller J (2003b) Trace element and Sr, Nd, Pb and O isotope variations in medium-K and high-K volcanic rocks from Merapi Volcano, Central Java, Indonesia: evidence for the involvement of subducted sediments in Sunda Arc magma genesis. J Petrol 44:457–486

Gertisser R, Charbonnier SJ, Troll VR, Keller J, Preece K, Chadwick JP, Barclay J, Herd RA (2011) Merapi (Java, Indonesia): anatomy of a killer volcano. Geol Today 27:57–62

Gertisser R, Charbonnier SJ, Keller J, Quidelleur X (2012a) The geological evolution of Merapi volcano, Central Java, Indonesia. Bull Volcanol 74:1213–1233

Gertisser R, Cassidy NJ, Charbonnier SJ, Nuzzo L, Preece K (2012b) Overbank block-and-ash flow deposits and the impact of valley-derived, unconfined flows on populated areas at Merapi volcano, Java, Indonesia. Nat Hazards 60:623–648

Gertisser R, Self S, Thomas LE, Handley HK, van Calsteren P, Wolff JA (2012c) Processes and timescales of magma genesis and differentiation leading to the great Tambora eruption in 1815. J Petrol 53:271–297

Gill JB, Williams RW (1990) Th isotope and U-series studies of subduction-related volcanic rocks. Geochim Cosmochim Acta 54:1427–1442

Global Volcanism Program (2013) Volcanoes of the World, v 4.9.4 (17 Mar 2021) Venzke E (ed) Smithsonian Institution. Downloaded 27 Apr 2021. https://doi.org/10.5479/si.GVP.VOTW4-2013

Global Volcanism Program (2019) Report on Merapi (Indonesia). In: Krippner JB, Venzke E (eds). Smithsonian Institution — Bull Global Volc Netw 44:10

Global Volcanism Program (2020) Report on Merapi (Indonesia). In: Bennis KL, Venzke E (eds). Smithsonian Institution — Bull Global Volc Netw 45:4

Gomez C, Janin M, Lavigne F, Gertisser R, Charbonnier S, Lahitte P, Hadmoko SR, Fort M, Wassmer P, Degroot V, Murwanto H (2010) Borobudur, a basin under volcanic influence: 361,000 years BP to present. J Volcanol Geotherm Res 196:245–264

Haggerty SE (1993) Oxide textures – a mini-atlas. In: Lindsley DH (ed) Oxide minerals: petrologic and magnetic significance. Rev Mineral 25:303–321

Hammer JE, Cashman KV, Voight B (2000) Magmatic processes revealed by textural and compositional trends in Merapi dome lavas. J Volcanol Geotherm Res 100:165–192

Handley HK, Macpherson CG, Davidson JP, Berlo K, Lowry D (2007) Constraining fluid and sediment contributions to subduction-related magmatism in Indonesia: Ijen Volcanic Complex, Indonesia. J Petrol 48:1155–1183

Handley HK, Davidson JP, Macpherson CG (2008) Untangling differentiation in arc lavas: constraints from unusual minor and trace element variations at Salak Volcano, Indonesia. Chem Geol 255:360–376

Handley HK, Macpherson CG, Davidson JP (2010) Geochemical and Sr-O isotopic constraints on magmatic differentiation at Gede Volcanic Complex, West Java, Indonesia. Contrib Mineral Petrol 159:885–908

Handley HK, Turner SP, Macpherson CG, Gertisser R, Davidson JP (2011) Hf-Nd isotope and trace element constraints on subduction inputs at island arcs: limitations of Hf anomalies as sediment input indicators. Earth Planet Sci Lett 304:212–223

Handley HK, Blichert-Toft J, Gertisser R, Macpherson CG, Turner SP, Zaennudin A, Abdurrachman M (2014) Insights from Pb and O isotopes into along-arc variations in subduction inputs and crustal assimilation for volcanic rocks in Java, Sunda arc, Indonesia. Geochim Cosmochim Acta 139:205–226

Handley HK, Reagan M, Gertisser R, Preece K, Berlo K, McGee LE, Barclay J, Herd R (2018) Timescales of magma ascent and degassing and the role of crustal assimilation at Merapi volcano (2006–2010), Indonesia: constraints from uranium-series and radiogenic isotopic compositions. Geochim Cosmochim Acta 222:34–52

Harris C, Pronost JJM, Ashwal LD, Cawthorn RG (2005) Oxygen and hydrogen isotope stratigraphy of the Rustenburg layered suite, Bushveld Complex: constraints on crustal contamination. J Petrol 46:579–601

Hartmann M (1935) Die Ausbrüche des G. Merapi (Mittel-Java) bis zum Jahre 1883. Neues Jahrb Mineral Geol Paläontol 75:127–162

Hatherton T, Dickenson WR (1969) The relationship between andesitic volcanism and seismicity in Indonesia, the lesser Antilles and other island arcs. J Geophys Res 74:5301–5310

Ijzerman JW (1891) Beschrijving der oudheden nabij de grens de Residentie's Soerakarta en Djogdjakarta. Batavia: Landsdrukkerij; 's Gravenhage: M. Nijhoff, 135 p

Innocenti S, Andreastuti S, Furman T, del Marmol M-A, Voight B (2013a) The pre-eruption conditions for explosive eruptions at Merapi volcano as revealed by crystal texture and mineralogy. J Volcanol Geotherm Res 261:69–86

Innocenti S, del Marmol M-A, Voight B, Andreastuti S, Furman T (2013b) Textural and mineral chemistry constraints on evolution of Merapi volcano, Indonesia. J Volcanol Geotherm Res 261:20–37

James DE (1981) The combined use of oxygen and radiogenic isotopes as indicators of crustal contamination. Ann Rev Earth Planet Sci 9:311–344

Katili JA (1975) Volcanism and plate tectonics in the Indonesian island arcs. Tectonophysics 26:165–188

Kemmerling GLL (1921) De hernieuwde werking van den vulkan G. Merapi (Midden Java) van den begin Augustus 1920 tot en met einde Februari 1921. Vulkanol Seismol Med 3:1–30

Kerinec F (1982) Le Merapi, volcan actif d'arc insulaire (Java): Petrographie et geochemie de materiaux solides; implications geotectonics. PhD Thesis (Thèse de Troisième Cycle), Université Paris-Sud, Orsay, France

Komorowski J-C, Jenkins S, Baxter PJ, Picquout A, Lavigne F, Charbonnier S, Gertisser R, Preece K, Cholik N, Budi-Santoso A, Surono, (2013) Paroxysmal dome explosion during the Merapi 2010 eruption: processes and facies relationships of associated high-energy pyroclastic density currents. J Volcanol Geotherm Res 261:260–294

Le Maitre RW (ed), Streckeisen A, Zanettin B, Le Bas MJ, Bonin B, Bateman P, Bellieni G, Dudek A, Efremova J, Keller J, Lameyre J, Sabine PA, Schmidt R, Sørensen H, Woolley AR (2002) Igneous rocks. A classification and glossary of terms. Recommendations of the International Union of Geological Sciences Subcommission on the systematics of igneous rocks. University Press, Cambridge

Li W, Costa F, Nagashima K (2021) Apatite crystals reveal melt volatile budgets and magma storage depths at Merapi volcano, Indonesia. J Petrol 62:egaa100

Leake BE, Woolley AR, Arps CES, Birch WD, Gilbert MC, Grice JD, Hawthorne FC, Kato A, Kinsch HJ, Krivovichev VG, Linthout K, Laird J, Mandarino JA, Maresch WV, Nickel EH, Rock NMS, Schumacher JC, Smith DC, Stephenson NCN, Ungaretti L, Whittaker EJW, Youzhi G (1997) Nomenclature of amphiboles: report on the subcommittee on amphiboles of the International Mineralogical Association, Commission on New Minerals and Mineral Names. Can Mineral 35:219–246

Luais B (1986) Pétrologie et géochemie (éléments trace et rapports isotopiques du Sr) du magmatisme associé aux zones de subduction: Exemples du bassin mediterraneen (Santorin, Arc Egeen; Stromboli, Arc Eolien) et des îles de la Sonde (Merapi, Java). PhD Thesis (Thèse de Troisième Cycle), Université de Montpellier, Montpellier, France

McDermott F, Hawkesworth C (1991) Th, Pb, and Sr isotope variations in young island arc volcanics and oceanic sediments. Earth Planet Sci Lett 104:1–15

Morimoto N (1988) Nomenclature of Pyroxenes. Mineral Petrol 39:55–76

Murwanto H, Gunnell Y, Suharsono S, Sutikno S, Lavigne F (2004) Borobudur monument (Java, Indonesia) stood by a natural lake: chronostratigraphic evidence and historical implications. The Holocene 14:459–463

Murwanto H (2014) Penelusuran jejak lingkungan danau di sekitar Candi Borobudur dengan pendekatan paleogeomorfologi. S3 Dissertation, University of Gadjah Mada, Yogyakarta, Indonesia

Nadeau O, Williams-Jones AE, Stix J (2013) Magmatic–hydrothermal evolution and devolatilization beneath Merapi volcano, Indonesia. J Volcanol Geotherm Res 261:50–68

Nandaka IGMA, Gertisser R, Walter TR, Troll VR, Ratdomopurbo A (2023) Merapi: evolving knowledge and future challenges. In: Gertisser R, Troll VR, Walter TR, Nandaka IGMA, Ratdomopurbo A (eds) Merapi volcano-geology, eruptive activity, and monitoring of a high-risk volcano. Springer, Berlin, Heidelberg, pp 553–572

Newhall CG, Bronto S, Alloway B, Banks NG, Bahar I, Del Marmol MA, Hadisantono RD, Holcomb RT, McGeehin J, Miksic JN, Rubin M, Sayudi SD, Sukhyar R, Andreastuti S, Tilling RI, Torley R, Trimble D, Wirakusumah AD (2000) 10,000 years of explosive eruptions of Merapi Volcano, Central Java: archaeological and modern implications. J Volcanol Geotherm Res 100:9–50

Newhall CG, Self S (1982) The volcanic explosivity index (VEI): an estimate of explosive magnitude for historical volcanism. J Geophys Res 87:1231–1238

Peccerillo A, Taylor SR (1976) Geochemistry of Eocene calc-alkaline volcanic rocks from the Kastamonu area, northern Turkey. Contrib Mineral Petrol 58:63–81

Peters STM, Troll VR, Weis FA, Dallai L, Chadwick JP, Schulz B (2017) Amphibole megacrysts as a probe into the deep plumbing system of Merapi volcano, Central Java. Indonesia. Contrib Mineral Petrol 172:16

Preece K (2014) Transitions between effusive and explosive activity at Merapi volcano, Indonesia: a volcanological and petrological study of the 2006 and 2010 eruptions. PhD Thesis, University of East Anglia, Norwich, UK

Preece K, Barclay J, Gertisser R, Herd RA (2013) Textural and micro-petrological variations in the eruptive products of the 2006 dome-forming eruption of Merapi volcano, Indonesia: implications for sub-surface processes. J Volcanol Geotherm Res 261:98–120

Preece K, Gertisser R, Barclay J, Berlo K, Herd RA, Facility EIM (2014) Pre- and syn-eruptive degassing and crystallisation processes of the 2010 and 2006 eruptions of Merapi volcano. Indonesia. Contrib Mineral Petrol 168:1061

Preece K, Gertisser R, Barclay J, Charbonnier SJ, Komorowski J-C, Herd RA (2016) Transitions between explosive and effusive phases during the cataclysmic 2010 eruption of Merapi volcano, Java. Indonesia. Bull Volcanol 78:54

Preece K, van der Zwan F, Hammer J, Gertisser R (2023) A textural perspective on the magmatic system and eruptive behaviour of Merapi volcano. In: Gertisser R, Troll VR, Walter TR, Nandaka IGMA, Ratdomopurbo A (eds) Merapi volcano—geology, eruptive activity, and monitoring of a high-risk volcano. Springer, Berlin, Heidelberg, pp 265–289

Rahardjo W, Sukandarrumidi, Rosidi HMD (1977) Geological Map of the Yogyakarta Quadrangle, Java, 1:100,000, Geol. Surv. of Indonesia, Ministry of Mines, Bandung

Ratdomopurbo A, Beauducel F, Subandriyo J, Nandaka IGMA, Newhall CG, Suharna SDS, Suparwaka H, Sunarta, (2013) Overview of the 2006 eruption of Mt. Merapi. J Volcanol Geotherm Res 261:87–97

Scheltema JF (1912) Monumental Java. Macmillan and Co., Limited, London, p 302

Selles A, Deffontaines B, Hendrayana H, Violette V (2015) The eastern flank of the Merapi volcano (Central Java, Indonesia): architecture and implications of volcaniclastic deposits. J Asian Earth Sci 108:33–47

Siebert L, Simkin T, Kimberly P (2011) Volcanoes of the world. University of California Press, Berkeley

Solikhin A, Thouret J-C, Liew SC, Gupta A, Sayudi DS, Oehler J-F, Kassouk Z (2015) High-spatial-resolution imagery helps map deposits of the large (VEI 4) 2010 Merapi Volcano eruption and their impact. Bull Volcanol 77:20

Subandriyo, Gertisser R, Aisyah N, Humaida H, Preece K, Charbonnier S, Budi-Santoso A, Handley H, Sumarti S, Sayudi DS, Nandaka IGMA, Wibowo HE (2023) An overview of the large-magnitude (VEI 4) eruption of Merapi in 2010. In: Gertisser R, Troll VR, Walter TR, Nandaka IGMA, Ratdomopurbo A (eds) Merapi volcano—geology, eruptive activity, and monitoring of a high-risk volcano. Springer, Berlin, Heidelberg, pp 353–407

Stewart RB, Price RC, Smith IEM (1996) Evolution of high-K arc magma, Egmont volcano, Taranaki, New Zealand: evidence from mineral chemistry. J Volcanol Geotherm Res 74:275–295

Sun SS, McDonough WF (1989) Chemical and isotopic systematics of oceanic basalts: implications for mantle composition and processes. In: Saunders AD, Norry MJ (eds) Magmatism in the ocean basins. Geol Soc Lond Spec Publ 42:313–345

Troll VR, Deegan FM (2023) The magma plumbing system of Merapi: The petrological perspective. In: Gertisser R, Troll VR, Walter TR, Nandaka IGMA, Ratdomopurbo A (eds) Merapi volcano—geology, eruptive activity, and monitoring of a high-risk volcano. Springer, Berlin, Heidelberg, pp 233–263

Troll VR, Hilton DR, Jolis EM, Chadwick JP, Blythe LS, Deegan FM, Schwarzkopf LM, Zimmer M (2012) Crustal CO_2 liberation during the 2006 eruption and earthquake events at Merapi volcano. Indonesia. Geophys Res Lett 39:L11302

Troll VR, Deegan FM, Jolis EM, Harris C, Chadwick JP, Gertisser R, Schwarzkopf LM, Borisova AY, Bindeman IN, Sumarti S, Preece K (2013a) Magmatic differentiation processes at Merapi volcano: inclusion petrology and oxygen isotopes. J Volcanol Geotherm Res 261:38–49

Troll VR, Chadwick JP, Jolis EM, Deegan FM, Hilton DR, Schwarzkopf LM, Blythe LS, Zimmer M (2013b) Crustal volatile release at Merapi volcano; the 2006 earthquake and eruption events. Geol Today 29:96–101

Turner S, Foden J (2001) U, Th and Ra disequilibria, Sr, Nd and Pb isotope and trace element variations in Sunda arc lavas: predominance of a subducted sediment component. Contrib Mineral Petrol 142:43–57

van Bemmelen RW (1949) The geology of Indonesia, Vol. 1A: General Geology. Government Printing Office, The Hague

van Bemmelen RW (1956) The influence of geologic events on human history (an example from Central Java). Verhand K Ned Geol Mijnbouw Genoot, Geol Serie, p 20–36

van der Zwan FM, Chadwick JP, Troll VR (2013) Textural history of recent basaltic-andesites and plutonic inclusions from Merapi volcano. Contrib Mineral Petrol 166:43–63

Vidal CM, Komorowski J-C, Métrich N, Pratomo I, Kartadinata N, Prambada O, Michel A, Carazzo G, Lavigne F, Rodysill J, Fontijn K, Surono (2015) Dynamics of the major plinian eruption of Samalas in 1257 A.D. (Lombok, Indonesia). Bull Volcanol 77:73

Voight B, Constantine EK, Siswowidjoyo S, Torley R (2000) Historical eruptions of Merapi volcano, Central Java, Indonesia, 1768–1998. J Volcanol Geotherm Res 100:69–138

White WM, Patchett J (1984) Hf-Nd-Sr isotopes and incompatible element abundances in island arcs: implications for magma origins and crust-mantle evolution. Earth Planet Sci Lett 67:167–185

Whitford DJ (1975a) Geochemistry and petrology of volcanic rocks from the Sunda arc, Indonesia: PhD Thesis, Australian National University, Canberra, Australia

Whitford DJ (1975b) Strontium isotopic studies of the volcanic rocks of the Sunda arc, Indonesia and their petrogenetic implications. Geochim Cosmochim Acta 39:1287–1302

Whitford DJ, Nicholls IA (1976) Potassium variation in lavas across the Sunda arc in Java and Bali. In: Johnson RW (ed) Volcanism in Australasia. Elsevier, Amsterdam, pp 63–75

Whitford DJ, Nicholls IA, Taylor SR (1979) Spatial variations in the geochemistry of Quaternary lavas across the Sunda arc in Java and Bali. Contrib Mineral Petrol 70:341–356

Whitford DJ, White WM, Jezek PA (1981) Neodymium isotopic composition of Quaternary island arc lavas from Indonesia. Geochim Cosmochim Acta 45:989–995

Whitley S (2020) Xenoliths as tracers of magmatic and intra-crustal processes at volcanic arcs. PhD Thesis, Keele University, Keele, UK

Whitley S, Gertisser R, Halama R, Preece K, Troll VR, Deegan FM (2019) Crustal CO_2 contribution to subduction zone degassing recorded through calc-silicate xenoliths in arc lavas. Sci Rep 9:8803

Whitley S, Halama R, Gertisser R, Preece K, Deegan FM, Troll VR (2020) Magmatic and metasomatic effects of magma-carbonate interaction recorded in calc-silicate xenoliths from Merapi volcano (Indonesia). J Petrol 61 (4):egaa048

Wirakusumah AD, Heriman AD, Hadisantono RD, Lubis H, Sutoyo (1980) Laporan kemajuan pemetaan geologi Daerah Gunung Merapi, Jawa Tengah. Unpublished Report – Volcanological Survey of Indonesia, Bandung

Wirakusumah AD, Juwarna H, Loebis H (1989) Peta Geologi Gunungapi Merapi. Jawa Tengah (geologic Map of Merapi Volcano, Central Java) 1(50):000

Woodhead JD, Hergt JM, Davidson JP, Eggins SM (2001) Hafnium isotope evidence for 'conservative' element mobility during subduction processes. Earth Planet Sci Lett 192:331–346